Power efficient adaptive mitigation of local interference in multimode wireless transceivers

DOI:
10.6100/IR770338

Document status and date:
Published: 13/03/2014

Document Version:
Publisher's PDF, also known as Version of Record (includes final page, issue and volume numbers)

Power efficient adaptive mitigation of local interference in multimode wireless transceivers

PROEFSCHRIFT

ter verkrijging van de graad van doctor aan de Technische Universiteit Eindhoven, op gezag van de rector magnificus prof.dr.ir. C.J. van Duijn, voor een commissie aangewezen door het College voor Promoties, in het openbaar te verdedigen op donderdag 13 maart 2014 om 16:00 uur

door

Hooman Habibi

geboren te Mahshahr, Iran

Dit proefschrift is goedgekeurd door de promotoren en de samenstelling van de promotiecommissie is als volgt:

voorzitter:	prof.dr. H. Corporaal
1e promotor:	prof.dr.ir. J.W.M. Bergmans
2e promotor:	prof.dr.ir. P.G.M. Baltus
copromotor:	dr. Y. Wu
leden:	prof.dr.ir. B. Nauta (University of Twente)
	prof.dr.Ing G. Ascheid (RWTH Aachen)
	prof.dr.ir. E.R. Fledderus
adviseur:	dr. D. Milosevic

To Sophie, Negar,
and my parents.

This research was kindly supported by STW, The Netherlands.

Power efficient adaptive mitigation of local interference in multimode wireless transceivers / by Hooman Habibi – Eindhoven University of Technology, Eindhoven, The Netherlands, 2014

A catalogue record is available from the Eindhoven University of Technology Library
ISBN: 978-90-386-3579-8
NUR 959
Subject headings: Multimode transceivers, Multiradio coexistence, Interference mitigation, Adaptive systems, Adaptive circuits, Nonlinear circuits.

This thesis was prepared with the LaTeX documentation system.
Cover design:Paul Verspaget
Reproduction:Eindhoven University of Technology, Print Service

Summary

Nowadays, handheld devices like mobile phones and tablets have become widespread. These devices support several wireless communication standards for various functionalities, e.g. voice and video calls, data transfer, and location finding. The collection of several transceivers in one device, which is required to implement these standards, is referred to as a multimode transceiver.

It is often required that two standards are used simultaneously in one multimode transceiver. Owing to the small size of the transceiver, a local transmitter for one standard induces a strong interference in the local receiver for the other standard, often many orders of magnitude stronger than the desired signal of the receiver. If the strong interference is not suppressed at an early stage of the receiver front-end, it will induce nonlinear distortion products and may cause a severe loss of receiver sensitivity, called desensitization. State of the art approaches to sufficiently suppress the interference require unpractical power consumption or analogue complexity. Hence they are not suitable for application in handheld devices.

In this thesis we study a novel hybrid approach, which combines mixed-signal circuits and digital signal processing techniques, to mitigate the local interference with low complexity and power consumption. The approach uses a memoryless Nonlinear Interference Suppressor (NIS) in the receiver front-end to significantly suppress the local interference and prevent desensitization. Design of this mixed-signal circuit is discussed in a companion PhD thesis [1]. For the NIS to suppress the interference, it must be dynamically adapted to accurately track the interference envelope. In this thesis we exploit the local availability of an interference reference to devise simple yet accurate digital NIS adaptation schemes.

Successful design and implementation of our approach is carried out in three stages. Firstly, based on ideal models we perform a system study, which shows the benefits and drawbacks of using the NIS. Secondly, accuracy requirements for the adaptation signal of the NIS are derived and a closed-loop adaptation method is designed to meet these requirements. Thirdly, the NIS circuit is integrated in a test bed transceiver, the ideal models are revised based on measurements, and adaptation methods are refined based on the revised models. Predictable and successful operation of the test bed validates the presented analysis and simulations.

When the combination of the strong interference and the weak desired signal experiences any nonlinearities in the receiver front-end, distortion products are generated. One of these is Cross-Modulation (CM) distortion, where the amplitude modulation of the interference transfers to modulation of the desired signal. CM distortion is particularly problematic, since it occurs independent of the frequency

separation of the desired signal and the interference. In this thesis we encounter CM distortion in two situations, namely without and with NIS. The first situation is of interest since the interference can be weak enough to be handled without NIS yet strong enough to cause CM distortion. In this situation the CM distortion can be compensated digitally. In Chapter 2, we propose a simple digital compensation method that exploits the local availability of the baseband interference to avoid the complexity and power dissipation of additional analogue circuits.

In Chapter 3, we introduce the NIS and study its potential benefits. Firstly, we derive an optimal adaptation signal for the NIS that yields complete suppression of the interference in the absence of the desired signal. For this optimal adaptation signal, residual distortion products of the NIS are identified. The impact of these products on the received desired signal is analyzed and rules of thumb are given to specify conditions for which adequate interference suppression is combined with negligible distortion. We show that these conditions are met in most cases of practical interest.

The optimal adaptation signal is proportional to the envelope of the received interference at the NIS input. A key feature in the multimode transceiver is the local availability of the interference source. Using a baseband linear model of the interference coupling path, from the local transmitter to the local receiver, the adaptation signal can be obtained digitally. In Chapter 4, we quantify the required accuracy for the adaptation signal to properly suppress the interference while keeping the degradation of the receiver Symbol Error Rate (SER) negligible. To provide the required accuracy, we propose a closed-loop method to dynamically adapt the path model such that the power of the residual interference at the output of the NIS is minimized. This method uses the baseband interference as a reference to combine simplicity with high accuracy and high speed. Our analysis and simulations show that the optimal adaptation signal can be estimated with sufficient accuracy, such that the interference is strongly suppressed while a SER close to that of an exactly linear receiver is achieved.

In Chapters 3 and 4, idealized models of the NIS and adaptation circuits are used to analyze the performance afforded by the NIS. In Chapter 5, we present experimental results of a multimode transceiver test bed that uses the mixed-signal integrated NIS circuit designed in [1]. The main circuit imperfections that limit the NIS performance are identified and simple imperfection models are described that explain the experimental results. Based on these models, the NIS adaptation method is extended with simple digital compensation and calibration techniques that unlock the full interference suppression potential of the NIS circuit. Furthermore, a low-complexity digital compensation method is proposed for the CM distortion that is caused by the imperfections. Successful operation of the test bed suggests that the NIS approach is practical and attractive for multimode transceivers.

Concluding remarks and suggestions for future work are collected in Chapter 6. The analysis, simulation and experimental results in this thesis show that the NIS can achieve substantial interference suppression at attractive complexity and power dissipation, and that the residual distortion products can be digitally compensated with a low complexity. Both fundamental and practical limitations of the proposed approach are identified, and directions for future improvements are sketched.

References:

[1] Ph.D. Thesis E.J.G. Janssen, "Methodologies for Multi-Radio Coexistence; Self-Interference Suppression Techniques".

Contents

List of Abbreviations

ADC	Analogue to Digital Converter
AGC	Automatic Gain Controller
AWGN	Additive White Gaussian Noise
BPF	Band Pass Filter
CDMA	Code Division Multiple Access
CM	Cross-Modulation
CSCG	Circularly-Symmetric Complex Gaussian
DAC	Digital to Analogue Converter
DFT	Discrete Fourier Transform
FE	Front-End
FIR	Finite Impulse Response
FMCW	Frequency Modulated Continuous Wave
FPGA	Field Programmable Gate Array
GMSK	Gaussian Minimum Shift Keying
GNSS	Global Navigation Satellite System
GPS	Global Positioning System
GSM	Global System for Mobile communication
GVD	Gain Variation Distortion
IM	Inter-Modulation
IIP3	Input third-order Intercept Point
IM3	third-order Intermodulation
LO	Local Oscillator
LPF	Low Pass Filter
LNA	Low Noise Amplifier
LRX	Local Receiver
LTX	Local Transmitter
LTE	Long Term Evolution for wireless communication
MBPS	Mega Bit Per Second
MER	Modulation Error Ratio
MSPS	Mega Symbol Per Second
MSE	Mean Square Error
MMSE	Minimum Mean Square Error
NAE	Normalized Adaptation Error
NIS	Nonlinear Interference Suppressor
OFDM	Orthogonal Frequency division Multiplexing
P1dB	1dB Compression Point
PAPR	Peak to Average Power Ratio
PSD	Power Spectral Density
QAM	Quadrature Amplitude Modulation
QPSK	Quaternary Phase Shift Keying

RF	Radio Frequency
RFID	Radio Frequency Identification
RX	Receiver
RTX	Remote Transmitter
SAW	Surface Acoustic Wave
SER	Symbol Error Rate
SDR	Signal to Distortion Ratio
SIMR	Signal to Inter-Modulation Ratio
SIR	Signal to Interference Ratio
SNR	Signal to Noise Ratio
SRCD	Sampling Rate Conversion and Delay block
TX	Transmitter
TRX	Transceiver
VSG	Vector Signal Generator
WiMax	Worldwide Interpretability for Microwave Access
WLAN	Wireless Local Area Network

List of Symbols

A_i	Envelope of the interference
A_d	Envelope of the desired signal
$A_{i,y}$	Envelope of the interference at the Nonlinear Interference Suppressor (NIS) output
$A_{d,y}$	Envelope of the desired signal at the NIS output
A_{IM}	Envelope of the third-order intermodulation at the NIS output
B_i	Bandwidth of the interference
B_d	Bandwidth of the desired signal
$d[n]$	Baseband discrete-time desired signal
Δf	Frequency separation between interference and the desired signal
$\mathrm{E}()$	Expected value
f_i	Frequency of the interference
f_d	Frequency of the desired signal
$\varphi_i(t)$	Phase of the interference
$\varphi_d(t)$	Phase of the desired signal
$g[n]$	Estimated baseband equivalent impulse response of interference coupling path
g_i	Gain of a block for the interference
g_d	Gain of a block for the desired signal
h	Baseband equivalent impulse response of interference coupling path
$i[n]$	Baseband discrete-time interference
$l(t)$	Adaptation signal of the NIS
$\tilde{l}(t)$	Optimal adaptation signal
$\hat{l}(t)$	Estimated adaptation signal
$P_i(t)$	Instantaneous power of the interference at NIS input
$P_d(t)$	Instantaneous power of the desired signal at NIS input
$\overline{P_i}$	Average power of the interference at NIS input
$\overline{P_d}$	Average power of the desired signal at NIS input
$x(t)$	NIS input signal
$y(t)$	NIS Output signal
$z(t)$	Signal received by the local receiver at the input of the Analogue to Digital Converter(ADC)

$z[n]$	Signal received by the local receiver at the output of the ADC

Chapter 1

Introduction

Nowadays, handheld devices like mobile phones and tablets have become widespread. These devices support several wireless communication standards for various functionalities, e.g. voice and video calls, data transfer, location finding. To enable these standards a number of transceivers is required(a transceiver is a pair of a transmitter and a receiver.) The collection of these transceivers in one device is referred to as a multimode transceiver. In this chapter, we first describe the problem of a strong local interference, which is encountered in multimode transceivers when a local transmitter and a local receiver are active simultaneously in the same handheld device. State of the art approaches to handle this problem are explored. It is concluded that these approaches are not adequate as they require an unpractical power consumption or are not suitable for application in handheld devices. Then the proposed solution for mitigation of the local interference is discussed. This solution uses an adaptive memoryless nonlinearity to suppress the interference at an early stage of the receiver front-end and uses digital signal processing techniques for its adaptation and for compensation of nonlinear distortion products, which are caused by application of this nonlinearity in the receiver. The chapter concludes by describing the outline and contributions in the following chapters of this thesis.

1.1 Wireless technologies in handheld devices

With the first handheld mobile device introduced in 1973 it became possible to make phone calls with a device portable by a human, without being restricted by wires. From then to this day, handheld devices, including phones and tablets, have changed dramatically to provide more functionalities. Beside their original purpose, i.e. voice communication, nowadays handheld devices offer wireless connectivity for a vast range of applications, with using a variety of communication standards. Short-range communication for transfer of data and connection to peripherals, near field communication for electronic wallet, Global Navigation Satellite System (GNSS) for navigation, and cellular long-range communication for transfer of voice and data over wide areas can be mentioned. The weight and size of these devices have been reduced to about 100 grams and the size of a palm of a hand.

To implement every communication standard a wireless transceiver is required. The inside of a modern mobile phone is shown in Fig. 1.1. Several transceivers (cellular transceiver, GNSS, WLAN and Bluetooth), are gathered in one small device to implement each of the standards. From the users' point of view, the simultaneous operation of these transceivers is highly desirable. For example during a phone call through a cellular network, the user may want to use a Bluetooth handsfree, he may want to acquire his position through GNSS, or look at his agenda stored in an online server. The combination of several transceivers, which is called a multimode transceiver, is required to implement these standards.

The mobility requirement necessities the handheld devices to rely on batteries as the energy source. The current trend shows that the power consumption of all devices is increasing faster than the capacity of the batteries. Hence minimizing the power consumption of the transceivers is of the utmost importance.

Fig. 1.2 shows a sample multimode transceiver in operation. The figure includes a Remote Transmitter (RTX), a Local Receiver (LRX), a Local Transmitter (LTX), and a remote receiver. The LRX and RTX belong to one communication standard and the LTX the remote receiver to another one. The RTX transmits a signal, shown in blue, which is received by the LRX antenna as the received desired signal, after propagation losses. At the same time the LTX transmits a signal, shown in red, to be received by the remote receiver. The LTX signal is partly received by the LRX antenna after a coupling loss, and induces a local interference. The distance between the LTX and LRX is dictated by the size of the handheld device and is typically a few centimeters. On the other hand the distance of the RTX and LRX can range from a few meters to a few kilometers. The propagation loss between a transmitter and receiver is proportional to the square of the distance between them. Hence the received signal by the LRX includes an interference which can be many orders of magnitude stronger than the desired received signal. The high level of this local interference compared to that of the desired signal is one of the main challenges in the implementation of a multimode transceiver. Owing to the extreme proximity of the LTX and LRX, the local interference is much stronger than interferences received from other devices, i.e. external interferences. Current techniques for mitigation of external interferences are not able to handle the local interference, thus severely limiting simultaneous operation. In the next section,

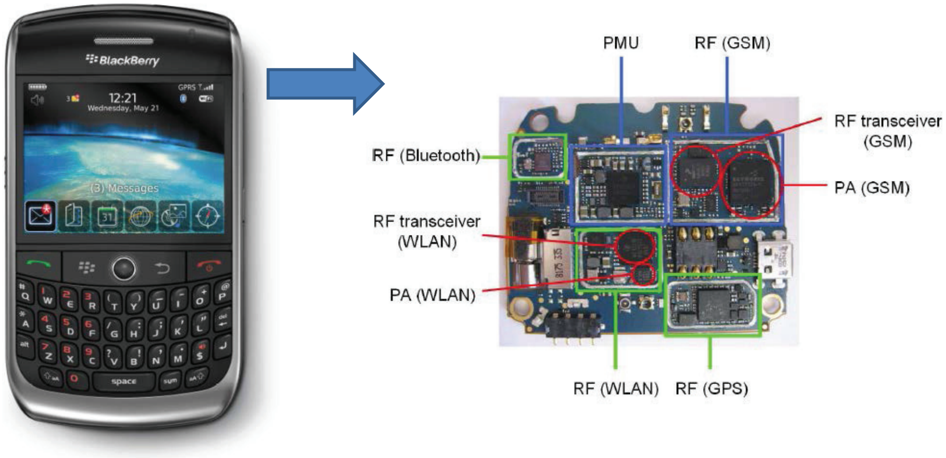

Figure 1.1: Inside view of a mobile phone.

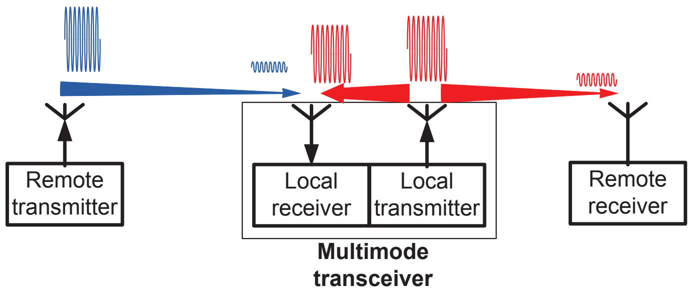

Figure 1.2: A multimode transceiver in operation.

we describe the impact of this strong interference on the LRX.

1.2 Local interference in local receiver

1.2.1 Receiver model

Fig. 1.3 shows a direct conversion receiver, which is a popular architecture for modern receiver design. Here in-phase and quadrature signals are shown with double lines. The combination of the desired signal and the interference is received by an antenna. The power spectral density of the received signal is shown and includes the desired signal and the local interference with center frequencies f_d

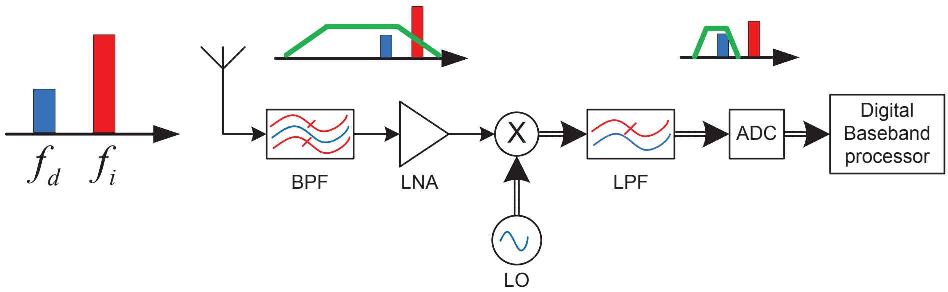

Figure 1.3: Direct conversion receiver

and f_i, respectively. The received signal is passed through a Band Pass Filter (BPF), which selects a frequency band of interest. The filtered signal is amplified by a Low Noise Amplifier (LNA) and is down-converted using a quadrature mixer, which is excited with a Local Oscillator (LO) that is locked to f_d. To select the frequency channel of the desired signal, the analogue baseband signal is filtered by a Low Pass Filter (LPF), and sampled and digitized by an Analogue to Digital Converter (ADC). Additional filtering and extracting the symbols transmitted by the RTX is performed in the digital baseband processor.

1.2.2 Interference classification

Three distinct scenarios can be considered based on the center frequency of the interference:
1-*Co-channel interference*: The interference is in the frequency channel of the desired signal. This is the most disruptive scenario and is generally prevented during standardization. Hence in this thesis we do not consider this scenario, and assume that the local interference and the desired signal do not have any spectral overlap.
2-*Co-band interference*: The interference is in the frequency band of the desired signal, although it is not co-channel. Typically, the co-band interference belongs to the same standard as the desired signal and it is an external interference. There are, however, cases like Bluetooth and WLAN that two standards share a frequency band and their simultaneous operation in one device is desired. Hence the co-band scenarios have some degree of importance for multimode operation. The BPF has no impact on the co-band interference and the receiver relies on low-pass filtering after down-conversion to filter out the interference.
3-*Out-of-band interference*: The interference is not in the band of the desired signal. This is the most common scenario for multimode operation. An out-of-band interference is suppressed by the BPF to some extent. Complete filtering of the interference is performed after down-conversion by the LPF or digital filters

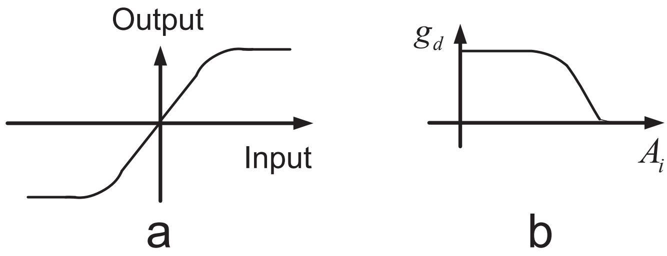

Figure 1.4: Input-output characteristics and weak signal gain versus envelope of a strong interference for a typical active component in the receiver FE

after the ADC.

1.2.3 Impact of a strong interference on the received signal

In principle, an interference which is not co-channel, can be completely suppressed by linear filtering. The BPF is meant to suppress the out-of-band interference. With the current technology, however, even after the BPF, the local interference can still be many orders of magnitude stronger than the desired signal. Moreover, the BPF becomes ineffective for a co-band interference or an interference in the transition band of the BPF. If the receiver Front-End (FE) is linear then the interference can be suppressed after down-conversion by the LPF or digital filtering. Active components of the FE, however, are linear only for a limited range of inputs. As shown in Fig. 1.4 a, the output eventually saturates as the input increases. Such a nonlinear IO characteristic leads to several undesirable effects:

E1- **Desensitization**: As the envelope A_i of the interference increases, the gain g_d of the weak desired signal decreases as shown in Fig. 1.4b, and eventually approaches zero. This excessive loss of gain leads to sensitivity loss of the receiver and is called desensitization [1]. Desensitization occurs for all interference scenarios in Section 1.2.2.

E2- **Cross-Modulation (CM) distortion:** It is seen in Fig. 1.4 b that there is a region where g_d depends on A_i. For a varying-envelope interference, variation of $A_i(t)$ leads to a variation of $g_d(A_i)$. Hence the modulation of the interference transfers to the modulation of the desired signal and leads to distortion of the desired signal. This form of distortion is called cross-modulation distortion. CM distortion occurs for all interference scenarios in Section 1.2.2.

E3-**Third-order intermodulation (IM3) product:** Suppose that, as shown in Fig. 1.5, besides the local interference an external interference with a center frequency f_e is present at the input of a nonlinear block with the characteristic

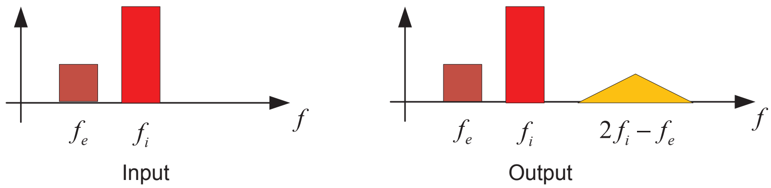

Figure 1.5: Generation of the IM3.

shown in Fig. 1.4. At the output of the block the third-order intermodulation (IM3) product of these two signals appears with a center frequency of $2f_i - f_e$. The power of this IM3 product approaches the power of the external interference as the local interference becomes stronger. The IM3 product can fall into the frequency channel of the desired signal, if f_e is close to $2f_i - f_d$. For out-of-band interference scenarios, f_e will be further out-of-band. Hence this effect is considerable only for co-band interference.

E4-**Spectral growth of the interference:** As the interference passes through the LRX nonlinear blocks, nonlinear distortion products of the interference are generated. The bandwidth of these products can be larger than the bandwidth B_i of the interference. If the frequency separation between the interference and the desired signal is small then these products can fall into the frequency channel of the desired signal. Hence this effect can only be considerable for co-band interference scenarios.

Besides the above effects, the following items can also affect the LRX reception. They originate from the LTX imperfections and the large coupling between the LTX and the LRX. Hence they will be present even for an exactly linear LRX FE.

E5-**Amplified LTX noise:** The LTX frond-end up-converts the baseband interference, amplifies and transmits it. At the same time the thermal noise at the input of the LTX front-end is amplified and is transmitted. Typically a bandpass filter is used before the LTX antenna to suppress the amplified noise and harmonics of the interference. For the co-band interference however, this bandpass filter has no effect. If the coupling between the LTX and LRX is large, the LTX noise can significantly affect the desired signal.

E6-**Spectral growth of the interference in the LTX power amplifier:** Similar to E4, owing to nonlinearity of the LTX Power Amplifier (PA), nonlinear products of the interference are generated. Similar to E4 this effect can only be considerable for co-band interference scenarios.

The above undesirable effects can severely disrupt the LRX reception. In the next section we look at state of the art approaches for mitigation of these effects. Since

E1,2 affects the received signal for all interference scenarios, the main focus of our work is on the mitigation of these two effects.

1.3 State of the art in interference mitigation

There are several approaches to mitigate the local interference.

1. It can be avoided by time multiplexing.

2. It can be suppressed in the analogue domain by linear filtering or by a nonlinearity as we will see in the next section.

3. It can be cancelled in the analogue domain by generating and subtracting a replica of the interference.

4. It can be filtered, cancelled, or its effect on the desired signal can be compensated in the digital domain.

Except for the first approach, these approaches are not mutually exclusive and may need to be combined to successfully mitigate the local interference. The digital mitigation approach is mainly a complementary approach and cannot mitigate desensitization. In this section we explore the above approaches, as found in the state of the art.

1.3.1 Time division multiplexing

The two conflicting standards can be time division multiplexed such that the RTX and LTX do not transmit at the same time. Such an approach is proposed in [2] to enable coexistence between Bluetooth and WLAN and in [3] to enable coexistence between LTE and Bluetooth, WLAN, and GNSS. This approach has two limitations:
1- it requires cooperation between two communication standards which is complex and is not yet a part of many standards,
2- it reduces the throughput of each standard by necessitating extra signaling and guard times.
Owing to these limitations, this approach is not commonly used.

1.3.2 Linear filtering

One may attempt to increase the dynamic range of the LRX FE to prevent E1-4, so that the LPF can suppress the interference. Unfortunately, to strongly increase the dynamic range for a certain technology and circuit topology, the power consumption of the FE circuits must be strongly increased [4]. Increasing the power consumption is highly undesirable, considering the limited energy supply of handheld devices.

1.3.3 Analogue cancellation of interference

By subtracting a replica of the received interference from the received signal, the interference can be cancelled while the desired signal remains unaffected. In principle, the cancellation can be done in the analogue or the digital domain. Digital cancellation, however, is not effective in mitigation of E1-6. Hence the cancellation must be done in an early stage of the LRX FE.

In multimode transceivers the received local interference originates from the locally known transmitted interference. The knowledge of the transmitted interference can be exploited for mitigation of the received interference. As shown in Fig. 1.6, a replica of the received interference at the LRX can be generated based on a linear model of the interference coupling path, shown with a bold line, and the transmitted interference as the input of this model. By subtracting this replica from the received signal in the analogue domain the local interference can be cancelled. The subtraction point in Fig. 1.6, is preferred to be before the active components of the LRX FE, i.e. after the LRX antenna or the BPF. Subtraction after the LNA however, may be explored with an aim to reduce the impact of added noise by cancellation [5]. If an exact model of the coupling path can be constructed this method can resolve E1-6. For this reason, this method is widely explored [5–10].

It must be considered that mitigation of E1-4 and E5-6 requires cancellation over both the frequency channels of the interference and desired signal, respectively. Hence the path model must be accurate over both frequency channels, otherwise mitigation of E1-4 may lead to aggravation of E5-6, or the other way around. Providing such an accuracy becomes more difficult as frequency separation $f_i - f_d$ between the desired signal and interference, or their bandwidths, increase.

The interference coupling path is subject to environmental changes. For example, the presence and movement of a user's hand changes the characteristics of the coupling path. Hence the path model should be adaptive. Such an adaptive model is shown in Fig. 1.7, where a_i are adaptable complex gains and τ_i are

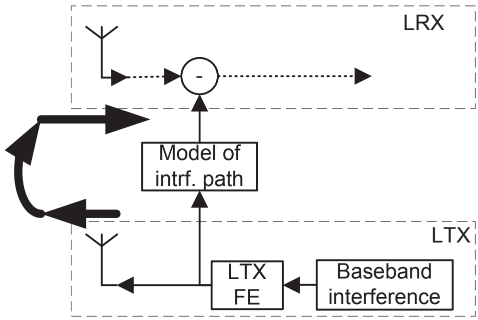

Figure 1.6: Analogue cancellation of the local interference

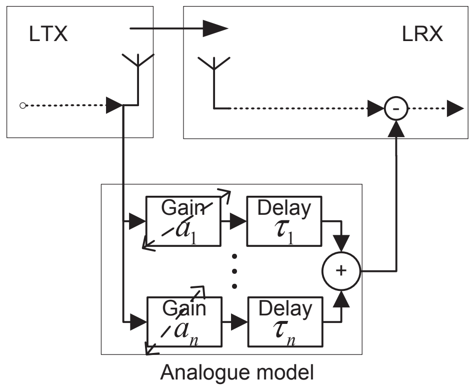

Figure 1.7: Adaptive analogue model

fixed delays. Our study in Appendix I shows that for wideband interferences, a multi-path model is required to achieve an adequate interference cancellation. In practice, however, even a single-path model requires a significant analog complexity and power consumption. In particular, implementing long delays (in the order of several nanoseconds) in an integrated circuit can be difficult. Hence in [5,7,9,10] only a single-path model without a delay element is implemented which suffices only to cancel the interference in a very narrow band. To improve the interference cancellation in [7] and [10], the coupling path is emulated using a bandpass filter or the input of the model is collected by an antenna similar to the LRX antenna. These two methods, however, are not suitable for mobile devices as they require more external components and also are not flexible (must be physically modified for each design).

In [11] the performance of a single-path model without delay or emulating the coupling path is studied. The interference is suppressed by only 10-20 dB, depending on the bandwidth of the interference. Such a single-path model not only fails to suppress the interference such that E1-4 are prevented, it even aggravates E4-5, since the model is not accurate enough over frequency channel of the interference nor that of the desired signal. A multipath (2-path) model approach is proposed in [6] to achieve cancellation at both f_i and f_d. The complexity and cost of such a multipath model makes it unsuitable for handheld devices.

Another limitation of the analog cancellation method is difficulty of its adaptation. For a reference-aided adaptation, analog circuits must be implemented to correlate the transmitted interference with the residual interference after the cancellation point [5]. Such an adaptation would increase the complexity further. Hence in [7] a search method over a_1 is used to minimize the energy of the residual interference. Such a search method, however, becomes increasingly slow when the number of paths increases.

Let us assume that an exact model of the coupling path can be constructed. For such an exact model E1-6 are completely resolved. Even such an exact model leads to introduction of an additional additive noise generated by the model itself. Another problem is the nonlinearity of the analogue circuits in the model. Even a small nonlinearity will limit the interference cancellation.

1.3.4 Digital compensation

The key motivation for digital compensation is the continuous reduction of cost and power consumption of digital signal processing, governed by Moore's law [12]. Hence by shifting complexity from the analogue to the digital domain, the cost and power consumption of the transceiver can be decreased. Digital compensation and cancellation techniques can be used to mitigate some of the effects in E1-6. For example cross-modulation or intermodulation components can be compensated in the digital domain [13] [14]. These methods, however, cannot mitigate the loss of sensitivity which was mentioned in E1. Therefore, to mitigate the local interference these methods can be used in conjunction with methods that mitigate the interference in the analogue domain, not as a stand-alone solution. Some of these methods require ADCs with higher sample rates or a larger number of bits. The power consumption of ADCs generally increases at least linearly with the sample rate and exponentially with the number of bits [15].

1.4 Proposed hybrid approach

As we saw in Section 1.2.3, as the level of interference increases the desired signal experiences cross-modulation and eventually the receiver becomes desensitized. To prevent desensitization the local interference must be mitigated in an early stage of the LRX FE. In this thesis, we propose to use an adaptive memoryless nonlinearity in the LRX FE to suppress the local interference and prevent desensitization. Application of this nonlinearity leads to introduction of cross-modulation distortion which is compensated digitally. A situation can be encountered where the interference is weak enough to be handled by the LRX FE without desensitization and strong enough to cause cross-modulation. In this situation the nonlinearity will be disabled and only the digital compensation of the cross-modulation is used. As outlined in the remainder of this thesis, our analysis, simulations, and experimental results show that the proposed hybrid approach can substantially suppress the local interference without an excessive power consumption.

1.4.1 Nonlinear Interference Suppressor

An interference much stronger than the desired signal can be suppressed by passing the received signal through a special memoryless nonlinearity [16]. This Nonlinear Interference Suppressor (NIS) can be built by adding outputs of a linear amplifier (with gain of $-c$) and a limiter with an adaptable limiting amplitude $l(t)$ as shown in Fig. 1.8. When passing through the hard limiter, the weak desired signal experiences a smaller gain than the strong interfering signal. The amplifier, on the other hand, has the same gain for both weak and strong signals. By adapting $l(t)$ proportional to the envelope of the received interference, the gains of the limiter and amplifier for the strong interference can be made equal but of opposite sign. Thus, the interference can be suppressed while the weak desired signal is passed with a gain of $\frac{-c}{2}$.

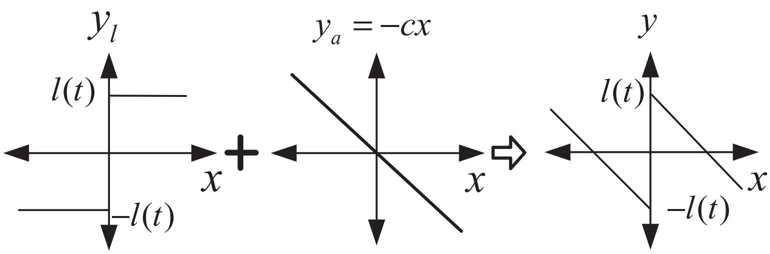

Figure 1.8: NIS input-output characteristic.

In the multimode transceiver the baseband transmitted interference is available locally. As shown in Fig. 1.9, using a discrete-time baseband model of the interference coupling path, shown with the tick line, the envelope of the receiver interference can be obtained digitally. The coupling path is subject to environmental changes. Hence the model must be adapted during the receiver operation to track these changes. The residual interference at the NIS output is measured using a mixer with the NIS input as its local oscillator port. A closed-loop adaptation method is designed that adapts the model such that the power of the residual interference is minimized.

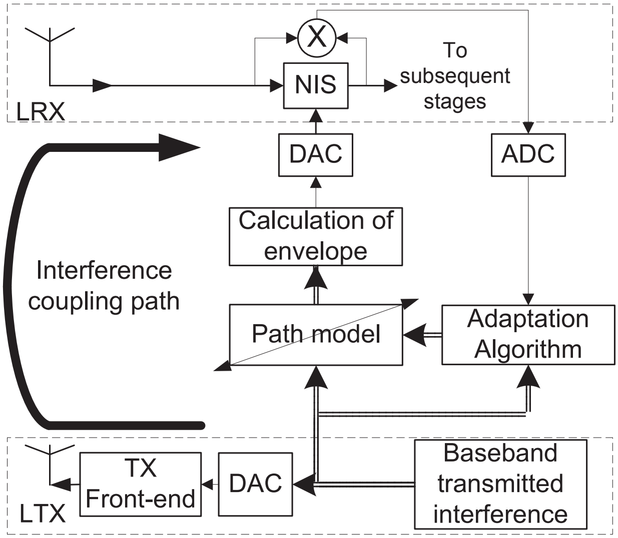

Figure 1.9: NIS and its adaptation in the multimode transceiver.

1.4.2 Digital compensation of CM distortion

In practice an analogue circuit can only approximate an ideal characteristic. For example the ideal NIS as shown in Fig. 1.8) has a linear characteristic for the weak desired signal. Another example is a typical receiver front-end. Although it is desired to be linear, it shows nonlinear effects. When the combination of the strong interference and the weak desired signal passes through a block with a nonlinear characteristic, amplitude modulation of the interference is transferred to modulation of the desired signal, resulting in CM distortion. In this thesis, in two chapters the CM distortion is encountered, firstly, in a typical receiver without the NIS (Chapter 2), and secondly, in the receiver with a practical NIS circuit(Chapter 5). The CM distortion in these two cases can be avoided by increasing the linearity and perfecting the NIS circuit, respectively. Alternatively, the CM distortion can be digitally compensated by identifying a model of the nonlinearity and estimating the envelope of the interference at the input of the nonlinearity. Considering the continuous increase of digital computation power governed by Moore's law, shifting the complexity from the analogue to the digital domain is advantageous in terms of circuit complexity and power consumption.

In Chapter 2, we study the case that the interference is strong enough to cause CM distortion, although it is not so strong that it leads to desensitization. In this case a weakly nonlinear model, i.e. a third-order polynomial, can be used for the receiver front-end. A method is proposed to compensate the CM distortion by estimating the envelope of the received interference and the parameter of the model. In Chapter 5, the CM distortion is the result of the strong nonlinear effect of the NIS circuit. For this type of nonlinearity, an efficient way to model the dependency of the envelope and phase of the desired signal to envelope of the interference is to use a look-up table. The look-up table is measured during a calibration stage. Since the envelope of the interference is already estimated to adapt the NIS, by using the look-up table the CM distortion is compensated.

1.4.3 Other areas of application for the NIS

Similar to multimode operation, there are other applications where a strong local interference disrupts operation of a local receiver.

- Frequency Division Duplex (FDD) transceivers: In FDD transceivers the local transmitter of a given communication standard induces an interference on the local receiver of the same standard. Typically a duplexer filter is used to isolate the local transmitter from the local receiver. The duplexer filter is realized using surface acoustic wave or ceramic technology as external components. These are expensive and have fixed frequencies. Hence if a transceiver is meant to operate in several frequency bands a bank of duplexers should be used. Alternatively, a combination of a circulator and the NIS can be used to achieve isolation between the local transmitter and receiver.

- Frequency Modulated Continuous Wave (FMCW) radar: In FMCW radar the transmitted signal is also received by the radar receiver and can be many order of magnitudes stronger than the echoes received from targets.

- In basestations several transceivers of different standards are placed in close proximity. The limitations regarding the size and power consumption for the basestation, however, are much more relaxed compared to handheld devices.

- Radio Frequency Identification (RFID) readers: In RFID systems a transceiver, called reader, powers and communicates with tags that are within range. To maintain the flow of power from the reader to tags and enable communication with multiple tags the reader operates in full duplex. Owing to insufficient isolation between the transmitter and receiver of the reader, the transmitted signal induces interference in the receiver that is many orders of magnitude stronger than the signal reflected by the tags. Currently, to maintain the receiver sensitivity in the presence of such a strong interference, a receiver with a large dynamic range and high power consumption is used.

1.5 Outline and contribution of this thesis

In this section we present a short summary of the content and contribution of each chapter of the rest of the thesis.

In Chapter 2, we analyze key distortion products which are generated in a receiver front-end having a memoryless nonlinear characteristic. When the combination of the strong interference and the weak desired signal experiences any nonlinearities in the receiver front-end, distortion products are generated. One of these is Cross-Modulation (CM) distortion, where the amplitude modulation of the interference transfers to modulation of the desired signal. CM distortion is particularly problematic, since it occurs independent of the frequency separation of the desired signal and the interference. In this thesis we encounter CM distortion in two situations, namely without and with NIS. The first situation is of interest since the interference can be weak enough to be handled without NIS yet strong enough to cause CM distortion. In this situation the CM distortion can be compensated digitally. In Chapter 2, we propose a fully digital compensation method that exploits the local availability of the baseband interference to avoid the complexity and power dissipation of additional analogue circuits. The baseband interference is used as the reference for estimation and then compensation of the CM distortion.

Although the proposed method in Chapter 2 is able to mitigate the CM distortion to some extent, it cannot alleviate the desensitization. In Chapter 3, we propose to use an adaptive Nonlinear Interference Suppressor (NIS), with the aim to prevent desensitization by suppressing the interference at an early stage of the receiver front-end. In previous work the NIS was only used for constant-envelope interference. For interference with arbitrary envelope variations, firstly, we derive an optimal adaptation signal for the NIS that yields complete suppression of the interference in the absence of the desired signal. For this optimal adaptation signal, residual distortion products of the NIS are identified which are not present in the case of a constant-envelope interference. The impact of these products on the received desired signal is analyzed and rules of thumb are given to specify conditions for which adequate interference suppression is combined with negligible distortion. We show that these conditions are met in most cases of practical interest.

The optimal adaptation signal is proportional to the envelope of the received interference at the NIS input. A key feature in the multimode transceiver is the local availability of the interference source. Using a baseband linear model of the interference coupling path, from the local transmitter to the local receiver, the adaptation signal can be obtained digitally. In Chapter 4, we quantify the required accuracy for the adaptation signal to properly suppress the interference while keeping the degradation of the receiver Symbol Error Rate (SER) negligible. To provide the required accuracy, we propose a closed-loop method to dynamically adapt the path model such that the power of the residual interference at the output of the NIS is minimized. This method uses the baseband interference as a reference in order to combine simplicity with high accuracy and high speed. Our analysis and simulations show that the optimal adaptation signal can be estimated with sufficient accuracy, such that the interference is strongly suppressed while a SER close to that of an exactly linear receiver is achieved.

In Chapters 3 and 4, idealized models of the NIS and adaptation circuits are used to analyze the performance afforded by the NIS. In Chapter 5, we present experimental results of a multimode transceiver test bed that uses the mixed-signal integrated NIS circuit designed in [17]. The main circuit imperfections that limit the NIS performance are identified. Simple imperfection models are described that explain the experimental results. Based on these models, the NIS adaptation method is extended with simple digital compensation and calibration techniques that unlock the full interference suppression potential of the NIS circuit. Furthermore, a low-complexity digital compensation method is proposed for the CM distortion that is caused by the imperfections. Successful operation of the test bed suggests that the NIS approach is practical and attractive for multimode transceivers.

Concluding remarks and suggestions for future work are collected in Chapter 6. The analysis, simulation and experimental results in this thesis show that the NIS can achieve substantial interference suppression at attractive complexity and power dissipation, and that the residual distortion products can be digitally compensated with a low complexity. Both fundamental and practical limitations of the proposed approach are identified, and directions for future improvements are sketched.

1.6 Publications

The research work of this thesis resulted in the following publications.

1.6.1 Journal publications

H. Habibi, E.J.G. Janssen, Wu Yan, D. Milosevic, P.G.M. Baltus, J.W.M. Bergmans, ”Experimental evaluation of an Adaptive Nonlinear Interference Suppressor for Multimode Transceivers”, To be published in *IEEE Journal on Emerging and Selected Topics in Circuits and Systems*, Dec. 2013.

H. Habibi, E.J.G. Janssen, Wu Yan, P.G.M. Baltus, J.W.M. Bergmans, "Closed-loop Adaptation of a Nonlinear Interference Suppressor for multimode Transceivers", Submitted to *IEEE Transaction on Vehicular Technology.*

H. Habibi, E.J.G. Janssen, Wu Yan, P.G.M. Baltus, J.W.M. Bergmans, "System Study on Nonlinear Suppression of Varying-Envelope Local Interference in Multimode Transceivers", *Submitted to International Journal of Electronics and Communications.*

H. Habibi, E.J.G. Janssen, Wu Yan, J.W.M. Bergmans, "Digital Compensation of Cross-Modulation Distortion in Multimode Transceivers" *IET communication, pp. 1724-1733, Aug. 2012.*

1.6.2 Conference proceedings

H. Habibi, P.E. Ling, E.J.G. Janssen, Wu Yan, J.W.M. Bergmans, P.G.M. Baltus, "Adaptive nonlinear interference suppressor for cognitive radio applications", *Proceedings of Workshop on Cognitive Radio*, Kista, Sweden, June, 2013.

H. Habibi, E.J.G. Janssen, Wu Yan, D. Milosevic, J.W.M. Bergmans, P.G.M. Baltus, "Suppression of Constant Modulus Interference in Multimode Transceivers Using an Adaptive Nonlinear Circuit". *Proceedings of NASA/ESA Conference on Adaptive Hardware and Systems (AHS-2013), Turin, Italy June, 2013.*

H. Habibi, E.J.G. Janssen, Wu Yan, P.G.M. Baltus, J.W.M. Bergmans, "Nonlinear Interference Suppressor for Varying-Envelope Local Interference in multimode transceivers". *Proceedings of 34th Symposium on Information Theory in the Benelux, Leuven, Belgium, May, 2013.*

H. Habibi, E.J.G. Janssen, Wu Yan, P.G.M. Baltus, J.W.M. Bergmans, "Closed-loop Adaptation of a Nonlinear Interference Suppressor for Local Interference in Multimode Transceivers". *Proceedings of 34th Symposium on Information Theory in the Benelux, Leuven, Belgium, May, 2013.*

H. Habibi, E.J.G. Janssen, Wu Yan, J.W.M. Bergmans, P.G.M. Baltus, "Suppression of constant modulus interference in multimode transceivers by closed-loop tuning of a nonlinear circuit". *Proceedings of IEEE 75th Vehicular Technology Conference, Yokohama, Japan, May, 2012.*

H. Habibi, E.J.G. Janssen, Wu Yan, J.W.M. Bergmans, "Digital Compensation of Cross-Modulation Distortion in Multimode Transceivers". *Proceedings of IEEE 75th Vehicular Technology Conference, Yokohama, Japan, May, 2012.*

E.J.G. Janssen, H. Habibi, D. Milosevic, P.G.M. Baltus and A.H.M van Roermund, "Smart Self-Interference Suppression by Exploiting a Nonlinearity," *Invited paper in 22nd Workshop on Advances in Analog Circuit Design (AACD)*, Grenoble, France, April, 2013.

E.J.G. Janssen, H. Habibi, D. Milosevic, P.G.M. Baltus, A.H.M. van Roermund, "Frequency-independent smart interference suppression for multi-standard transceivers", *Proceedings of the 42st European Microwave Conference (EuMC)*, Amsterdam, The Netherlands, November, 2012.

E.J.G. Janssen, H. Habibi, D. Milosevic, P.G.M. Baltus, A.H.M. van Roermund, "Digital hardware resources for steering a nonlinear interference suppressor". *Proceedings of the 19th International Conference Mixed Design of Integrated Circuits and Systems (MIXDES), Warsaw, Poland, May 2012.*

E.J.G. Janssen, H. Habibi, D. Milosevic, P.G.M. Baltus, "Modeling and Analysis of Nonlinearities and Bandwidth Limitations in RF Receivers". *Proceeding of IEEE International Symposium on Circuits and Systems (ISCAS), Rio de Janeiro, Brazil, May, 2011.*

Appendix I:Single-branch analogue cancellation

In this appendix firstly we present the frequency response of the interference coupling path from the LTX to the LRX. Secondly, we analyze the performance of analogue cancelation using a single-branch model of the path. The simple investigation performed in this appendix, clarifies the limitations of the analogue cancellation.

System setup

A simplified diagram of the multimode transceiver including a LTX and a LRX is shown in Fig. 1.10. we have two objectives to study the frequency response $H_s(f) = \frac{V_r(f)}{V_t(f)}$ of the antenna coupling system. Firstly, $|H_s(f)|^2$ shows the power of the interference that is coupled from the LTX to the LRX. Secondly, we use this frequency response to study the performance of the analogue cancellation approach, which was described in Section 1.3.3. In this appendix, we consider the simple system of Fig. 1.10 with simple antennas for the LTX and the LRX. Absence of highly frequency-selective components in Fig. 1.10 leads to favorable results for analogue cancellation approach compared to a practical multimode transceiver, where the antennas are designed to achieve more frequency selectivity and a filter is used after the LRX antenna. The performance of the cancellation attained in this appendix, however, can be considered as an upper bound on the performance of the cancellation approach. For the LTX and the LRX we consider frequency

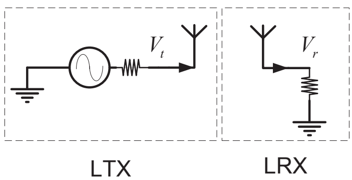

Figure 1.10: A simplified block diagram of LTX and LRX.

bands of 1.9 to 2 GHz and 2.4 to 2.5 GHz, respectively. Planar dipole antennas are used for both the LTX and the LRX. The distance d between the antennas is assumed to be 3, 5, or 10 cm. Scattering parameters S_{11} of both antennas are shown in Fig. 1.11 for $d = 5$ cm. The LTX and LRX antenna are tuned to have minimum reflections at 1.95 GHz and 2.45 GHz, repectively. For $d = 5$ cm, however, a slight deviation in S_{11} is observed, owing to the mutual coupling between the antennas. For $d = 3$,5 ,10 cm, the S-parameters of the antenna system is calculated using CST simulation software. Using the S-parameters, $H_s(f) = \frac{V_r(f)}{V_t(f)}$

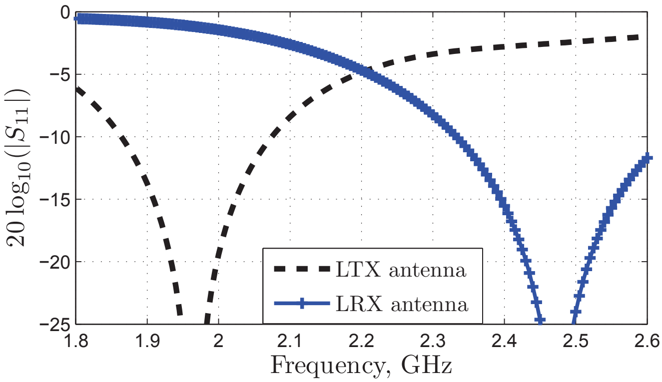

Figure 1.11: Scattering parameters S_{11} of LTX and LRX antenna.

can be calculated[1]. The amplitude response $10\log_{10}(|H_s|^2)$, shown in Fig. 1.12, indicates the amount of power that is transferred from the LTX to the LRX versus frequency. In two frequency ranges $|H_s|$ is of interest.

1- *In the band from 1.9 to 2 GHz*: it indicates the amount of out-of-band interference received by the LRX from the LTX. For example if the LTX transmits at 30 dBm, then at the LRX an interference of about 13 dBm is received, for $d = 5$ cm. Such a strong interference can lead to desensitization of the receiver front-end if it is not suppressed sufficiently.

2-*In the band from 2.4 to 2.5 Ghz*: it indicates the amount of in-band interference. The amplified thermal noise accompanied by the LTX can be 50 dB stronger than the thermal noise floor. A 20 dB coupling loss between LTX and LRX in this band, as seen in Fig. 1.12, leads to an in-band noise which can be 30 dB stronger than the LRX input thermal noise. Hence the transmitted noise by the LTX can significantly disrupt the LRX.

At a first sight, the analogue interference cancellation seems to provide a solution for both out-of-band interference and in-band noise. This would be possible if an analogue model of H_s could be constructed with enough accuracy over both frequency bands of the LTX transmission and the LRX reception. In principle an analogue model with several branches, as shown in Fig. 1.13, can be used to construct $H_s(f)$. As discussed in Section 1.3.3, owing to complexity of a multi-branch analogue model, most works in the state of the art consider a single-branch variant of the model in Fig. 1.13, without any delay element. In the following sections, we analyze the performance of the single-branch model with and without a delay element.

[1] An impedance of 50 Ω is assumed for both terminations

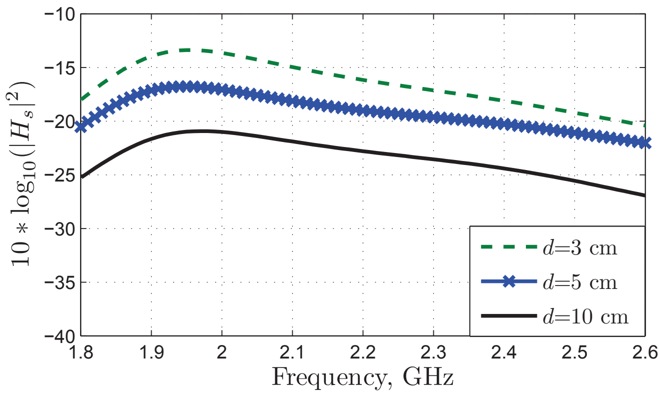

Figure 1.12: Frequency response of the system for different spacing between antennas.

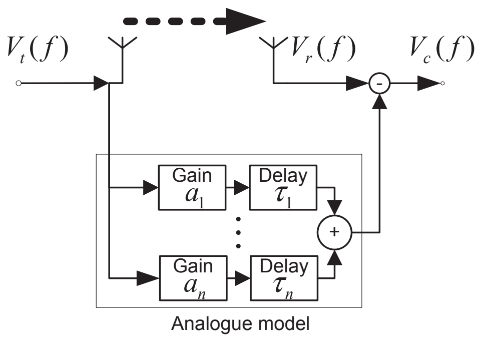

Figure 1.13: Interference cancellation using an analogue model of $H_s(f)$.

Single-branch model without delay

A single-branch variant of Fig. 1.13, without a delay element is shown in Fig. 1.14. To make the cancellation possible, a_1 must be complex-valued. A complex-valued scaling can be implemented by combining a variable gain amplifier and a vector modulator. By adapting a_1 the frequency response of the cancellation system $H_c(f, a_1) = \frac{V_c(f)}{V_t(f)}$ can be nulled at a single frequency. Fig. 1.15 shows $H_c(f, a_1)$ and compares it with $H_s(f)$, when a_1 is tuned to obtain a null at 1.95 GHz. We see that a narrowband null is attained at 1.95 GHz at the expense of an increased coupling of the LTX noise at the frequency range of 2.4-2.5 GHz. To measure effectiveness of the cancellation system we define Interference Cancellation (IC)

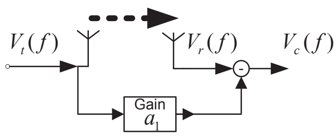

Figure 1.14: Cancellation using a single-branch without delay.

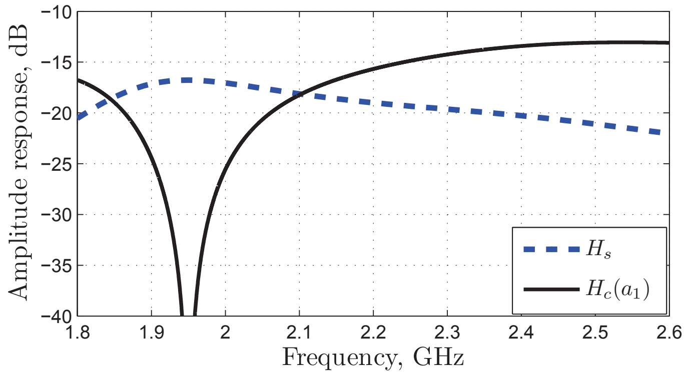

Figure 1.15: Frequency response of the system before and after cancellation.

for a center frequency f_i and bandwidth B_i of the interference as:

$$\mathrm{IC} = \frac{\int_{f_i-\frac{B_i}{2}}^{f_i+\frac{B_i}{2}} |H_s(f)|^2}{\int_{f_i-\frac{B_i}{2}}^{f_i+\frac{B_i}{2}} |H_c(f)|^2}. \tag{1.1}$$

For an interference with a flat spectrum over $[f_i - \frac{B_i}{2},\ f_i + \frac{B_i}{2}]$, IC indicates the ratio of the interference power before cancellation to the interference power after cancellation. For f_i in range of 1.9 to 2 GHz, IC is maximized by adapting a_1. The maximum of IC versus f_i for B_i=20 MHz is shown in Fig. 1.16. We see that an IC of about 25-27 dB can be attained.

Single-branch model with adaptable complex-valued gain and adaptable delay

The group delay of the system in Fig. 1.10 is shown in Fig. 1.17. We see a group delay in the order of 1 ns, which the model without the delay cannot handle. To improve the performance of the cancellation, in this section we consider a single-branch model with adaptable a_1 and τ_1. Fig. 1.18 shows $H_c(f, a_1, \tau_1)$ when a_1 and τ_1 are tuned to obtain a null at 1.95 GHz. For comparison $H_s(f)$ and $H_c(f, a_1)$ are

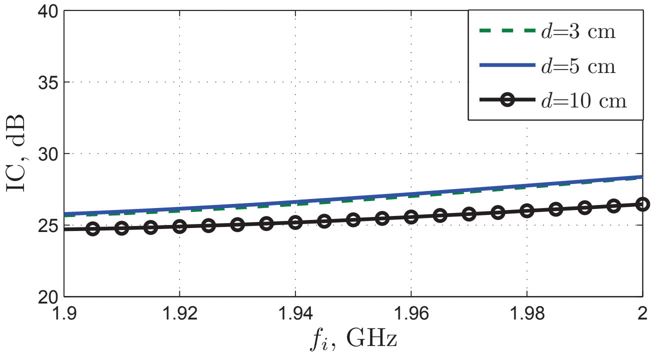

Figure 1.16: Interference cancellation with a single complex-valued gain, B_i =20 MHz and d=5 cm.

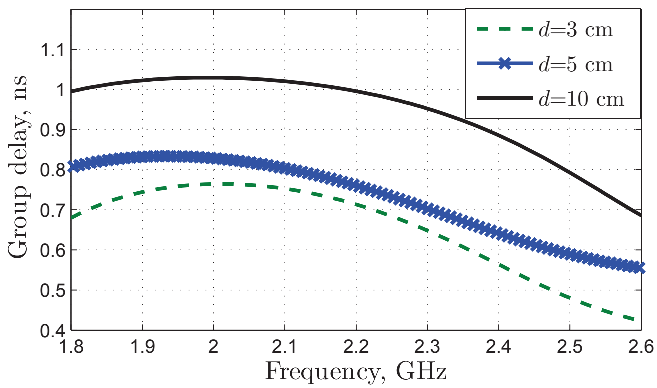

Figure 1.17: Group delay of the system in Fig. 1.10.

also shown. We see that although the null for $H_c(f, a_1, \tau_1)$ is widened compared to $H_c(f, a_1)$, the coupling across the band from 2.4 to 2.5 GHz is still increased by about 10 dB. For f_i in the range of 1.9 to 2 GHz, IC is maximized by adapting a_1 and τ_1. The maximum of IC versus f_i for B_i=20 MHz is shown in Fig. 1.19. We see that an IC of better than 40 dB can be attained.

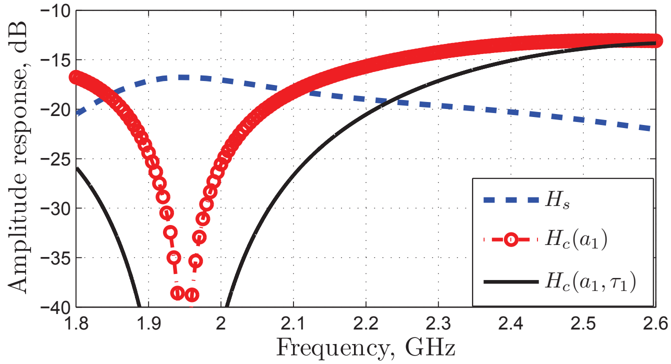

Figure 1.18: Amplitude response before and after cancellation with adaptable gain and delay.

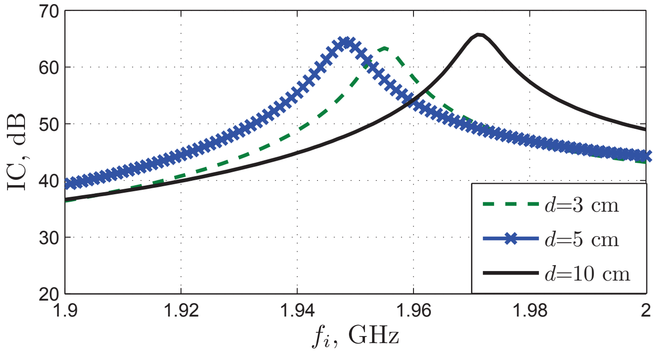

Figure 1.19: Interference cancellation with an adaptable gain and delay, B_i =20 MHz and d=5 cm.

Chapter 2

Digital Compensation of Cross-Modulation Distortion in Multimode Transceivers[1]

2.1 Abstract

In a multimode transceiver, several communication standards may be active at the same time. Due to the small size of the transceiver, the transmitter for one standard induces a large interference on the receiver for another one. When this large interference passes through the inherently nonlinear receiver Front-End (FE), distortion products are generated. Among these products, the Cross-Modulation (CM) product is the most problematic one, as it always has the same center frequency as the desired signal. Increasing the FE linearity to lower the CM distortion leads to unacceptable power consumption for a handheld device. Considering the continuous increase of digital computation power governed by Moore's law an attractive alternative approach is to digitally compensate for the CM distortion. An existing solution to compensate for the CM distortion is tailored to single-mode transceivers and requires an auxiliary FE. By using the locally available transmitted interference in the multimode transceiver, we propose a CM compensation method which requires no additional analog hardware. Hence the power consumption and complexity of the multimode transceiver can be reduced significantly. The simulation results demonstrate that the proposed method can lower distortion to

[1]This chapter is reproduced from the paper published as H. Habibi, E.J.G. Janssen, Wu Yan, J.W.M. Bergmans, "Digital Compensation of Cross-Modulation Distortion in Multimode Transceivers", *IET communication*, pp. 1724-1733, Aug. 2012.

a negligible amount at realistic interference levels.

2.2 Introduction

The communication features of handheld devices have been increasing rapidly in the past years. Some of the possible communication standards that may be supported by a handheld device are GSM, CDMA, WLAN, WiMAX, Bluetooth, and GPS. To implement these standards, a combinations of several transceivers is required which is called a multimode transceiver [18]. In a multimode transceiver, several standards may be active at the same time.

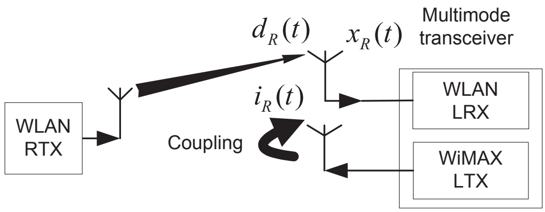

Figure 2.1: A sample scenario in a multi-mode transceiver.

Fig. 2.1 shows a sample scenario which includes a Remote WLAN Transmitter (RTX), a Local WLAN receiver (LRX), and a Local WiMAX Transmitter (LTX). The RTX transmits a WLAN signal with a carrier frequency f_d in the range of 2400-2483 MHz. This signal passes through a communication channel and is received by the LRX antenna as the received desired signal $d_R(t)$. At the same time the LTX transmits a WiMAX signal with a carrier frequency f_i in the range of 2496-2690 MHz, which is partly received by the LRX antenna after a coupling loss and induces an interferer $i_R(t)$. The coupling loss between transceivers in a multimode transceiver is typically between 10 to 30 dB [19]. The LTX output power can be as high as 23 dBm while the LRX sensitivity can be as low as -83 dBm [20]. Hence the received signal $x_R(t)$ includes both $d_R(t)$ and $i_R(t)$ where the power of $i_R(t)$ can be 96 dB larger than that of $d_R(t)$. The high level of $i_R(t)$ compared to that of $d_R(t)$ is one of the main challenges in the implementation of a multimode transceiver.

The direct conversion receiver architecture is a popular choice for implementation in integrated circuits. Fig. 2.2 shows such a receiver tuned to a center frequency f_d. The received signal $x_R(t)$ is passed through a Band Pass filter (BPF) which limits the input frequency range to frequency band of the standard. The BPF suppresses $i_R(t)$ to some extent. However the BPF suppression is limited to about 0-40 dB depending on the frequency separation between $i_R(t)$ and $d_R(t)$ (0 dB for standards that share the same frequency band). Hence the BPF output $x_B(t)$

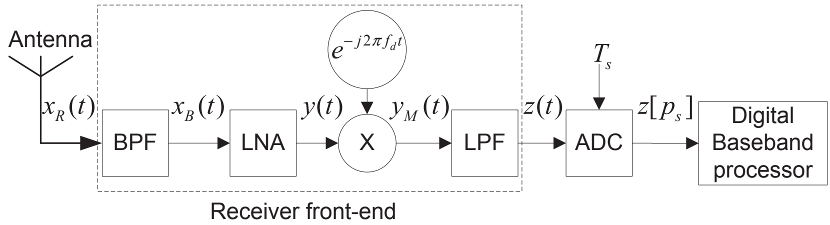

Figure 2.2: Direct conversion receiver.

includes the combination of $d_B(t)$ and $i_B(t)$, which are the BPF outputs with $d_R(t)$ and $i_R(t)$ as inputs, respectively. A Low Noise Amplifier (LNA) amplifies $x_B(t)$ and the amplified signal $y(t)$ is down-converted to zero frequency by a quadrature mixer. The frequency of the local oscillator of this mixer is f_d. Complex-valued output $y_M(t)$ of the mixer is filtered by a Low Pass Filter (LPF) to select a desired frequency channel. The LPF complex-valued output $z(t)$ is sampled by an Analog to Digital Converter (ADC) with sampling period of T_s seconds. The ADC output $z[p_s]$ is processed in a digital baseband processor to extract the transmitted information. The symbol p_s is used for the indices that belong to the clock domain T_s.

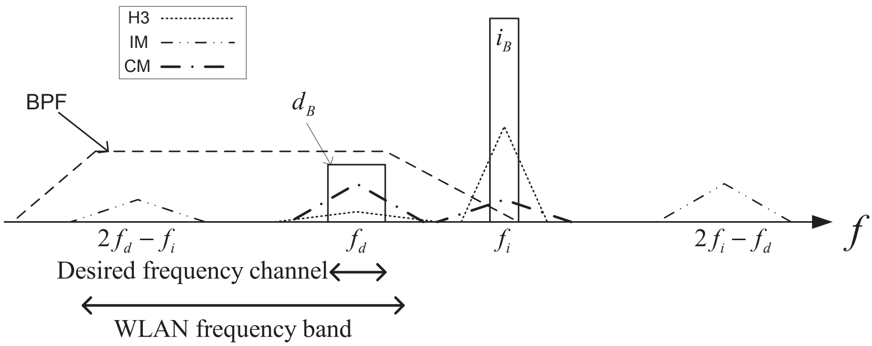

Figure 2.3: Power spectrum of $y(t)$, illustrating the nonlinear effect of the LNA.

Since $i_R(t)$ does not have any spectral overlap with $d_R(t)$, for an exactly linear Front-End (FE), $i_R(t)$ can be filtered out after down-conversion by the LPF without any undesirable effect. However in a practical receiver, LNA, mixer and other active circuits exhibit a nonlinear behavior for large input signals. When the combination of $d_B(t)$ and $i_B(t)$ passes through these circuits, this nonlinear behavior leads to generation of nonlinear distortion products. This nonlinear behavior is commonly modeled by a third-order polynomial [21]. Fig. 2.3 shows the power spectrum of $y(t)$ where the LNA is modeled by a third-order polynomial. The WLAN signal $d_B(t)$, centered at the desired frequency channel, and the WiMAX signal $i_B(t)$, beside the WLAN frequency band, are shown with rectangles. Because of the limited suppression of the BPF, the power of $i_B(t)$ can be much higher than that of $d_B(t)$. The distortion products are shown with triangles which indicate the bandwidth growth resulting from cross-multiplication of signals. The products centered at $3f_d$, $3f_i$, $2f_i + f_d$ and $2f_d + f_i$ will be filtered out by the LPF, hence they are not shown. As we see $y(t)$ includes the following distortion products:

- Harmonic (H3) products: Generated from third-order harmonics of $d_B(t)$ and $i_B(t)$ and located at center frequencies of f_d,f_i,$3f_d$ and $3f_i$.

- Intermodulation (IM) products: Generated by multiplication of $d_B(t)$ and $i_B(t)$ with center frequencies of $2f_d \pm f_i$ and $2f_i \pm f_d$.

- Cross-modulation (CM) products: Generated by multiplication of $d_B(t)$ and $i_B(t)$ with center frequencies of f_d and f_i.

For most standards, distortion products at f_i, $2f_i - f_d$ and $2f_d - f_i$ do not have any spectral overlap with $d_B(t)$ and they can be filtered out by the LPF. The H3 product at f_d is the response of the nonlinearity to $d_B(t)$ as input. By proper design of the receiver FE the power of this product can be kept negligible compared to the power of $d_B(t)$. On the other hand the power of the CM product at f_d depends on the power of $i_B(t)$ and can be large enough to degrade the receiver performance significantly [13]. Hence in this paper we focus on the compensation of distortion caused by the CM product presence. In the rest of the paper, the CM product at f_d will be referred to as the CM product and the distortion caused by the presence of the CM product will be referred to as CM distortion.

To decrease the power of distortion products, linearity of the FE circuits can be increased. To increase the linearity for a certain input-referred noise, technology and circuit topology, the power consumption of circuits must be increased [4]. However increasing the power consumption is highly undesirable, considering the limited energy supply of handheld devices [22].

According to Moore's law, the number of transistors on a certain surface of silicon is doubling every two years which results in continuous price reduction of digital circuits [12]. Hence a potentially attractive approach is to digitally compensate for the receiver FE nonlinearities. Although the power consumption and chip area of the digital section will be increased, the total power consumption and chip area can be reduced compared to the solution based on increasing the FE linearity.

An example of digital compensation is given in [23] where harmonics and IM products are digitally canceled while the CM distortion is left uncompensated. In [13] a technique is reported to compensate for the CM distortion in single-mode transceivers. As illustrated in Fig. 2.4a, two FEs and two ADCs are used. The main FE and ADC capture the combination of the desired signal plus the

CM product in the desired frequency channel. At the same time an auxiliary FE (tuned to f_i) and ADC capture the received interferer. Samples of the received interference and pilot symbols of the desired signal are processed together to estimate and compensate for the nonlinear distortion and communication channel of the desired signal at the same time.

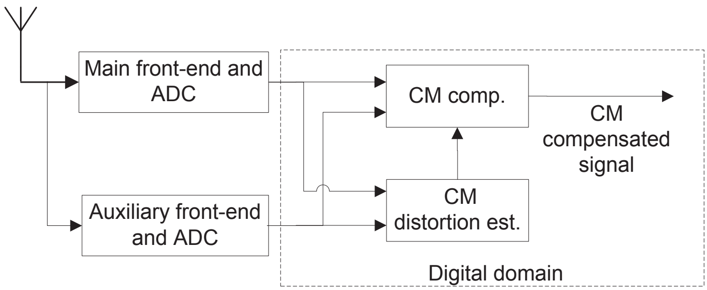

(a) Compensation scheme in [13].

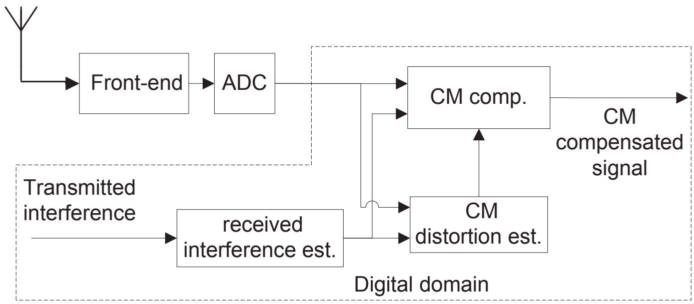

(b) Proposed compensation scheme for the multimode transceiver.

Figure 2.4: Receiver with CM compensation.

One disadvantage of the method in [13] is that it uses an auxiliary FE and ADC to capture the interferer, which leads to additional complexity and power consumption. However in the multimode transceiver, discrete-time samples of the transmitted interference are locally available. As shown in Fig. 2.4b, we propose to estimate the received interference from the available baseband information. The proposed method does not require any additional analog hardware, at the expense of slightly higher complexity in the digital domain. Hence the chip area and power consumption of the multimode receiver can be significantly reduced compared to the method in [13]. The proposed compensation method is based on the statistical independence of the desired signal and the interference. Hence it is more generic than [13] and it does not require presence of the pilot symbols in the desired signal, neither of channel estimation as required in [13]. The simulation results for a WLAN RX and WiMAX TX scenario demonstrate the effectiveness of the compensation method to improve the input third-order intercept point of the receiver, e.g. 8 dB for 64QAM modulation of the desired signal.

This paper is organized as follows. In section 2.3 we develop a simplified system model to describe the discrete-time received baseband signal in the presence of the CM distortion in most cases of practical interest. Based on this simplified model, we propose a CM compensation method in section 2.4. Simulation results are presented in section 2.5. Concluding remarks are given in section 2.6.

2.3 System Model

In this section, impact of the FE nonlinearity on the receiver operation is analyzed and a simplified model to describe the CM distortion is presented. This model will be used in section III to design a compensator for the CM distortion.

2.3.1 Derivation of the LNA input

The signal $x_R(t)$ received by the LRX antenna, in Fig. 2.1, is a combination of the received desired signal and interference as:

$$x_R(t) = d_R(t) + i_R(t). \tag{2.1}$$

In (2.1) the input referred noise is neglected. The input referred noise includes the thermal noise, and added circuit noise by the receiver referred to the FE input . Typically the added circuit noise is dominated by the circuit noise of the LNA and the passive components before the LNA. Hence the input referred noise can be assumed statistically independent of $d_R(t)$ and $i_R(t)$. For practical Symbol Error Rates (SER) the desired signal is at least one or two orders of magnitude larger than input referred noise. As we will see in section 2.5.1 and 2.5.2, the proposed CM compensation method only relies on statistical independence of $d_R(t)$ and $i_R(t)$. Hence neglecting the input referred noise does not have a significant impact on the accuracy of the CM compensator. This is verified in the simulation results section, where the the performance of the CM compensator is shown both for noise-free scenarios and for scenarios with the input noise.

The LNA input in Fig. 2.2 is obtained as:

$$x_B(t) = x_R(t) \circledast h_B(t) = (d_R(t) + i_R(t)) \circledast h_B(t) = d_B(t) + i_B(t), \tag{2.2}$$

where $h_B(t)$ is the impulse response of the BPF and $\circledast$ denotes convolution. The interference component $i_R(t)$ originates from the complex-valued baseband interference $i(t)$. First $i(t)$ is up-converted to a carrier frequency f_i. Then it is transmitted by the LTX antenna, and is received by the LRX antenna resulting in $i_R(t)$. To model the transmit-receive path of the interference from $i(t)$ to $i_B(t)$, we make the following practical assumptions:

1. The LTX is linear. Because the nonlinearities in the LTX are typically kept at minimum to guarantee a high quality transmitted signal.

2. Transmit-receive path approximately has a flat frequency and group-delay response over the interference bandwidth B_i. The only possibility for a non-flat frequency response over B_i is the case when f_i falls in the transition band of the BPF. However for most practical scenarios, f_i falls in the flat region of the frequency response of the BPF.

Based on these assumptions the transmit-receive path of the interference can be modeled as multiplication by a complex number α_i and a time delay τ_i. Hence $x_B(t)$ is obtained as:

$$x_B(t) = \mathrm{Re}\left\{\left(d(t) + \alpha_i i(t-\tau_i)e^{j2\pi\Delta f t}\right)e^{j2\pi f_d t}\right\}, \tag{2.3}$$

where $d(t)$ is the baseband equivalent of $d_B(t)$, Δf is the frequency separation between $d_B(t)$ and $i_B(t)$, defined as $\Delta f = f_i - f_d$.

Both α_i and τ_i depend on the changes happening in the handheld device environment. For example moving the user hand can change α_i by changing the coupling between the LRX and LTX antennas. The same variability also occurs for τ_i. The rate of change for α_i and τ_i, even in extreme cases, are assumed to be much smaller than 1 kHz. Hence α_i and τ_i can be assumed constant for time spans in the order of 1 ms.

2.3.2 Derivation of analog baseband signal

To simplify the analysis, we assume that the only nonlinear element of the FE is the LNA. It is common to model this nonlinearity by a third order polynomial as [13], [14]:

$$y(t) = a_1 x_B(t) + a_3 x_B^3(t). \tag{2.4}$$

The values of a_1 and a_3 are related to the LNA parameters. The small signal gain of the LNA is represented by a_1. Without loss of generality, in the rest of this paper we will assume that $a_1 = 1$. As long as we one interferer and one desired signal are present, a second-order term $(x_B^2(t))$ does not generate any in-band distortion component. Hence such a term is omitted in (2.4).

Using (2.4) and (2.3), the mixer output $y_M(t)$ in Fig. 2.2 can be written as:

$$
\begin{aligned}
y_M(t) = d(t) &+ \underbrace{\frac{3}{4}a_3 d(t)|d(t)|^2}_{\mathrm{H}_3} + \underbrace{\frac{3}{2}a_3|\alpha_i|^2 d(t)|i(t-\tau_i)|^2}_{\mathrm{CM}} \qquad (2.5)\\
&+ \left(\alpha_i i(t-\tau_i) + \frac{3}{4}a_3|\alpha_i|^2 i(t-\tau_i)|i(t-\tau_i)|^2 + \frac{3}{2}a_3\alpha_i i(t-\tau_i)|d(t)|^2\right)e^{j2\pi\Delta f t}\\
&+ \left(\frac{3}{4}a_3|\alpha_i|^2 d^*(t)\,|i(t-\tau_i)|^2\right)e^{j4\pi\Delta f t} + \left(\frac{3}{4}\alpha_i a_3 i^*(t-\tau_i)|d(t)|^2\right)e^{-j2\pi\Delta f t}\\
&+ \text{high frequency terms around } 2f_d \text{ and } 2f_i,
\end{aligned}
$$

where $*$ in the superscripts denotes complex conjugate. In (2.5) the first term is the baseband desired received signal, the second term is the H3 product, and the third term is the CM product.

We use the following practical assumptions to derive a simple description for the received analog baseband signal $z(t)$:

1. The frequency separation Δf is large enough, so that the components in (2.5) with center frequency of Δf, $2\Delta f$ and $-\Delta f$ do not have any spectral overlap with $d(t)$. Hence they will be filtered out by the LPF.

2. The receiver FE is designed to process $d_r(t)$ with negligible nonlinear distortion in the absence of $i_R(t)$. Therefore H3 product of $d_r(t)$ is negligible compared to $d(t)$.

3. To simplify compensation of the CM distortion, we choose the bandwidth B_{LPF} of the LPF larger than bandwidth B_{CM} of the CM product. B_{CM} depends on modulation and statistical characteristics of $d(t)$ and $i(t)$. However in all cases B_{CM} won't be more than $B_d + 2B_i$, where B_d is the bandwidths of the $d(t)$.

Using the above assumptions, $z(t)$ can be approximated by:

$$
z(t) \simeq d(t)\left(1 + c|i(t-\tau_i)|^2\right) \qquad (2.6)
$$

where c is defined as:

$$
c = \frac{3a_3}{2}|\alpha_i|^2. \qquad (2.7)
$$

Typically, active circuits have a compressive behavior so that $a_3 < 0$ and hence $c < 0$. Since c depends on a_3 and α_i, it can be assumed constant for time spans in the order of 1 ms.

2.3.3 Derivation of discrete-time received signal

Equation (2.6) describes how the CM distortion affects $z(t)$. To digitally compensate for the CM distortion, we must obtain the discrete-time counterpart of (2.6). Suppose that $z(t)$ is sampled with the rate of $\frac{1}{T_s}$, which is high enough to prevent aliasing of $z(t)$. The resulted discrete-time signal will be:

$$z[p_s] = z(t)|_{t=p_sT_s} \simeq d[p_s]\left(1 + c|i[p_s]|^2\right), \tag{2.8}$$

where

$$d[p_s] = d(t)|_{t=p_sT_s}, \tag{2.9}$$

$$i[p_s] = i(t - \tau_i)|_{t=p_sT_s}. \tag{2.10}$$

The analog signal $i(t)$ is generated by analog conversion of discrete-time samples of the interference $i[p_i]$ with a conversion period T_i. The symbol p_i denotes the time indices in the clock domain T_i. According to (2.10), $i[p_s]$ can be generated digitally by re-sampling $i[p_i]$ from sampling period T_i to T_s, and applying a digital delay of τ_i seconds by a Sampling Rate Conversion and Delay block (SRCD).

For an exactly linear FE, the ADC output would be $d[p_s]$. Based on (2.8), the CM distortion can be interpreted as the multiplication of $d[p_s]$ by the time varying factor $(1 + c|i[p_s]|^2)$. The Signal to Distortion Ratio (SDR) for $z[p_s]$ in (2.8) can be defined as power ratio of $d[p_s]$ to the CM product $cd[p_s]|i[p_s]|^2$:

$$\mathrm{SDR}\{z\} \triangleq \frac{E\{|d[p_s]|^2\}}{E\{|cd[p_s]|i[p_s]|^2|^2\}}. \tag{2.11}$$

Considering that $d[p_s]$ and $i[p_s]$ are statistically independent (2.11) can be written as:

$$\mathrm{SDR}\{z\} = \frac{1}{c^2 E\{|i[p_s]|^4\}}. \tag{2.12}$$

According to (2.12), $\mathrm{SDR}\{z\}$ does not depend on the power of the desired signal and only depends on the interference power at the LNA input and the LNA nonlinearity. The probability distribution of a baseband OFDM signal can be approximated by a zero mean Circularly-Symmetric Complex Gaussian (CSCG) random signal. If $i[p_s]$ is a unit variance CSCG random signal by using (2.51) we will have $E\{|i[p_s]|^4\} = 2$, and (2.12) becomes:

$$\mathrm{SDR}\{z\} = \frac{1}{2c^2}. \tag{2.13}$$

The defined SDR reflects the impact of CM distortion on the time domain signals. For a complete analysis of impact of nonlinear distortion on OFDM signals in the frequency domain the interested reader can consult [24], [25].

2.4 Proposed compensation method

According to (2.8) the CM distortion can be compensated by dividing $z[p_s]$ by the factor $(1 + c|i[p_s]|^2)$. Hence the core part of our compensation scheme will be estimation of $(1+c|i[p_s]|^2)$, which leads to estimation of two unknown parameters: τ_i and c.

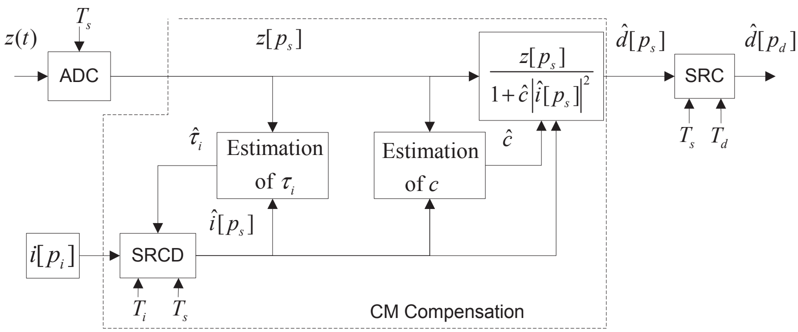

Figure 2.5: Proposed compensation scheme.

The proposed compensation scheme is illustrated in Fig. 2.5. The baseband received signal $z(t)$ is sampled with the sampling period T_s. The signal $i[p_i]$ is re-sampled from the sampling period T_i to T_s and delayed $\hat{\tau}_i$ seconds by the SRCD. The estimated time-delay $\hat{\tau}_i$ is used to make the output $\hat{i}[p_s] = i(p_sT_s - \hat{\tau}_i)$ of the SRCD time-aligned with $i[p_s] = i(p_sT_s - \tau_i)$. The estimation of τ_i is performed by processing $z[p_s]$ and $\hat{i}[p_s]$ together, as explained in Section 2.4.1. Then c is estimated by processing $z[p_s]$ and $\hat{i}[p_s]$ together, as explained in Section 2.4.2. The estimated values, $\hat{c}$ and $\hat{i}[p_s]$, are used to calculate $(1 + \hat{c}|\hat{i}[p_s]|^2)$. The CM distortion is compensated by dividing $z[p_s]$ by $(1 + \hat{c}|\hat{i}[p_s]|^2)$. The compensated signal $\hat{d}[p_s]$ is re-sampled from the sampling period T_s to T_d by a Sampling Rate Converter (SRC), where T_d is the symbol clock of the transmitted desired signal which can be recovered by processing $\hat{d}[p_s]$ as usual.

2.4.1 Estimation of τ_i

To find the time difference between $z[p_s]$ and $\hat{i}[p_s]$ we propose a cost function $f(\tau)$ of which the absolute minimum occurs at $\tau = \tau_i$. Therefore τ_i can be found as:

$$\tau_i = \underset{\tau}{\operatorname{argmin}}\, f(\tau). \tag{2.14}$$

We define $f(\tau)$ as:

$$f(\tau) = E\{|z(p_sT_s)||i(p_sT_s - \tau)|^2\}, \tag{2.15}$$

and prove in Appendix I that the absolute minimum of $f(\tau)$ occurs for $\tau = \tau_i$. In practice the exact Probability Distribution Functions (PDF) of $d[p_s]$ and $i[p_s]$ are not known. Hence we have to approximate the expected value by the corresponding time average as:

$$\hat{f}(\tau) = \frac{1}{N} \sum_{p_s=1}^{N} |z(p_s T_s)||i(p_s T_s - \tau)|^2, \tag{2.16}$$

where N is the number of samples used in the estimation of expected value. By minimizing $\hat{f}(\tau)$ an estimate of τ_i is obtained as:

$$\hat{\tau}_i = \underset{\tau}{\operatorname{argmin}}\, \hat{f}(\tau). \tag{2.17}$$

By increasing N, the time average in (2.16) becomes closer to $f(\tau)$. To increase N, the time span that we collect the samples can be increased. Since τ_i can be assumed constant for time spans in the order of 1 ms, for an interference with a bandwidth of 10 MHz, we can collect about $N = 10^4$ independent samples. In the limit when $N \to \infty$, we will have $\hat{\tau}_i \to \tau_i$. We use (2.16) to calculate $\hat{f}(\tau)$ in a possible range of τ_i. Then $\hat{\tau}_i$ is estimated by finding the argument that minimizes $\hat{f}(\tau)$.

2.4.2 Estimation of c

In this section we propose an estimator for c. In Appendix II we show that the mean square error of this estimator is proportional to $\frac{1}{N}$, where N is the number of independent samples used in the estimation. We estimate c, where $i[p_s]$ and $z[p_s]$, $p_s = 1..N$ are known and $d[p_s]$, $p_s = 1..N$ is unknown. In this section $\simeq$ in (2.8) is replaced with $=$ to clarify where new approximations are made. Since $d[p_s]$ and $i[p_s]$ originate from two independent transmitters they can be assumed to be statistically independent. Taking absolute value of both sides of (2.8) results in:

$$|z[p_s]| = |d[p_s]| \left(1 + c|i[p_s]|^2\right), \tag{2.18}$$

where we assumed that $(1+c|i[p_s]|^2)$ is positive. By calculating the expected value of both sides of (2.18), we obtain:

$$E\{|z[p_s]|\} = E\{|d[p_s]|\}(1 + cE\{|i[p_s]|^2\}). \tag{2.19}$$

By multiplying both sides of (2.18) by $|i[p_s]|$ and calculating the expected value of both sides, we obtain:

$$E\{|z[p_s]i[p_s]|\} = E\{|d[p_s]|\}(E\{|i[p_s]|\} + cE\{|i[p_s]|^3\}). \tag{2.20}$$

Suppose that E_k, $E_{|d|}$ and I_k are defined as:

$$E_k = E\{|z[p_s]i[p_s]|^k\}, E_{|d|} = E\{|d[p_s]|\}, I_k = E\{|i[p_s]|^k\}, \tag{2.21}$$

then by dividing (2.19) by (2.20) and solving for c we obtain:

$$c = \frac{E_0 I_1 - E_1}{I_2 E_1 - I_3 E_0}. \tag{2.22}$$

In practice, it is impossible to find E_0,E_1,I_1,I_2 and I_3, since the PDF of $d[p_s]$ and $i[p_s]$ are not exactly known. Instead they can be approximated by their corresponding time averages as:

$$\hat{E}_k = \frac{1}{N}\sum_{p_s=1}^{N} |z[p_s]i[p_s]|^k, \quad \hat{I}_k = \frac{1}{N}\sum_{p_s=1}^{N} |i[p_s]|^k. \tag{2.23}$$

Using these approximated values c can be estimated as:

$$\hat{c} = \frac{\hat{E}_0 \hat{I}_1 - \hat{E}_1}{\hat{I}_2 \hat{E}_1 - \hat{I}_3 \hat{E}_0}. \tag{2.24}$$

In Appendix II, the Mean Square Error (MSE) of the estimator for c in the case of N independent identically distributed samples is derived as:

$$\mathrm{MSE}\{\hat{c}\} = E\{|\hat{c} - c|^2\} \simeq \frac{1}{N}\frac{\sigma^2_{|d|}}{E^2_{|d|}} A(I_1..I_6, c) \tag{2.25}$$

where $\sigma^2_{|d|}$ is the variance of $|d[p_s]|$ and $A(I_1..I_6, c)$ is a function which is defined in appendix II. From (2.25) the following inferences are made:

- The MSE of $\hat{c}$ decreases proportional to $\frac{1}{N}$. Hence by using more independent samples the accuracy of the estimator can be increased.

- The MSE of $\hat{c}$ is proportional to $\frac{\sigma^2_{|d|}}{E^2_{|d|}}$. Hence the estimation error will be higher for received desired signals with larger envelope variations.

When $i[p_s]$ and $d[p_s]$ are zero mean unit variance CSCG random signals then (2.25) can be approximated as (Appendix II):

$$\mathrm{MSE}\{\hat{c}\} \simeq \frac{1}{N}(0.3 + 1.8c + 4c^2 + 3.4c^3 + c^4). \tag{2.26}$$

The simulation results in section 2.5.2 confirm the accuracy of the derived formula in (2.26).

We assumed that the factor $(1 + c|i[p_s]|^2)$ in (2.18) is always positive. This factor represents the effective gain that $d[p_s]$ experiences. For a typical amplifier, the gain decreases from 1 to 0 when $|i[p_s]|$ increase from 0 to a very large value. However for the third order model, $(1 + c|i[p_s]|^2)$ becomes negative when $|i[p_s]|$ is very large. As we will see in section 2.5.2, violation of the positivity assumption increases MSE$\{\hat{c}\}$ for strong interferers. To solve this problem, we can discard all the samples for which $1 + c|i[p_s]|^2 < 0$ from the summations in (2.23). Although we do not know c, we can use the largest possible value of $|c|$ in a given scenario, and discard all the samples that:

$$1 - \max(|c|)|i[p_s]|^2 < 0. \tag{2.27}$$

The performance of the estimator that uses all the samples and the one which discards some of the samples based on (2.27), will be discussed in section 2.5.2.

2.5 Simulation results

In this section simulation results are presented. First we investigate the accuracy of the estimators for τ_i and c. Then we evaluate and compare the Symbol Error Rate (SER) of the receiver affected by the CM distortion before and after compensation. For simulation we consider the multimode transceiver scenario of Fig. 2.1. The WLAN signal transmitted by RTX is located at the uppermost part of the WLAN frequency band, channel 11 with the center frequency of 2462 MHz. The WiMAX signal transmitted by LTX is located at the lowermost part of the WiMAX frequency band with center frequency of 2501 MHz, hence Δf =39 MHz. The bandwidths of WLAN and WiMAX signals are 20 MHz and 10 MHz, respectively. Three types of modulation for the WLAN signal are simulated, Single carrier QPSK, 64 QAM and Orthogonal Frequency Division Multiplexing (OFDM) with 64 subcarriers where each carrier has a 64 QAM modulation. In all simulations a zero mean unit variance CSCG random signal, which approximates a baseband OFDM signal, is used for the WiMAX baseband signal $i[p_i]$. The maximum allowable transmitted power of the WiMAX transmitter is 23 dBm. We assume -20 dB coupling between the LTX and the LRX and 23 dB suppression of the WiMAX signal by the BPF. Hence the maximum power of $i_B(t)$ will be -20 dBm which is equivalent to $|\alpha_i|^2 = 10^{-3}$ in a 50 Ω system $(10\log_{10}(\frac{|\alpha_i|^2}{2\times 50}/10^{-3}) = -20)$. The IIP3 of the LNA is chosen at least 10 dB larger than maximum power of $i_B(t)$ to prevent excessive loss of the LNA gain. Loosing the LNA gain leads to loss of the receiver's sensivity, which is called desensitization. Here we require an IIP3 of -10 dBm which is a moderate value [26]. The IIP3 of a circuit in dBm can be related to the third-order polynomial model in (2.4) [21] and results in $a_3 = -133$, considering that $a_1 = 1$. Based on (2.7), c is in the range of $[0, -0.20]$, where 0 and -0.20 correspond to zero interference ($|\alpha_i|^2 = 0$) and maximum interference ($|\alpha_i|^2 = 10^{-3}$), respectively. According to (2.13), SDR$\{z\} > 11$ dB. Since for smaller SDRs, the degradation to receiver performance because of the desensitization dominates the CM distortion, all the simulation results are shown for SDR$\{z\}$ >11 dB.

2.5.1 Accuracy of $\hat{\tau}_i$

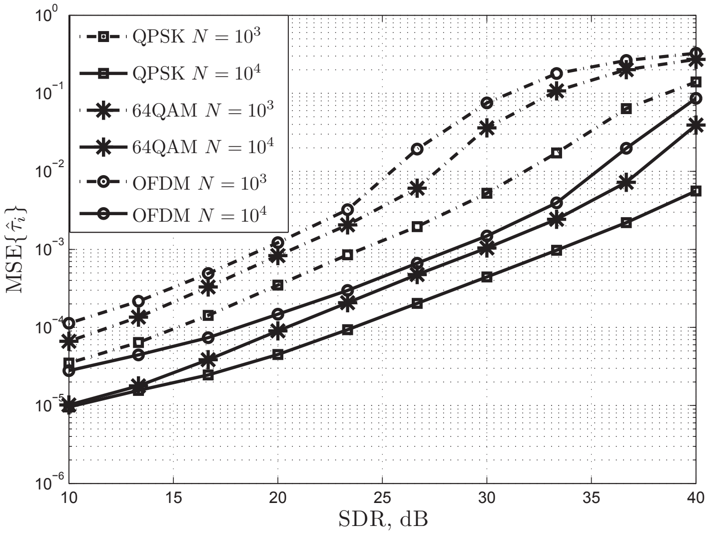

Figure 2.6: MSE $\{\hat{\tau}_i\}$ versus SDR$\{z\}$ for $N = 10^3, 10^4$, $d[p_d]$: QPSK, 64 QAM and OFDM.

The MSE for estimating τ_i is evaluated by simulation and plotted versus SDR$\{z\}$ in Fig. 2.6. The number of independent samples of $i[p_i]$ is $N = 10^3, 10^4$. These values of N corresponds to 0.1 ms and 1 ms of collecting samples of the received signal, respectively. The transmitted desired signal $d[p_d]$ has QPSK, 64 QAM or OFDM modulation as mentioned before. We use p_d for time indices that belongs to the clock domain T_d. Since the bandwidth of the desired signal is 20 MHz, the number of independent samples of $d[p_d]$ will be 2×10^3 and 2×10^4 samples.

The simulator interpolates $i[p_i]$ and $d[p_d]$, 10 and 5 times to simulate the received analog signal $z(t)$. The interpolating filter for OFDM modulations is designed such that the analog signal would have a rectangular frequency spectrum. For single carrier modulations of $d[p_d]$, a raised cosine pulse shaping filter with a roll-off-factor of 0.5 is used to interpolate the samples of $d[p_d]$. Uniform random numbers in the range of $\pm T_i$ are used as the values of τ_i. An exhaustive search is performed in a range of $\pm T_i$ with a step size of $\frac{T_i}{10}$ to find the minimum of $\hat{f}(k\frac{T_i}{10})$, where $k = -10, .., 10$. Then a parabola is fitted to the minimum of $\hat{f}(k\frac{T_i}{10})$ and its two adjacent points. Then the minimum of the parabola is found as $\hat{\tau}_i$ [27]. The step size is decreased with trial and error to have a negligible impact on the measured MSE$\{\hat{\tau}_i\}$. The measured error $\hat{\tau}_i - \tau_i$ is normalized to T_i.

We observe that MSE$\{\hat{\tau}_i\}$ increases when SDR$\{z\}$ increases. Since we are estimating the time delay between the transmitted and received interference and a stronger interference leads to a more accurate estimate. When the received interference is small, the cross-modulation is already negligible and there is no need for an accurate estimation. In the extreme case when $c \to 0$, $f(\tau)$ becomes constant and MSE$\{\hat{\tau}_i\}$ converges to the variance of a uniform random variable in [-1 1], which is $\frac{1}{3}$, as seen for OFDM and 64 QAM modulation with $N = 10^3$. By increasing N the accuracy of the estimation improves. As we will see in section 2.5.3 by choosing $N = 10^4$, the SER performance of the compensator which uses $\hat{\tau}_i$, is almost the same as the compensator which uses τ_i. MSE$\{\hat{\tau}_i\}$ increases when the envelope variation of $d[p_d]$ increases from QPSK to 64 QAM and to OFDM modulation. In fact, envelope variation of $d[p_d]$ acts as a disturbing factor when measuring the cross correlation between $|z(p_sT_s)|$ and $|i(p_sT_s - \tau)|$.

2.5.2 Accuracy of $\hat{c}$

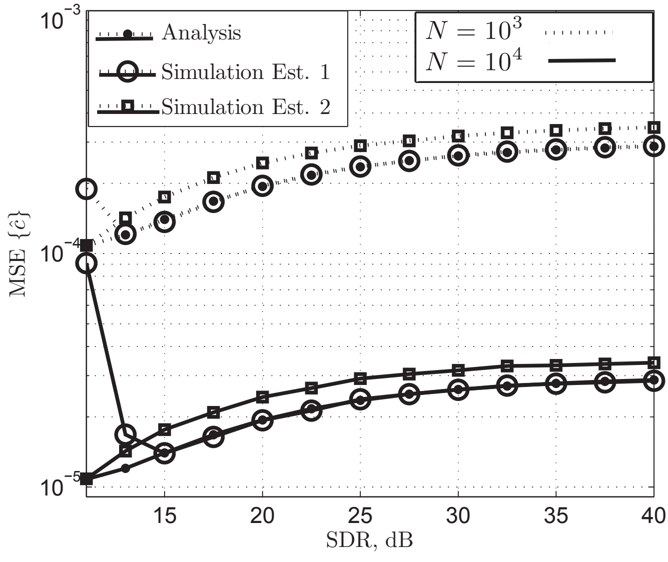

Figure 2.7: MSE$\{\hat{c}\}$versus SDR, $N = 10^3$, 10^4, $d[p_d]$: OFDM..

Fig. 2.7 shows MSE$\{\hat{c}\}$ versus SDR$\{z\}$ when $d[p_d]$ has the OFDM modulation and $N = 10^3, 10^4$ independent samples of $i[p_i]$ and $d[p_d]$ are used to estimate c. The simulation is performed for the estimator that uses all the samples (Est. 1) and the estimator that discards the samples that $1 - 0.2|i[p_s]|^2 < 0$ (Est. 2). The simulation results are compared with the derived MSE in (2.26). For Est. 1 two

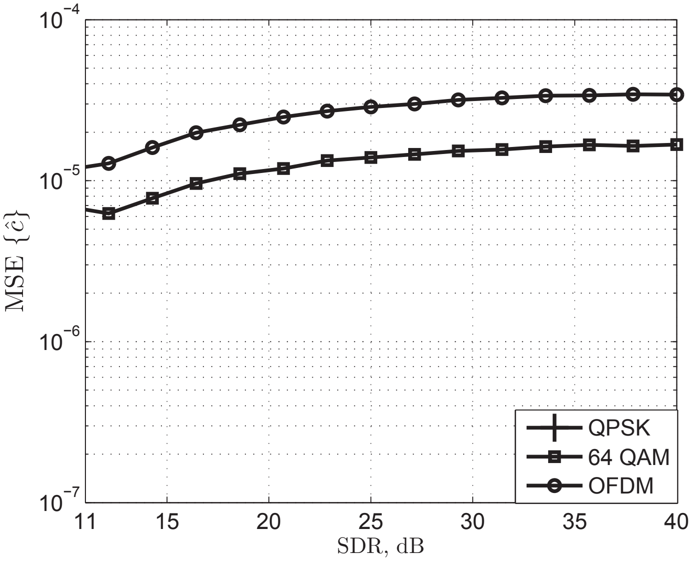

Figure 2.8: MSE$\{\hat{c}\}$versus SDR, $N = 10^4$, $d[p_d]$: QPSK, 64 QAM and OFDM..

trends are observed for SDR$\{z\} > 16$ dB and SDR$\{z\} < 16$ dB. For SDR$\{z\} > 16$ dB the main error source originates from replacing expected values with time averages. The curves based on the analysis in (2.26) match exactly with the curves resulted from the simulation. MSE$\{\hat{c}\}$ is slightly decreased by decreasing SDR$\{z\}$ (i.e. we have a smaller error in estimating c for larger amounts of the CM distortion). MSE$\{\hat{c}\}$ is proportional to $\frac{1}{N}$ as predicted by (2.26). For SDR$\{z\} < 16$ dB, MSE$\{\hat{c}\}$ increases by decreasing SDR$\{z\}$. This phenomenon originates from our assumption on positivity of $1 + c|i[p_s]|^2$ in (2.18). Since $i[p_s]$ has a Gaussian distribution, this assumption will be violated for some samples of $i[p_s]$. This violation causes an error that is unaccounted for in (2.22) and becomes dominant for SDR$\{z\}$ <16 dB compared to the other error source in estimating c (i.e. replacing I_k and E_k with $\hat{I}_k$ and $\hat{E}_k$). Since this error is not taken into account when deriving (2.26), the derived formula does not predict MSE$\{\hat{c}\}$ correctly in this region.

For Est. 2, since we use less samples for the estimation, we achieve a slightly larger MSE$\{\hat{c}\}$ (here about 8%) when SDR$\{z\}$ is large, compared to Est. 1 that uses all the samples. On the other hand for $N = 10^4$, Est. 2 has a significantly smaller MSE$\{\hat{c}\}$ when SDR$\{z\}$ dB is small. Since we are mainly interested to improve the receiver SER for small values of SDR$\{z\}$, we will use Est. 2 in the rest of simulations.

Fig. 2.8 shows MSE$\{\hat{c}\}$ for various modulations of $d[p_d]$ where $N = 10^4$ independent samples of $i[p_i]$ and $d[p_d]$ are used to estimate c.. The modulation of $d[p_d]$ can be QPSK, 64QAM, or OFDM. For QPSK modulation $d[p_d]$ is constant. Hence we achieve a very small value for MSE$\{\hat{c}\}$ (less than 10^{-7}). We observe that MSE$\{\hat{c}\}$ increases for modulations with larger envelope variations (i.e. larger variance), as predicted by (2.25).

2.5.3 SER performance of the compensation scheme

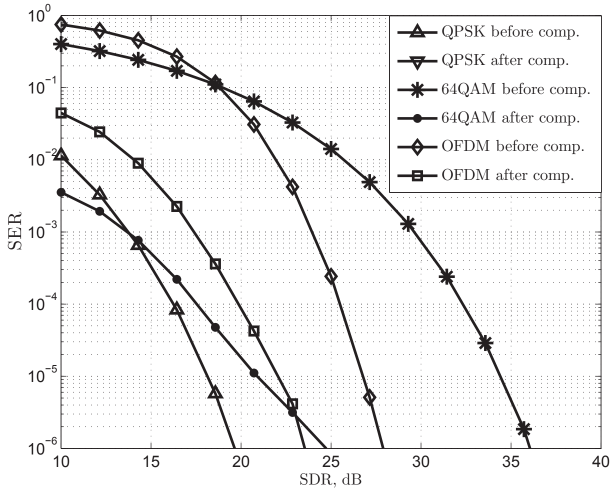

Figure 2.9: SER versus SDR$\{z\}$, $N = 10^4$, a) $d[p_d]$: QPSK, 64 QAM and OFDM, b)$d[p_d]$: 64 QAM, compensation with exact τ_i and estimated c.

The CM distortion leads to additional degradation of the receiver performance, on top of the errors due to the additive input noise. To isolate the impact of CM distortion, firstly, we consider a noise free scenario where the symbol errors are solely caused by the CM distortion. First we assume an ideal estimation and implementation of τ_i ($i[p_s] = \hat{i}[p_s]$) to isolate the effects of inaccuracies in the estimation of c on the SER. In Fig. 2.9 uncoded SER vs SDR $\{z\}$ is shown. The number of samples used for the estimation of c is $N = 10^4$. The modulation of $d[p_d]$ can be QPSK, 64QAM, or OFDM. The power of the transmitted interferer is varied from 23 dBm to 8 dBm, resulting in a received interference power of -20 dBm to -35 dBm at the LNA input (equivalent to 11 dB$<$ SDR$\{z\}$ $<$41 dB), while the power of the received desired signal is kept at -60 dBm.

In QPSK modulation, information is carried in phase. As we showed previously, the CM distortion is multiplication of the desired signal by $1+c|i[p_s]|^2$. For QPSK

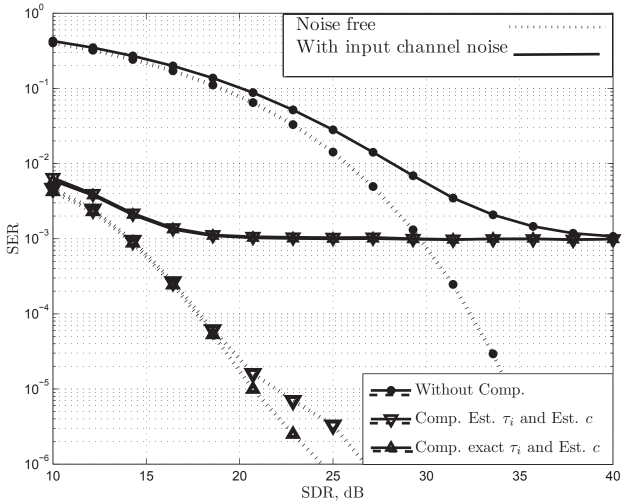

Figure 2.10: SER versus SDR$\{z\}$, $N = 10^4$, a) $d[p_d]$: QPSK, 64 QAM and OFDM, b)$d[p_d]$: 64 QAM. compensation with estimated τ_i and estimated c in noise free (shown with dashed lines ...) and noisy environment (shown with solid lines $-$)..

the CM distortion causes an error only when $1 + c|i[p_s]|^2 < 0$, which happens very rarely for practical interference levels. Hence the QPSK has the lowest SER before compensation compared to the other modulations. When we compensate for the CM distortion, no error is observed for QPSK modulation. We observe that before compensation, the SER vs. SDR curve of the OFDM has a steeper slope than 64 QAM modulation. The reason is that the amplitude of the CM distortion product is $cd[p_s]|i[p_s]|^2$. As $i[p_s]$ has a CSCG distribution, $|i[p_s]|^2$ will have a Chi-square distribution (with 2 degrees of freedom). Hence for single carrier modulation of $d[p_d]$, each symbol experiences a Chi-square distributed disturbance. Due to the discrete Fourier transform in OFDM demodulation, the disturbance that each symbol experience has a Gaussian distribution (According to central limit theorem). The Gaussian PDF decays faster than a Chi-square PDF. Hence the probability of making errors with a Gaussian distributed disturbance decreases with a faster rate by increasing SDR compared to a Chi-square distributed disturbance. Here we want to limit the SER degradation because of the CM distortion to about an order of magnitude smaller than the SER due to the the input noise, (around 10^{-2}). Hence we consider an SER of 10^{-3} to measure the improvement in SDR after CM compensation. As we see for the 64QAM modulation, the SDR of the compensated signal (SDR $\{\hat{d}\}$) is improved by 16 dB, which is equivalent to 8 dB improvement in the effective IIP3 of the receiver. Compared to 64QAM, OFDM shows a smaller improvement in SDR after compensation, 7 dB at SER of 10^{-3}. Since with the same N and c, MSE$\{\hat{c}\}$ is larger for the OFDM than 64QAM modulation.

In Fig. 2.10 uncoded SER vs SDR$\{z\}$ is shown when the compensation is performed with estimated values of for τ_i and c. The same simulation parameters and search method as Section IV.A are used for estimation of τ_i. The desired signal has the 64 QAM modulation. The simulation is performed both for a noise free environment and a noisy environment. For the noise free environment we see a small degradation in the performance of the compensator that uses $\hat{c}$ and $\hat{\tau}_i$ compared to a compensator that uses $\hat{c}$ and τ_i. For simulation of the noisy environment, the desired signal is passed through an Additive White Gaussian Noise (AWGN) channel. The desired Signal to Noise Ratio (SNR) is chosen such that an SER of 10^{-3} would be resulted in the absence of the interference, which requires an SNR of 24 dB for 64QAM modulation. This SER results in an error free communication after the forward error correction in the WLAN receiver. For the SDRs up to 40 dB we still observe the degradation of the receiver performance by the cross-modulation. After the CM compensation the SER improves significantly. We choose an SER of 2×10^{-3} for measuring the SDR improvement after the CM compensation, to take into account both impacts of the imperfect CM compensation and the channel noise together. At this SER the amount of SDR improvement is about 18 dB. Hence the introduction the channel noise has not affected the performance of the compensation method.

2.6 Conclusion

The simultaneous operation of the transmitter of one communication standard and the receiver of another one in the multimode transceiver leads to strong Cross Modulation (CM) distortion of the desired signal of the receiver. In this paper we proposed a fully digital method to compensate for the CM distortion. A third-order polynomial is used to model the nonlinear Front-End (FE) and the transmit-receive path of the interferer is modeled by a time delay and attenuation. Based on these models a discrete nonlinear model for the received signal is presented, which includes two priori unknown parameters, namely a time delay τ_i and an amplitude c. We proposed estimators for these two parameters. Based on these estimated values and by using baseband transmitted interferer the CM distortion is compensated. Our simulation results show the effectiveness of our method to improve the receiver's SER in the presence of a strong interferer for different modulations of the desired signal. With compensation an improvement of 16 dB in SDR for 64 QAM modulation is observed which is equivalent to 8 dB improvement of the receiver IIP3. The proposed compensation method does not require any major modification to the receiver FE or the digital stages of the receiver after the CM compensator.

Appendix I: Estimation of τ

The cross-correlation of $|z(p_sT_s)|$ with $|i(p_sT_s-\tau)|^2$ is obtained as:

$$\begin{aligned} f(\tau) &= E\{|z(p_sT_s)||i(p_sT_s-\tau)|^2\}, \\ &= E\{|d(p_sT_s)|(1+c|i(p_sT_s-\tau_i)|^2)|i(p_sT_s-\tau)|^2\}. \end{aligned} \tag{2.28}$$

Because $d[p_s]$ and $i[p_s]$ are independent (2.28) can be written as:

$$f(\tau) = E\{|d(p_sT_s)|\}\left(E\{|i[p_s]|^2\} + cE\{|i(p_sT_s-\tau_i)|^2|i(p_sT_s-\tau)|^2\}\right) \tag{2.29}$$

According to the Cauchy Schwartz inequality:

$$\begin{aligned} &E\{|i(p_sT_s-\tau_i)|^2|i(p_sT_s-\tau_i)|^2\}^2 \leq \\ &E\{|i(p_sT_s-\tau_i)|^4\}E\{|i(p_sT_s-\tau)|^4\} = E\{|i[p_s]|^4\}^2, \end{aligned} \tag{2.30}$$

where equality happens only, when $|i(p_sT_s-\tau)| = |i(p_sT_s-\tau_i)|$ or equivalently $\tau=\tau_i$, (assuming that $i[p_s]$ has a varying envelope modulation). Because $c<0$, using (2.30), we will have:

$$f(\tau) \geq E\{|m[p_s]|\}\left(E\{|i[p_s]|^2\} + cE\{|i[p_s]|^4\}\right). \tag{2.31}$$

Hence the absolute minimum of $f(\tau)$ is $E\{|d[p_s]|\}\left(E\{|i[p_s]|^2\} + cE\{|i[p_s]|^4\}\right)$ and occurs for $\tau=\tau_i$.

Appendix II: Proof for variance of $\hat{c}$

Lemma: Suppose that $x[n]$ and $y[n]$ are wide sense stationary, independent and identically distributed random signals. Besides $x[n]$ and $y[n]$ are independent from each other. If R is defined as:

$$R = \frac{1}{N}\sum_{n=1}^{N} x[n]y[n] - \frac{1}{N^2}\sum_{n=1}^{N} x[n]\sum_{n=1}^{N} y[n], \tag{2.32}$$

then

$$\begin{aligned} E\{R\} &= 0 \\ E\{R^2\} &= \frac{1}{N}(1-\frac{1}{N})\sigma_x^2\sigma_y^2, \end{aligned} \tag{2.33}$$

where

$$\sigma_x^2 = E\{(x - E\{x\})^2\}, \quad \sigma_y^2 = E\{(y - E\{y\})^2\}. \tag{2.34}$$

Proof:

$$\begin{aligned} E\{R\} &= \frac{1}{N}\sum_{n=1}^{N} E\{x[n]\}E\{y[n]\} - \frac{1}{N^2}\sum_{n=1}^{N} E\{x[n]\}\sum_{n=1}^{N} E\{y[n]\} \\ &= \frac{1}{N}NE\{x\}E\{y\} - \frac{1}{N^2}N^2E\{x\}E\{y\} = 0 \end{aligned} \tag{2.35}$$

We define $x'[n]$ and $y'[n]$ as:

$$x'[n] = x[n] - E\{x\}, \quad y'[n] = y[n] - E\{y\}. \tag{2.36}$$

After simple manipulations we will have:

$$R = \frac{1}{N}\sum_{n=1}^{N} x'[n]y'[n] - \frac{1}{N^2}\sum_{n=1}^{N} x'[n]\sum_{n=1}^{N} y'[n] \tag{2.37}$$

Using (2.37), $E\{R^2\}$ can be calculated as:

$$\begin{aligned} E\{R^2\} =& \frac{1}{N^2}\underbrace{E\left\{\left(\sum_{n=1}^{N} x'[n]y'[n]\right)^2\right\}}_{T_1} - \frac{2}{N^3}\underbrace{E\left\{\sum_{n=1}^{N} x'[n]\sum_{n=1}^{N} y'[n]\sum_{n=1}^{N} x'[n]y'[n]\right\}}_{T_2} \\ &+ \frac{1}{N^4}\underbrace{E\left\{\left(\sum_{n=1}^{N} x'[n]\sum_{n=1}^{N} y'[n]\right)^2\right\}}_{T_3} \end{aligned} \tag{2.38}$$

$$T_1 = \sum_{n_1=1}^{N} \sum_{n_2=1}^{N} E\left\{x'[n_1]x'[n_2]\right\} E\left\{y'[n_1]y'[n_2]\right\}$$
$$= \sum_{n_1=1}^{N} E\left\{x'^2[n_1]\right\} E\left\{y'^2[n_1]\right\} = N\sigma_x^2\sigma_y^2 \tag{2.39}$$

In a similar manner, it can be proved : $T_2 = N\sigma_x^2\sigma_y^2$ and $T_3 = N^2\sigma_x^2\sigma_y^2$ and therefore (2.33) will be resulted.

To calculate MSE $\{\hat{c}\}$, we write (17) and (18) in terms of sample means and introduce two error terms, namely R_0 and R_1 as:

$$\hat{E}_0 + R_0 = \hat{E}_{|d|}(1 + c\hat{I}_2), \tag{2.40}$$

$$\hat{E}_1 + R_1 = \hat{E}_{|d|}(\hat{I}_1 + c\hat{I}_3). \tag{2.41}$$

From the above lemma, mean and variance of R_0 and R_1 can be calculated as :

$$\begin{aligned}
&E(R_0) = E(R_1) = 0\\
&E(R_0^2) = \frac{1}{N}\sigma_{|d|}^2\sigma_{(1+c|i|^2)}^2 = \frac{1}{N}\sigma_{|d|}^2 c^2(I_4 - I_2^2)\\
&E(R_1^2) = \frac{1}{N}\sigma_{|d|}^2\sigma_{(|i|+c|i|^3)}^2 = \frac{1}{N}\sigma_{|d|}^2\left((I_2 - I_1^2) + 2c(I_4 - I_1I_3) + c^2(I_6 - I_3^2)\right)
\end{aligned} \tag{2.42}$$

Also in a similar way as the above lemma it can be proved that:

$$E(R_0R_1) = \frac{1}{N}\sigma_{|d|}^2\left(c(I_3 - I_1I_2) + c^2(I_5 - I_2I_3)\right). \tag{2.43}$$

By dividing (2.40) by (2.41) we have:

$$\frac{\hat{E}_0 + R_0}{\hat{E}_1 + R_1} = \frac{1 + c\hat{I}_2}{\hat{I}_1 + c\hat{I}_3}. \tag{2.44}$$

From (2.44), c is obtained as:

$$c = \frac{(\hat{E}_0 + R_0)\hat{I}_1 - (\hat{E}_1 + R_1)}{(\hat{E}_1 + R_1)\hat{I}_2 - (\hat{E}_0 + R_0)\hat{I}_3} = \frac{\hat{A} + \varepsilon_1}{\hat{B} + \varepsilon_2} = \frac{A}{B}, \tag{2.45}$$

where A, B, $\hat{A}$ and $\hat{B}$ and the error terms ε_1 and ε_2 are defined as:

$$\begin{array}{ll}
A = E_0I_1 - E_1 & B = E_1I_2 - E_0I_3\\
\hat{A} = \hat{E}_0\hat{I}_1 - \hat{E}_1 & \hat{B} = \hat{E}_1\hat{I}_2 - \hat{E}_0\hat{I}_3\\
\varepsilon_1 = R_0\hat{I}_1 - R_1 & \varepsilon_2 = R_1\hat{I}_2 - R_0\hat{I}_3
\end{array} \tag{2.46}$$

According to (24), $\hat{c} = \frac{\hat{A}}{\hat{B}}$. When $\frac{\varepsilon_2}{B}$ is small $(c - \hat{c})$ is obtained as:

$$c - \hat{c} = \frac{A}{B}\left(\frac{1 - \frac{\varepsilon_1}{A}}{1 - \frac{\varepsilon_2}{B}}\right) - \frac{A}{B} \simeq -\frac{1}{B}\varepsilon_1 + \frac{A}{B^2}\varepsilon_2. \tag{2.47}$$

Hence MSE$\{\hat{c}\}$ will be:

$$\text{MSE}\{\hat{c}\} = E\{(c - \hat{c})^2\} \simeq \frac{1}{B^2}E(\varepsilon_1^2) + \frac{A^2}{B^4}E(\varepsilon_2^2) - \frac{A}{B^3}E(\varepsilon_1\varepsilon_2). \tag{2.48}$$

Using (2.42) and (2.43), (2.48) can be simplified as:

$$\text{MSE}\{\hat{c}\} \simeq \frac{1}{N}\frac{\sigma_{|d|}^2}{E_{|d|}^2}A(I_1..I_6, c), \tag{2.49}$$

where

$$A(I_1..I_6, c) = \frac{1}{(I_1 I_2 - I_3)^2}\left(\begin{array}{l} c^2(I_4 - I_2^2)(I_1 + cI_3)^2 + \\ (I_2 - I_1^2 + c^2(I_6 - I_3^2) + 2c(I_4 - I_1 I_3))(1 + cI_2)^2 - \\ 2c(c(I_5 - I_2 I_3) + I_3 - I_1 I_2)(I_1 + cI_3)(1 + cI_2) \end{array}\right). \tag{2.50}$$

To evaluate (2.49), I_k and $E_{|d|}$ can be calculated for specific modulations of $i[p_s]$ and $d[p_s]$. If the $i[p_s]$ and $d[p_s]$ are zero mean unit variance CSCG random variables then $|i[p_s]|$ and $|d[p_s]|$ have Rayleigh distributions and we obtain [28]:

$$I_k = E\{|i[p_s]|^k\} = E\{|d[p_s]|^k\} = \Gamma(\frac{k}{2} + 1), \quad E_{|d|} = I_1, \quad \sigma_{|d|}^2 = I_2 - {I_1}^2, \tag{2.51}$$

where $\Gamma(.)$ is the Gamma function. Using (2.51), (2.49) is simplified as:

$$\text{MSE}\{\hat{c}\} \simeq \frac{1}{N}(0.3 + 1.8c + 4c^2 + 3.4c^3 + c^4). \tag{2.52}$$

Chapter 3

System Study on Nonlinear Suppression of Varying-Envelope Local Interference[1]

3.1 abstract

In multimode transceivers, a local transmitter may induce a large interference in a local receiver, often several orders of magnitude larger than the desired received signal. To suppress this interference linearly, the receiver would need a very large dynamic range, resulting in excessive power consumption. A potentially much more power-efficient approach involves a memoryless nonlinearity that can strongly suppress interference when accurately adapted to the interference envelope. This approach has so far been limited to constant-envelope interferers owing to the difficulty of extracting accurate interference envelope information from the compound received signal. In this paper, we observe that in multimode transceivers the locally available baseband interference enables accurate adaptation for varying-envelope interferences. The paper performs a system study to explore the resulting performance. Specifically, we show that for varying-envelope interferences, nonlinear

[1]This chapter is reproduced from the paper submitted as H. Habibi, E.J.G. Janssen, Wu Yan, P.G.M. Baltus, J.W.M. Bergmans, "System Study on Nonlinear Suppression of Varying-Envelope Local Interference in Multimode Transceivers", to *International Journal of Electronics and Communications.*

distortion products emerge that are negligible for constant-envelope interferences. We analyze these products, identify the conditions for which adequate interference suppression is combined with negligible distortion, and show that these conditions are met in most cases of practical interest. Simulations for a broad set of modulation schemes corroborate this analysis.

3.2 Introduction

The number of communication standards supported by handheld devices has been increasing rapidly in recent years. To implement these standards in a single device, a combination of several transceivers is required, which is called a multimode transceiver [18]. Owing to the small size of a multimode transceiver, the transmitted signal of a Local Transmitter (LTX) is received by the Local Receiver (LRX) for another communication standard with a small attenuation, inducing a large interference on the received desired signal. For example, let us consider simultaneous operation of a WLAN Receiver (RX) operating in the frequency range of 2400-2483 MHz and a local WiMAX transmitter (TX) operating in the frequency range of 2496-2690 MHz. The transmitted WiMAX signal can be as high as 23 dBm, while the WLAN received signal can be as low as -82 dBm [20]. The coupling loss between transceivers in a multimode transceiver is typically between 10 to 30 dB [19]. Hence the locally induced interference by the WiMAX TX can be as high as 13 dBm, resulting in a Signal to Interference Ratio (SIR) of -95 dB at the input of the WLAN RX Front-End (FE).

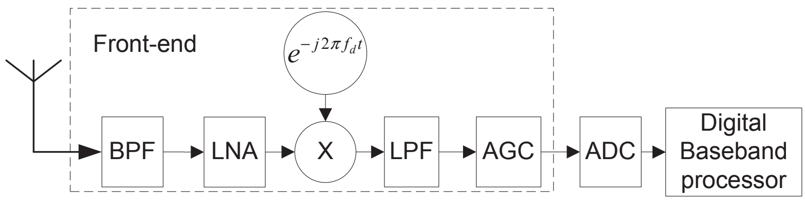

Figure 3.1: Direct conversion receiver.

In this paper, we consider a direct-conversion architecture for the receiver, which is a popular choice for implementation in integrated circuits. Fig. 3.1 shows such a receiver tuned to the center frequency f_d of the received desired signal. The received signal is collected by an antenna and is passed through a bandpass filter (BPF) to limit the input frequency range. The BPF output is amplified by a Low Noise Amplifier (LNA). The amplified signal is down-converted to zero frequency by a quadrature mixer with local oscillator frequency of f_d. The complex-valued output of the mixer is filtered by a Low-Pass filter (LPF) to select a certain frequency channel. The LPF output is amplified by an Automatic Gain Control

(AGC) block before sampling and quantizing by an Analog to Digital Converter (ADC). The ADC output is processed in a digital baseband processor to extract the transmitted information.

3.2.1 Interference suppression by linear filtering

In the direct-conversion receiver FE, any interference is partly suppressed by the BPF and the LPF. Firstly, the BPF suppresses out-of-band interference to some extent. Secondly, the LPF suppresses all the components outside the frequency channel of the received desired signal. However, when the frequency separation between the desired signal and interference is small, the linear filtering cannot sufficiently suppress the interference, as we will see in Section 3.3.2. For example in the WLAN LRX and WiMAX LTX scenario, for the smallest possible frequency separation, the SIR at the ADC input of the WLAN LRX can be as low as -60 dB.

After sampling and quantizing the combination of the desired signal and interference, further suppression of the interference is possible in principle. The interference can be suppressed by digital filtering and nonlinear distortion, caused by presence of the large interference, can be compensated [13]. However, to quantize the desired signal in the presence of a large interference, we have to increase the maximum amplitude that the ADC can handle. With a fixed quantization step, this is achieved by increasing the number of ADC bits n_b. As we will see in Section 3.3.2, to handle the worst case condition for the WLAN RX and WiMAX TX scenario we need 10 additional ADC bits compared to what is required to quantize the desired signal in the absence of any interference. The ADC power consumption for a certain technology and architecture is proportional to 2^{n_b} [29]. Hence the additional 10 bits result in a 1000-fold increase of the power consumption. To avoid this excessive power penalty the interference must be suppressed before the ADC. Also, the presence of a large interference along with the small desired signal can lead to excessive loss of gain of the active components of the receiver, e.g. LNA, mixer and LPF (in case of active mixer and LPF) [21]. Hence it is very desirable to suppress the interference at an early stage in the receiver.

3.2.2 Interference cancellation

In the multimode transceiver, the transmitted interference is available locally. Hence we can use the transmitted interference as a reference signal to generate a replica of the received interference and subtract it from the received signal. If the reference signal is taken from the Radio Frequency (RF) output of the LTX then the generation is done solely in the analog domain [30] [5]. Analog generation of the replica is complex and leads to a high power consumption. Also the replica cannot be constructed accurately, especially if the cancellation point is postponed till after the LNA and the BPF. If the discrete-time baseband interference is used as the reference signal, then a baseband equivalent of the replica can be generated digitally with a high accuracy. The drawback of using the discrete-time reference is that it requires an auxiliary transmitter for generation of the replica, including 2 DACs, up-converters and amplifiers.

3.2.3 Nonlinear interference suppression

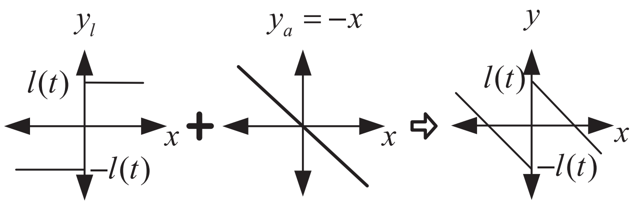

Figure 3.2: NIS input-output characteristic.

An alternative approach to linear filtering and cancellation is to suppress the interference by passing the input signals through a memoryless nonlinearity [16]. Its input-output characteristic as shown in Fig. 3.2, can be realized by combining a limiter with a variable limiting amplitude $l(t)$ and a linear amplifier (here with gain of -1). We call this a Nonlinear Interference Suppressor (NIS). The NIS input includes an interference much larger than the desired signal. The limiter gain for the interference is positive and proportional to $l(t)$ divided by the input envelope. For a constant-modulus interference, $l(t)$ can be tuned such that the limiter gain for the interference equals to 1. Hence the NIS gain for the interference equals to 0 and the interference is suppressed at the NIS output. On the other hand, owing to the compressive behavior of the limiter, the limiter gain for the desired signal is smaller than 1. Hence the NIS gain for the desired signal will be strictly larger than 0. An early implementation of the NIS was used in [31] to suppress a strong constant-envelope interference in spread spectrum receivers.

The limiting amplitude $l(t)$ that results in complete interference suppression depends on the envelope of the received interference at the NIS input. For a constant-envelope interference, $l(t)$ must be tuned to track the slow changes in the power of the received interference. This slowly varying tuning signal can be extracted accurately from the NIS input [31]. For a varying-envelope interference, $l(t)$ must be adapted proportional to the envelope of the received interference. Extracting the adaptation signal $l(t)$ from the compound received signal at the NIS input has the following drawbacks:
1- requires an auxiliary receiver for the received interference,

2- introduces a considerable delay. Hence the same delay must be added before the NIS input to synchronize the NIS input with $l(t)$.
The added complexity of the auxiliary receiver and the difficulty of implementing an analog synchronization scheme make the method in [31] unattractive for varying-envelope interferences.

3.2.4 Adaptive nonlinear interference suppression

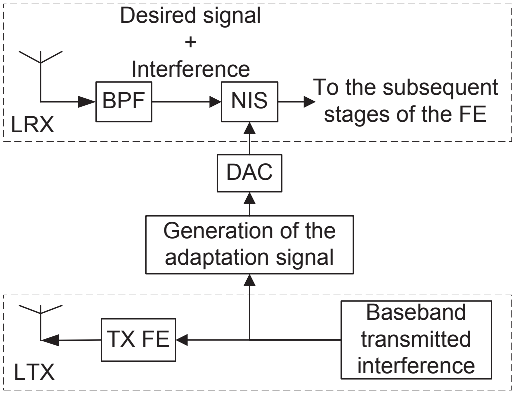

Figure 3.3: Proposed adaptation method for the multimode transceivers.

In multimode transceivers the transmitted baseband interference is locally available. We propose to generate the adaptation signal from the baseband interference, as shown in Fig. 3.3. Unlike the method in [31], for the proposed method:
1- the adaptation signal is generated digitally and hence an auxiliary receiver is not required,
2- the transmitted interference is known in advance and a digital delay can be introduced in the LTX FE or calculation of the adaptation signal to exactly synchronize $l(t)$ with the NIS input.
Hence the proposed method is not limited to constant-envelope interferences as in [31]. The impact of LTX and LRX components on the envelope of the received interference, from the baseband transmitted interference to the received interference at the NIS input, can be taken into account digitally. The coupling between LTX and LRX can be accurately estimated as shown in [32]. Hence in this paper we assume that the adaptation signal $l(t)$ can be determined accurately. A novel state of the art implementation of the NIS for varying-envelope interferences can be found in [33]. The required analog hardware for the nonlinear suppression method is one DAC and the NIS circuit. Hence compared to the cancellation method, the proposed method has a lower power consumption and complexity. We show that by using the combination of the NIS and the channel filter (the LPF), the local interference is suppressed such that SIR at the ADC input will be

much larger than 0 dB. Hence the number of required ADC bits and the power consumption of the receiver with the NIS will be reduced significantly compared to a direct-conversion receiver without NIS (which we henceforth call the baseline receiver).

We will see that using the NIS for varying envelope interferences leads to introduction of in-band nonlinear distortion products, which are negligible for constant-envelope interferences. These products, which were not identified in previous work [16] [31] [34] [35] [36] [37], can be categorized as:

1. Gain Variation Distortion (GVD): The NIS gain for the desired signal depends on the ratio of envelope of the desired signal to envelope of the interference. As a result the gain varies over time and this leads to distortion of the desired signal. The GVD can degrade the Symbol Error Rate (SER) of the receiver. As we will see in section 3.4.3, the GVD and consequently the SER degradation increases when SIR at the NIS input increases. We show that when the SIR at the NIS input is smaller than a threshold, the SER degradation due to the GVD will be negligible. Also, in section 3.5.3 we will see that for SIRs larger than this threshold, the baseline receiver can handle the interference with no or at most a few additional ADC bits. Hence we can cover the complete range of input SIRs with no or at most a few additional ADC bits.

2. Inter-modulation (IM) leakage: The IM is centered at a frequency different from the center frequency of the desired signal. However, depending on the frequency separation of the desired signal and interference, a part of the IM may leak into frequency channel of the desired signal. For the smallest frequency separation of the desired signal and interference this IM leakage can limit the SER performance of the receiver. However the IM leakage vanishes rapidly with increasing the frequency separation and is negligible for most conditions of practical interest.

The rest of this paper is organized as follows. In Section 3.3, we describe the models of the baseline receiver and of the receiver with the NIS. In Section 3.4, we describe the NIS model, and derive the ideal adaptation signal for interference suppression. We then analyze the NIS interference suppression and the impact of the NIS on the desired signal. In Section 3.5 the simulation results are presented. The concluding remarks are provided in Section 3.6.

3.3 System model

In this section, we describe models of the baseline receiver, i.e. the receiver without the NIS, and of the receiver with the NIS. The ADC input will be analyzed so as to determine the number of required bits for each receiver and evaluate the effects of using the NIS in the receiver. While the developed methods are general, we choose typical specifications of a WLAN receiver as an example. Fig. 3.1 and Fig. 3.4 show the baseline receiver and the receiver with the NIS, respectively. First we analyze the received signal in the baseline receiver and then we perform the same analysis for the receiver with the NIS.

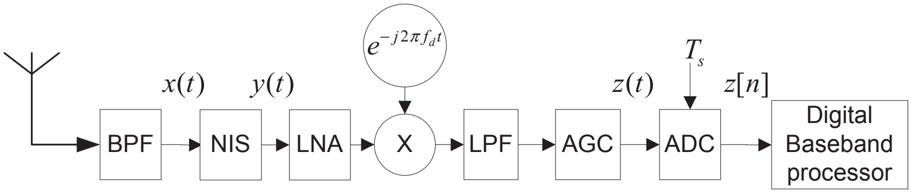

Figure 3.4: Direct conversion receiver with NIS.

3.3.1 The received signal after the BPF

The signal collected by the antenna is passed through the BPF. In both receivers we have the same signal after the BPF. The desired signal is almost passed unchanged through the BPF. The interferences with large frequency separation from the desired signal are suppressed by the BPF. With a small frequency separation, the local interference is attenuated only slightly by the BPF. Then the BPF output $x(t)$ includes both the desired signal and interference as:

$$x(t) = A_d(t)\cos(2\pi f_d t + \varphi_d(t)) + A_i(t)\cos(2\pi f_i t + \varphi_i(t)). \tag{3.1}$$

where A_i, φ_i, f_i, A_d, φ_d, f_d are envelope, phase and center frequencies of the interfering and desired signals after the BPF, respectively. We neglect the input channel noise in (3.1). The reason is that the input noise is bandlimited by the BPF. Hence its power is much smaller than power of the desired signal and it does not necessitate any additional ADC bits for the baseline receiver. For the receiver with the NIS the effect of input noise will be discussed in section 3.4.5. In the simulations of section 3.5, we take into account the input noise by adding Gaussian noise bandlimited by the BPF to $x(t)$ in (3.1). The SIR after the BPF is defined as:

$$\mathrm{SIR}_x = \frac{\mathrm{E}(A_d^2)}{\mathrm{E}(A_i^2)}, \tag{3.2}$$

where E() denotes statistical expectation. For the sample scenario mentioned before SIR_x can be low as -90 dB.

3.3.2 baseline receiver

For the baseline receiver of Fig. 3.1, the BPF output $x(t)$ is amplified by the LNA, and down-converted by a quadrature mixer. The complex-valued output of the mixer is passed through the LPF and amplified by the AGC. The complex-valued AGC output $z'(t)$ will be:

$$z'(t) = A'_{d,z}(t)e^{j\varphi_d(t)} + A'_{i,z}(t)e^{j(2\pi\Delta ft+\varphi_i(t))}, \tag{3.3}$$

where $A'_{d,z}(t)$ and $A'_{i,z}(t)$ are desired signal and interference envelopes. Frequency separation $f_i - f_d$ is denoted as Δf. During processing in the FE, both the desired signal and the interference are amplified by the LNA and AGC and the interference is suppressed by the LPF. As a result the SIR for $z'(t)$, defined as:

$$\mathrm{SIR}_{z'} = \frac{\mathrm{E}((A'_{d,z})^2)}{\mathrm{E}((A'_{i,z})^2)}, \tag{3.4}$$

equals SIR_x multiplied by the suppression by the LPF of the interference centered at Δf. The AGC output is sampled and quantized by the ADC at a sampling rate of $F_s = \frac{1}{T_s}$.

The baseline receiver relies on linear suppression of the interference, partly by the LPF and the BPF and partly by digital filtering after ADC conversion. In the case that both standards share the same frequency band, like WLAN and Bluetooth, the BPF does not attenuate the interference. In the case of standards with small frequency separation, like WLAN and WiMAX, the suppression that can be achieved is limited to about 5 to 30 dB. The LPF suppression depends on the type of the LPF and on Δf. For example, consider a fourth order Butterworth LPF with 3 dB bandwidth of 10-12 MHz, commonly used in WLAN receivers [38], [39]. For $\Delta f = 30$ MHz, the suppression at 30 MHz is about 30 dB. As a result for the WLAN RX plus WiMAX TX scenario mentioned in the introduction, $\mathrm{SIR}_{z'}$ can be as low as -60 dB. Here to achieve a 0 dB SIR at the ADC input, an analog low pass filter with an impractical order of 12 should be used. One can verify that for negative SIRs at the ADC input, for every 6 dB decrement of SIR we have to add one additional ADC bit to quantize the desired signal in the presence of the interference (Appendix I). As a result we require 10 additional ADC bits compared to an ADC that quantizes only the desired signal. These 10 additional bits result in a 10^3 fold increase in the ADC power consumption.

3.3.3 Receiver with NIS

For the receiver with the NIS, shown in Fig. 3.4, $x(t)$ is passed through the NIS to suppress the interference. As we will see in section 3.4.2, the NIS output $y(t)$ includes three dominant components with center frequencies close to f_d:

$$y(t) \cong A_{d,y}(t)\cos(2\pi f_d t + \varphi_d(t)) + A_{i,y}(t)\cos(2\pi(f_d + \Delta f)t + \varphi_i(t)) \\ + A_{\mathrm{IM}}(t)\cos(2\pi(f_d + 2\Delta f)t + 2\varphi_i(t) - \varphi_d(t)), \tag{3.5}$$

where $A_{d,y}(t)$, $A_{i,y}(t)$ and $A_{\mathrm{IM}}(t)$ are envelopes of the interference, desired signal and main Inter-Modulation (IM) component at the NIS output, respectively. The NIS output $y(t)$ is amplified by the LNA, and down-converted by a quadrature mixer. The complex-valued output of the mixer is passed through the LPF and amplified by the AGC. The complex-valued AGC output $z(t)$ is:

$$z(t) \cong A_{d,z}(t)e^{j\varphi_d(t)} + A_{i,z}(t)e^{j(2\pi\Delta f t + \varphi_i(t))} \\ + A_{\mathrm{IM},z}(t)e^{j(4\pi\Delta f t + 2\varphi_i(t) - \varphi_d(t))}. \tag{3.6}$$

Similar to the baseline receiver, $z(t)$ is sampled and quantized by the ADC with a sampling rate of F_s. Compared to the baseline receiver, $z(t)$ in (3.6) includes the IM component.

3.4 Nonlinear interference suppressor

In this section, firstly we present a model of the NIS and derive the adaptation signal that leads to complete interference suppression in the absence of the desired signal. For this adaptation signal we then derive the NIS output in the presence of the desired signal and identify and analyze the key distortion products at the NIS output.

3.4.1 NIS modeling and adaptation

As shown in Fig. 3.2, the NIS can be built by combining a linear Input/Ouput (I/O) curve and a nonlinear I/O curve (a hard limiter) with a variable limiting amplitude. The combined output $y(t)$ will be:

$$y(t) = y_l(t) + y_a(t) = f(x(t)) = \begin{cases} -l(t) - x(t) & x < 0, \\ 0 & x = 0, \\ l(t) - x(t) & x > 0, \end{cases} \tag{3.7}$$

where $x(t)$ is the NIS input, $y_a(t)$ is the amplifier output, $y_l(t)$ is the limiter output, and $l(t)$ is the limiting amplitude. Although this simple model may not reflect all characteristics of an analog implementation of the NIS, it captures the main benefits and drawbacks of using the NIS and makes it possible to analyze the NIS impact on the receiver.

By changing $l(t)$, we can change the I/O curve of the NIS, i.e. $f(x)$. In this section, we show how to adapt $l(t)$ to null the interference at the NIS output. Because we are interested in the conditions that the interference is much larger than the desired signal, first we look at the simple case where only interference is present. In this case the NIS input will be:

$$x(t) = A_i(t)\cos(2\pi f_i t + \varphi_i(t)) = A_i(t)\cos(\theta_i(t)). \tag{3.8}$$

The NIS output $y(t) = f(x(t))$ has harmonic components with center frequencies at integer multiples of f_i. We assume that all the harmonic components, except the fundamental component at f_i, will be filtered out by the LPF. Hence, we only consider the fundamental component of $y(t)$. We assume that the bandwidth of $x(t)$ is small enough compared to f_i so that $A_i(t)$ and $\varphi_i(t)$ can be assumed constant during one period of the carrier ($0 < \theta_i(t) < 2\pi$). Using this assumption the NIS output can be written as:

$$y(t) = A_{i,y}(A_i(t))\cos(2\pi f_i t + \varphi_i(t)),$$

where $A_{i,y}$ is envelope of the NIS output at the fundamental frequency f_i and $A_{i,y}(A_i(t))$ is obtained as [34]:

$$A_{i,y}(A_i) = \frac{2}{\pi}\int_0^{\pi} f(A_i\cos(\theta_i))\cos(\theta_i)d\theta_i = \frac{4l(t)}{\pi} - A_i(t).$$

By solving $A_{i,y}(A_i) = 0$, the adaptation signal that nulls the interference at the NIS output is obtained as:

$$\tilde{l}(t) = \frac{\pi A_i(t)}{4}. \tag{3.9}$$

3.4.2 NIS output in the presence of the desired signal

In this section we analyze the NIS output $y(t)$ in (3.5) in the presence of the desired signal. In the limit when $A_d \to 0$, adapting the NIS according to (3.9) results in the full suppression of the interference. Hence for the situation that the desired signal is much smaller than the interference, we expect a large suppression of the interference by adapting the NIS according to (3.9).

The NIS output is described in (3.5), where $A_{i,y}$, $A_{d,y}$ and $A_{\mathrm{IM}}(t)$ can be calculated as [40]:

$$
\begin{aligned}
A_{i,y}(A_i, A_d) &= \frac{2}{\pi^2}\int_0^{\pi}\int_0^{\pi} f(A_i\cos\theta_i + A_d\cos\theta_d)\cos\theta_i d\theta_i d\theta_d \\
A_{d,y}(A_i, A_d) &= \frac{2}{\pi^2}\int_0^{\pi}\int_0^{\pi} f(A_i\cos\theta_i + A_d\cos\theta_d)\cos\theta_d d\theta_i d\theta_d \\
A_{\mathrm{IM}}(A_i, A_d) &= \frac{2}{\pi^2}\int_0^{\pi}\int_0^{\pi} f(A_i\cos\theta_i + A_d\cos\theta_d)\cos(2\theta_i - \theta_d) d\theta_i d\theta_d. \quad (3.10)
\end{aligned}
$$

In (3.10), it is assumed that the bandwidths of the desired signal and interference are small compared to f_m and f_i so that $A_i(t)$, $A_d(t)$, $\varphi_i(t)$ and $\varphi_d(t)$ can be assumed constant during one period of the carriers ($0 < \theta_i(t) = 2\pi f_i t + \varphi_i(t) < 2\pi$ and ($0 < \theta_d(t) = 2\pi f_d t + \varphi_d(t) < 2\pi$)). An odd-symmetric input-output characteristic, e.g the NIS in Fig. 3.2, only produces odd-order IM components at its output. Such a characteristic can be implemented using a differential topology.

For the receiver with the NIS, to determine the number of required additional ADC bits, we can calculate the ratios of the desired signal envelope to the interference and IM component envelopes at the ADC input and use (3.27), in Appendix I. The LPF suppression for the interference and IM depends on Δf and on the LPF type. Hence, we analyze these ratios before the LPF to make our analysis easily applicable to other types of LPF and values of Δf. The ratios at the ADC input can be calculated easily by multiplying the LPF suppression to the ratios at the NIS output. The Instantaneous ratio of the desired Signal to Interference ISIR_y at the NIS output is defined as:

$$\mathrm{ISIR}_y(t) = \left(\frac{A_{d,y}(t)}{A_{i,y}(t)}\right)^2. \quad (3.11)$$

The Instantaneous ratio of the desired Signal to IM component ISIMR_y at the NIS output is defined as:

$$\mathrm{ISIMR}_y(t) = \left(\frac{A_{d,y}(t)}{A_{\mathrm{IM}}(t)}\right)^2. \quad (3.12)$$

Also we need to calculate the instantaneous gain $g_d(t)$ of the desired signal, defined as:

$$g_d(t) = \frac{A_{d,y}(t)}{A_d(t)}. \quad (3.13)$$

To prevent distortion of the desired signal, $g_d(t)$ should be independent of t. However we will see that this is not true here. Using (3.10), the ratios in (3.11)-(3.13) can be evaluated. One can easily verify that the quantities in (3.11)-(3.13) are fully determined by Instantaneous SIR $\mathrm{ISIR}_x(t)$ at the NIS input defined as:

$$\mathrm{ISIR}_x(t) = \left(\frac{A_d(t)}{A_i(t)}\right)^2. \quad (3.14)$$

When $\mathrm{ISIR}_x(t) \ll 1$, the integrals in (3.10) can be approximated as: $A_{i,y} = 0$ and $A_{d,y} = A_{\mathrm{IM}} = -\frac{A_d}{2}$ [35], which results in:

$$\mathrm{ISIMR}_y(t) = 1, \quad \mathrm{ISIR}_y(t) = \infty, \quad g_d(t) = -\frac{1}{2}. \tag{3.15}$$

Although the NIS is targeted for scenarios with $\mathrm{SIR}_x \ll 1$, ISIR_x may span $[0+\infty]$ for varying envelope signals (e.g. for an OFDM interference $A_i(t)$ can become momentarily zero resulting the $\mathrm{ISIR}_x(t)$ to become $+\infty$). Hence we should evaluate the quantities in (3.11)-(3.13) more accurately than (3.15). Because the integrals in (3.10) do not have closed form solutions, we use numerical integration to evaluate the ratios in (3.11)-(3.13).

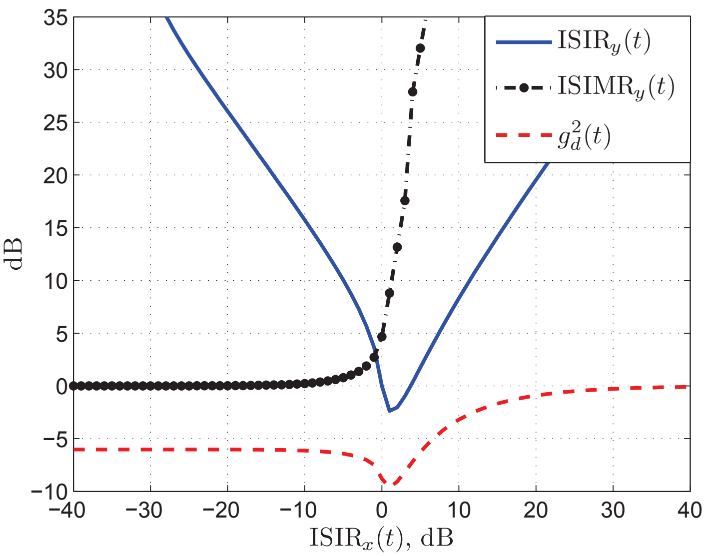

Figure 3.5: $\mathrm{ISIR}_y(t)$, $\mathrm{ISIMR}_y(t)$ and $g_d^2(t)$ versus $\mathrm{ISIR}_x(t)$.

Fig. 3.5 shows $\mathrm{ISIR}_y(t)$, $\mathrm{ISIMR}_y(t)$ and ${g_d}^2(t)$ versus $\mathrm{ISIR}_x(t)$.

1. From the ISIR_y curve, we see that the interference is not entirely nulled at the NIS output, especially for $\mathrm{ISIR}_x(t)$ values in the vicinity of 0 dB. However the minimum of $\mathrm{ISIR}_y(t)$ equals -3 dB. The LPF further suppresses the interference after the NIS. For example for the WLAN and WiMAX scenario, the suppression of the discussed LPF at $\Delta f = 30$ MHz, equals 30 dB. Hence the power of the residual interference at the ADC input will be much smaller than the power of the desired signal.

2. From the ISIMR_y curve, we see that the IM component is present at the NIS

output, especially for $\text{ISIR}_x(t) < 0$ dB . The minimum of ISIMR_y is 0 dB and the LPF further suppress the IM component prior to the ADC. For the same scenario and LPF, the LPF suppression at the center frequency of the IM component (here $2\Delta f = 60$ MHz) will be 60 dB. Hence the power of the IM at the ADC input will be much smaller than the power of the desired signal. It must be considered that 60 dB is the LPF suppression at $2\Delta f$. The exact amount of LPF suppression of the IM depends on spectrum of the IM and Δf. Actually a part of the IM may leak into frequency channel of the desired signal. In section 3.5.1 we evaluate this IM leakage versus Δf for the WLAN RX plus WiMAX TX scenario.

3. From the g_d^2 curve, we see that $g_d(t)$ depends on $\text{ISIR}_x(t)$. The variation of $g_d(t)$ leads to in-band nonlinear distortion of the desired signal. In section 3.4.3 we quantify this gain-variation distortion.

Considering the small power of the residual interference and IM component at the ADC input, the receiver with the NIS does not require any additional ADC bits in the presence of the local interference. Compared to the baseline receiver this is a major reduction in the required number of ADC bits and power consumption.

3.4.3 Gain Variation Distortion

The variation of $g_d(t)$ over time leads to in-band distortion of the desired signal. The GVD is a general form of cross-modulation distortion. The cross-modulation is the transfer of interference modulation to the small desired signal and is only a function of $A_i(t)$ [21]. In this section we will evaluate this Gain Variation Distortion (GVD). Based on Bussgang's decomposition [41], the desired signal $A_{d,y}(t)e^{j\varphi_d(t)}$ at the NIS output can be decomposed into a component proportional to $A_d(t)e^{j\varphi_d(t)}$ and one that is uncorrelated with $A_d(t)e^{j\varphi_d(t)}$:

$$A_{d,y}(t)e^{j\varphi_d(t)} = \bar{g_d}A_d(t)e^{j\varphi_d(t)} + A_e(t)e^{j\varphi_d(t)}, \tag{3.16}$$

where $\bar{g_d}$ is constant and is determined such that $\mathrm{E}\{A_e(t)A_d(t)\} = 0$. We can interpret $\bar{g_d}$ as the average gain of the NIS for the desired signal. By multiplying both sides of (3.16) by $A_d(t)$ and taking the expected value $\bar{g_d}$ is obtained as:

$$\bar{g_d} = \frac{\mathrm{E}(A_{d,y}A_d)}{\mathrm{E}(A_d^2)}. \tag{3.17}$$

Using (3.16) and (3.17) power of the GVD component is obtained as:

$$\mathrm{E}(A_e^2) = \mathrm{E}(A_{d,y}^2) - \bar{g_d}^2\mathrm{E}(A_d^2). \tag{3.18}$$

Using (3.18),the desired Signal to GVD power Ratio (SDR) at the NIS output is obtained as:

$$\mathrm{SDR} = \frac{\mathrm{E}(A_d^2)\bar{g_d}^2}{\mathrm{E}(A_e^2)}. \tag{3.19}$$

3.4.3.1 Case 1: constant-envelope interference and OFDM desired signal

Firstly we consider the case that the interference has a constant-envelope modulation, i.e. $A_i(t) = A_i$, and the desired signal has an OFDM modulation. The desired signal component $A_{d,y}$ at the NIS output can be approximated as [42]:

$$A_{d,y}(t) \cong -\frac{1}{2}A_d(t) + \frac{1}{16A_i^2}A_d^3(t) \qquad \text{for} \qquad A_i > A_d(t). \tag{3.20}$$

For a constant-envelope interference we have $\overline{P_i} = \frac{A_i^2}{2R}$[2], where $\overline{P}_i$ is the interference average power at the NIS input defined as $\overline{P_i} = \mathrm{E}(\frac{A_i^2}{2R})$. Eq. (3.20) can be used to define an Input third-order Intercept point (IIP3) and 1 dB compression point (P1dB) for the desired signal as [21]:

$$\begin{aligned} \mathrm{IIP3} &= 10\log_{10}\left(\frac{32A_i^2}{3}\right) \text{ dBm} + 10 \text{ dB} \\ &\cong \overline{P}_i \text{ dBm} + 10 \text{ dB} \\ \mathrm{P1dB} &\cong \mathrm{IIP3} - 10 \text{ dB} = \overline{P_i}\mathrm{dBm}. \end{aligned} \tag{3.21}$$

In (3.21), we have considered a 50 Ω system. Based on (3.21) the NIS effect on the desired signal can be interpreted as that of a third-order polynomial nonlinear system with an IIP3 point proportional to the power of the local interference. As a rule of thumb, when the power of the desired signal approaches P1dB, the nonlinear distortion becomes evident. The desired signal has an OFDM modulation. Hence the complex-valued baseband desired signal approximately has a Gaussian distribution and its envelope A_d is Rayleigh distributed $A_d \sim \mathrm{Rayleigh}(\sqrt{\overline{P_d}})$ with probability density function as:

$$f_{A_d}(A) = \frac{2A}{\overline{P_d}}e^{-\frac{A^2}{\overline{P_d}}}, \tag{3.22}$$

where A is a positive real number and $\overline{P}_d = \mathrm{E}(\frac{A_d^2}{2R})$ is average power of the desired signal at the NIS input. Now we can approximate SDR at the NIS output as (Appendix III):

$$\mathrm{SDR} \cong 32\frac{(1 - 0.25\mathrm{SIR}_x)^2}{\mathrm{SIR}_x^2}. \tag{3.23}$$

[2] $R = 50\Omega$ is the reference impendence

Using (3.10), $A_{d,y}$ can be calculated numerically and thus SDR can be calculated using (3.17)-(3.19). In Fig. 3.6, the approximate formula in (3.23) is compared with SDR calculated numerically using (3.10). We see that the approximate formula of (3.23) matches the numerical calculation when $\text{SIR}_x = \frac{\overline{P_d}}{\overline{P_i}}$ is small. The SDR decreases as SIR_x increases. When SIR_x increases, the probability of having an ISIR_x close to 0 dB becomes larger. Variations of $g_d(t)$ are largest around ISIR_x=0 dB as observed in Fig. 3.5. Hence the GVD increases by increasing SIR_x which leads to a decrement of SDR.

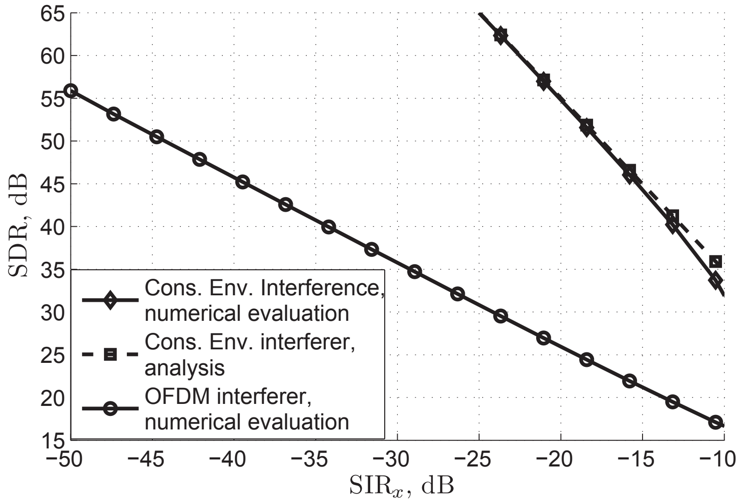

Figure 3.6: SDR vs. SIR_x.

3.4.3.2 Case 2: OFDM interfering and desired signals

Now consider the case that both desired signal and interference are OFDM modulated. Then both A_d and A_i are Rayleigh distributed, $A_d \sim \text{Rayleigh}(\sqrt{\overline{P_d}})$ and $A_i \sim \text{Rayleigh}(\sqrt{\overline{P_i}})$. SDR is evaluated numerically by using (3.10) and (3.17)-(3.19) and is shown in Fig. 3.6 vs. SIR_x. Similar to case 1, SDR decreases as SIR_x increases. Because the variations of $\text{ISIR}_x = \frac{A_d}{A_i}$ are larger when both A_d and A_i are Rayleigh distributed, SDR for case 2 is worse than for case 1. Among typical modulations, OFDM has the largest envelope variations. Hence we can conclude that case 2 has the worst SDR among typical modulations.

3.4.4 IM leakage

The IM component in (3.6) is a nonlinear mixture of the desired signal and interference centered at $2\Delta f$. The IM bandwidth may be large enough to leak into frequency channel of the desired signal. As we saw in Fig. 3.5 for small values of $\text{ISIR}_x(t)$, $A_{\text{IM}}(t) \cong A_{d,y}(t) \cong -\frac{A_d}{2}(t)$. Here we assume that SIR_x is small enough such that $\text{ISIR}_x < -10$ dB most of the time. Hence $A_{\text{IM}}(t)$ can be approximated by $-\frac{A_d(t)}{2}$ and the IM component at the ADC input will be:

$$\text{IM}_z \cong -\frac{1}{2}\left(A_d(t)e^{-j\varphi_d(t)}\right)\left(e^{j\varphi_i(t)}\right)^2 e^{j(2\pi)2\Delta f t}. \tag{3.24}$$

In (3.24), $e^{j\varphi_i(t)}$ is baseband interference after removing the amplitude information. When the interference is constant-envelope, $e^{j\varphi_i(t)}$ is just a scaled version of the interference. Suppose that the bandwidths of the desired and interfering signals are B_d and B_i, respectively. Then the bandwidth of the IM will be $B_d + 2B_i$. As a result for a constant-envelope interference, when $\Delta f > \frac{B_d+B_i}{2}$ there will not be any IM leakage.

For an OFDM interference with a rectangular frequency spectrum, the bandwidth of the phase-modulated component $\psi(t) = e^{j\varphi_i(t)}$ of the interference is infinite [43]. Hence a part of the IM will leak into the frequency channel of the desired signal. In section 3.5.1 the IM leakage will be evaluated for the WLAN RX plus WiMAX TX scenario.

3.4.5 Effect of input channel noise on the receiver with NIS

In section 3.4.2 we saw that the NIS gain $g_d(t)$ for a signal centered at f_d and much smaller than interference is $-\frac{1}{2}$, approximately. For most practical situations, the desired signal power is larger than the in-band noise power. Here the input channel noise is filtered by the BPF and as a result it is roughly centered around f_d. Being a small signal compared to the interference, the effect of the NIS on the input channel noise can be approximated by a constant gain of $-\frac{1}{2}$. As a result the NIS will not change power ratio of the desired signal to the channel noise centered around f_d.

One problem may arise when the channel noise around center frequency of $f_n = 2f_i - f_d$ is not filtered by the BPF. In this case, the input channel noise will be mapped to the frequency of $2f_i - f_n$, which equals f_d (i.e. the desired signal center frequency). This phenomenon will be referred to as spectral mirroring. One example is a WLAN RX and a local Bluetooth TX scenario, where for some of the possible values of f_d and f_i, $f_n = 2f_i - f_d$ can be in the pass-band of the BPF. In this case the power ratio of the desired signal to noise at the NIS output will be 3 dB less than this ratio at the NIS input. This 3 dB loss of signal to noise ratio is likely to be intolerable. However, we have significantly reduced the power consumption for the receiver with the NIS. A part of this saving can be spent on reducing the receiver noise figure as a remedy for this 3 dB loss. For the WLAN RX plus WiMAX TX scenario the channel noise around $f_n = 2f_i - f_d$ is filtered out by the BPF. Hence for this scenario we do not have this problem.

3.5 Simulation Results

In this section, simulation results are presented. We consider the scenario of a WLAN RX with a local WiMAX TX as the interference. The received desired WLAN signal is located at the uppermost part of the WLAN frequency band, channel 13 with center frequency of 2472 MHz and bandwidth of 20 MHz. The WLAN signal has Orthogonal Frequency Division Multiplexing (OFDM) modulation with 64 sub-carriers, where each subcarrier can have QPSK, 16 QAM or 64 QAM modulation. The transmitted WiMAX signal occupies the frequency range of 2496-2690 MHz with bandwidth of 10 MHz. We consider two center frequencies for the WiMAX signal: 2502 MHz and 2532MHz, resulting in frequency separations of Δf =30 MHz and Δf =60 MHz. We consider two cases for WiMAX signal modulation: constant-envelope modulation and OFDM modulation. The maximum allowable transmitted power of the WiMAX TX is 23 dBm. We assume that there is -10 dB coupling between the WiMAX TX and the WLAN RX and the WiMax signal is further attenuated 5 dB by the BPF. Hence SIR_x can be as low as -90 dB.

The IM component is the largest component with small frequency separation from the desired signal. A part of the IM component may leak into frequency channel of the desired signal. We numerically evaluate the IM leakage in the next section. Then we compare SER performance of the receiver with the NIS and the baseline receiver to see the amount of SER degradation due to the GVD and IM leakage. Finally, we evaluate and compare the required number of ADC bits to achieve a certain SER for the baseline receiver and the receiver with NIS.

3.5.1 Evaluation of IM leakage

Fig. 3.7 shows the average power ratio of the desired signal to the IM leakage vs. Δf for the WLAN RX plus WiMAX TX scenario. The WLAN and WiMAX signals both are OFDM modulated and have rectangular shaped frequency spectrums. The power of IM leakage in 20 MHz bandwidth of the WLAN signal is measured by simulation. We observe that the amount of IM leakage decreases 9 dB by doubling Δf when Δf is large. The IM leakage adds to the channel noise and it can degrades the SNR and hence the SER. For 0.5 dB and 0.1 dB degradation to the SNR, the IM leakage should be 9 dB and 16 dB less than the channel noise, respectively.

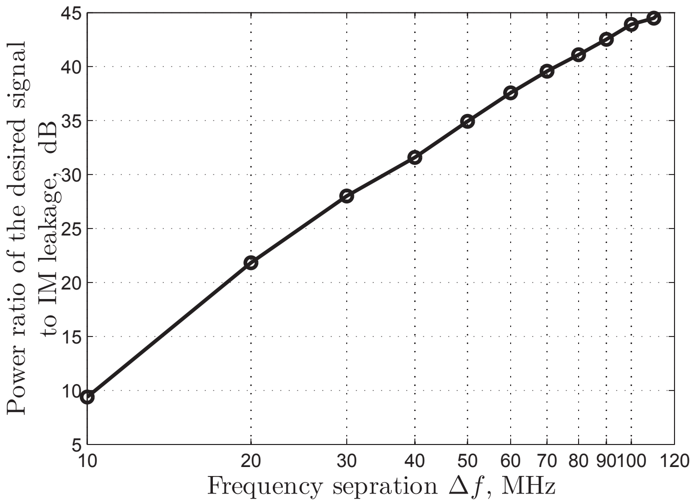

Figure 3.7: Power ratio of desired signal to IM leakage vs. Δf for WLAN RX and WiMAX TX scenario.

3.5.2 SER comparison of the baseline RX and the RX with NIS

We assume that the received WLAN signal is passed through an Additive White Gaussian Noise (AWGN) channel. Hence the SER performance of the baseline RX depends only on the desired Signal to Noise power Ratio (SNR), where the noise power is measured in the frequency channel of the desired signal. The SNR is chosen such that it results in an un-coded SER of 10^{-3} for the baseline RX, which leads to an error free reception after forward error correction of the WLAN RX. The required SNR for QPSK, 16 QAM and 64 QAM is 10.34, 17.6 and 24 dB, respectively [44]. On the other hand, because of the GVD and IM leakage, the SER of the RX with the NIS depends on the SNR, SIR_x and Δf.

In the following sections, firstly we present the simulation results for the constant-envelope interference. Then we continue with the OFDM interference. In all the simulations the desired signal has OFDM modulation.

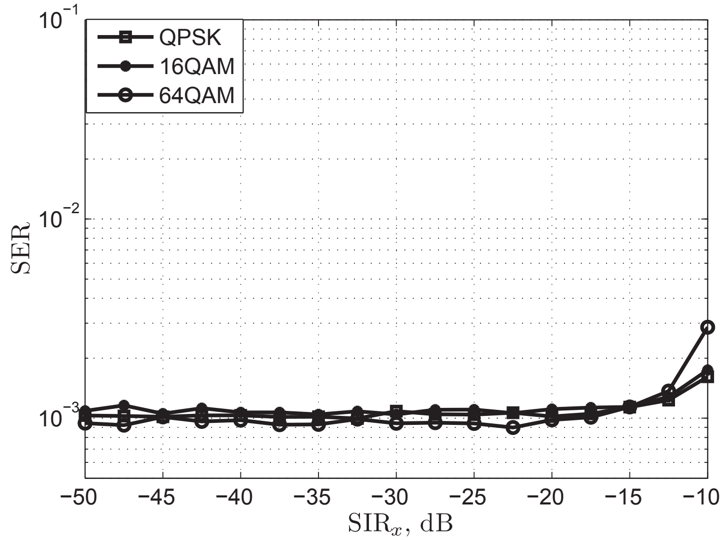

Figure 3.8: SER vs. SIR_x, constant envelope interference and OFDM desired signal, SER of the baseline RX: 10^{-3}, Frequency separation Δf : 30 MHz.

3.5.2.1 SER performance for constant-envelope interference and OFDM desired signal

Consider the case that the interference has a Gaussian Minimum Shift Keying (GMSK) modulation and the desired signal has an OFDM modulation. In Fig. 3.8 and Fig. 3.9 the SER for the RX with the NIS vs. SIR_x is shown for $\Delta f = 30$ MHz and 60 MHz, respectively. In both figures we see that by decreasing SIR_x, SER decreases and reaches 10^{-3}, i.e. SER of the baseline receiver.

The SER degradation due to the GVD depends on SIR_x and becomes evident in both figures when SIR_x increases. This observation is in agreement with Fig. 3.6, where SDR decreases when SIR_x increases. The GVD limits the largest SIR_x for which the NIS offers a negligible SER degradation. We can use Fig. 3.9 to determine this limit for a certain amount of SER degradation. For example when $\Delta f = 30$ MHz, if we want to keep SER less than 1.2×10^{-3} (equivalent to an SNR degradation less than 0.1 dB) then we should stop using the NIS when SIR_x is larger than about -12 dB, -13 dB and -15 dB for desired signal with QPSK, 16 QAM and 64 QAM modulation, respectively.

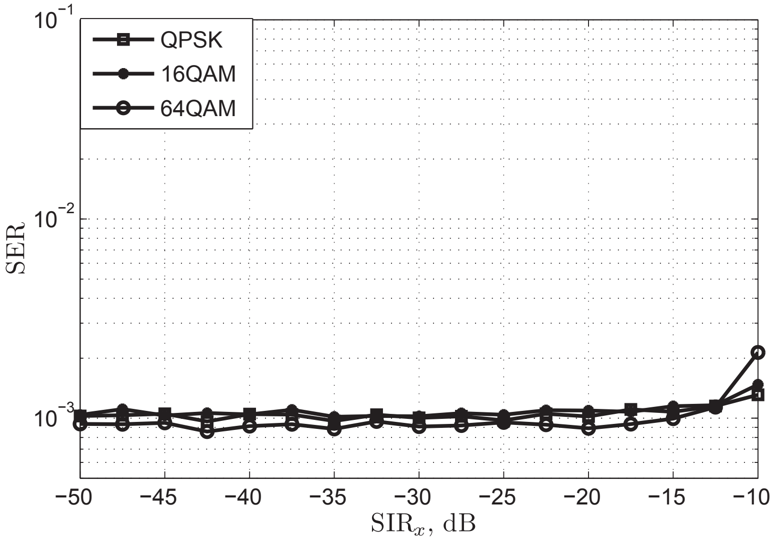

Figure 3.9: SER vs. SIR$_x$, constant envelope interference and OFDM desired signal, SER of the baseline RX: 10^{-3}, Frequency separation Δf : 60 MHz..

3.5.2.2 SER performance for OFDM modulated desired signal and OFDM interference

Now consider the case that both the desired signal and interference have OFDM modulations. In Fig. 3.10 and Fig. 3.11 the SER for the RX with the NIS vs. SIR$_x$ is shown for $\Delta f = 30$ MHz and 60 MHz, respectively. Both figures show that by decreasing SIR$_x$, SER decreases and reaches a floor.

Similar to constant-envelope interference case, the SER degradation due to the GVD becomes evident in both figures when SIR$_x$ increases. However, the observed GDV for an OFDM interference is much larger than for a constant-envelope interference. This observation agrees with the SDR curves in Fig. 3.6. The GVD limits the largest SIR$_x$ which for the NIS offers a negligible SER degradation. Fig. 3.11 can be used to determine this limit for a certain amount of SER degradation. For example when $\Delta f = 60$ MHz, if we want to keep the SER less than 2×10^{-3} (equivalent to an SNR degradation less than 0.5 dB) then we should stop using the NIS when SIR$_x$ is larger than -12 dB, -18 dB and -27 dB for QPSK, 16 QAM and 64 QAM, respectively. Based on this simulation we can find a threshold on SIR$_x$ to use the NIS within a certain amount of SER degradation. Since the degradation for the case that both signals have OFDM modulations is the largest, the threshold calculated for this case guarantees to limit the degradation for all other types of modulation of both signals. As a rule of thumb for the both OFDM

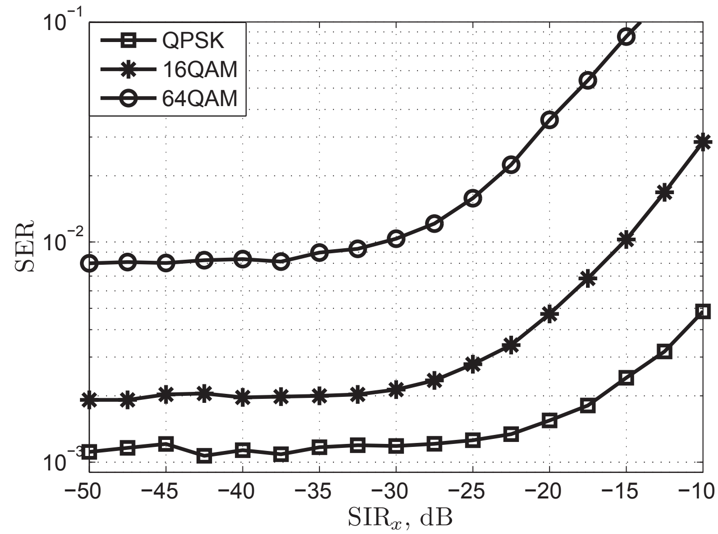

Figure 3.10: SER vs. SIR$_x$ for OFDM modulations, SER of the baseline RX: 10^{-3}, Frequency separation Δf: 30 MHz.

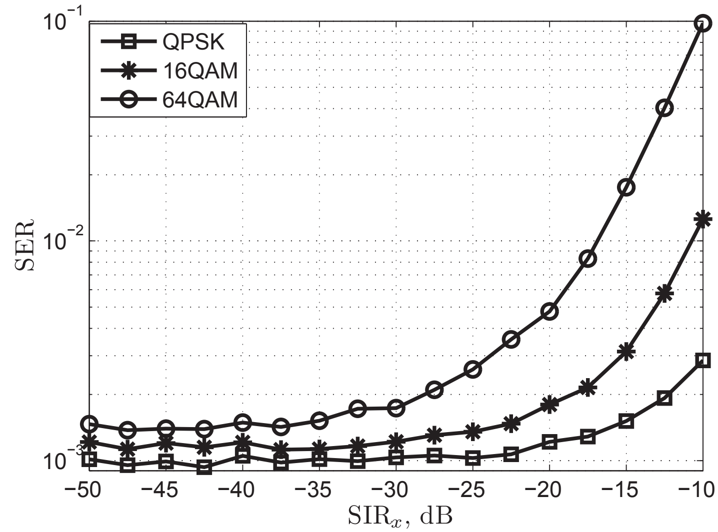

Figure 3.11: SER vs. SIR$_x$ for OFDM modulations, SER of the baseline RX: 10^{-3}, Frequency separation Δf: 60 MHz.

case the threshold for 0.5 dB degradation will be $-$SNR [dB] $-$ 3 and for 0.1 dB degradation it will be $-$SNR [dB] $-$ 7. As we will see in section 3.5.3, when SIR_x is larger than the threshold the baseline receiver can operate with no or a few additional ADC bits.

The distance of the SER floor from the ideal SER of 10^{-3} is very small for $\Delta f =$ 60 MHz as we see in Fig. 3.11. This SER floor, which is independent of SIR_x, originates from the IM leakage and decreases by increasing Δf from 30 MHz (Fig. 3.10) to 60 MHz (Fig. 3.11). The amount of degradation due to the IM leakage can be calculated using Fig. 3.7. For example for $\Delta f = 30$ MHz, the IM leakage power is 28 dB smaller than the desired signal power. For 16 QAM the SNR to achieve an SER of 10^{-3} is 17.6 dB. Hence the ratio of the desired signal to noise plus IM leakage will be 17.2 dB. This 0.4 dB degradation to the SNR translates into an SER floor of about 2×10^{-3}, when GVD becomes negligible (for small SIR_x), as we see in Fig. 3.10. For $\Delta f = 60$ the IM leakage power becomes 37 dB smaller than the desired signal power and the amount of SNR degradation decreases to 0.05 dB which results in an SER floor of 1.1×10^{-3} as we see in Fig. 3.11.

3.5.3 Comparison of the required number of ADC bits

We consider a case that the WLAN received signal has a 16 QAM (OFDM) modulation with an SNR of 17.6 dB, which results in a SER of 10^{-3} for the baseline RX. The frequency separation Δf equals 30 MHz. The ADC sampling frequency is 60 MHz. Hence we can sample $z'(t)$ in (3.3) such that $A'_{i,z}(t)e^{j(2\pi\Delta f t+\varphi_i(t))}$ would not alias into the frequency channel of the desired signal after sampling. This is important for the baseline RX, where the interference is mainly suppressed by digital filtering. Fig. 3.12 shows the required number of bits vs. SIR_x to achieve a target SER smaller than 2×10^{-3} for the baseline RX and the RX with NIS.

For the baseline RX, when $\text{SIR}_x > -30$ dB we have $\text{SIR}_z > 0$ dB. Hence we don't need any additional ADC bits beyond what is required to quantize $A'_{d,z}(t)e^{j\varphi_d(t)}$. When $\text{SIR}_x < -30$ dB, for the same SER performance, we have to increase the number of ADC bits proportional to SIR_x (in dB), as analyzed in section 3.3.2. In [45], a low-power 10 bits ADC suitable for WLAN applications is reported with a power consumption of 12 mW. To handle the interference this ADC already has 3 additional bits compared to 7 bits which are required to quantize only the desired signal. Increasing the number of bits to 17, would increase the ADC power consumption by 2^7 times [29], i.e. to 1536 mW from 12 mW. On the other hand for the receiver with NIS, when $\text{SIR}_x < -30$ dB, the target SER is achieved with only 7 bits. Total power consumption of the NIS circuit [33] and the required blocks to generate the adaptation signal [46] is well below 100 mW. Considering that the power consumption of a typical WLAN transceiver is around 200 mW [47], using

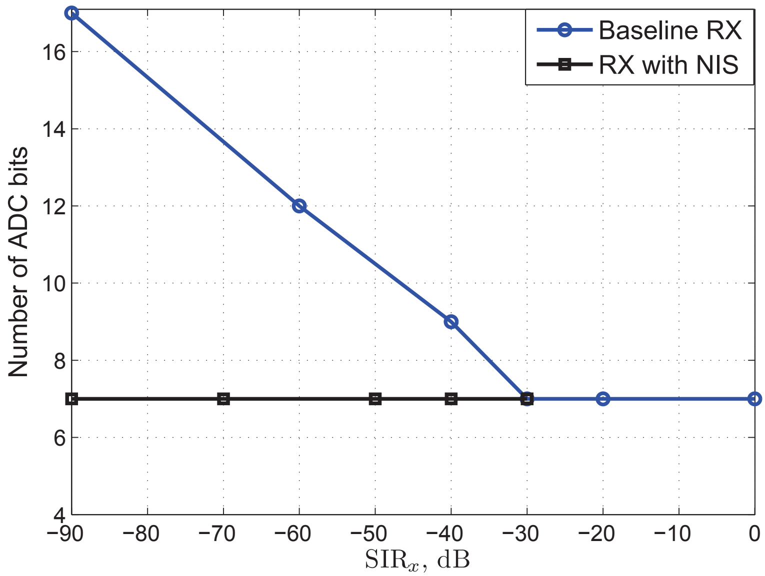

Figure 3.12: Required number of ADC bits to achieve a SER smaller than 2×10^{-3}, 16 QAM modulation, SNR=17.6 dB.

the NIS reduces the power consumption of the multimode transceiver by an order of magnitude.

It must be noted that in Fig. 3.12, due to the IM leakage, 2×10^{-3} is the smallest SER that the RX with NIS can achieve. Based on Fig. 3.7 for $\Delta f > 50$ MHz when $\mathrm{SIR}_x < -30$ dB, the SER will be better than 1.2×10^{-3} (equivalent to 0.1 dB SNR degradation).

3.6 Conclusion

In multimode transceivers, the transmitter for one communication standard may induce a large interference in the receiver for another one. Due to the limitations of linear analog filtering, the interference can still be several orders of magnitude larger than the desired signal at the input of Analog to Digital Converter (ADC) of the receiver. Quantizing the desired signal in the presence of this interference leads to an unrealistic number of ADC bits and excessive power consumption of the receiver. A much more power efficient approach is to use an adaptive Nonlinear Interference Suppressor which was only used for constant-envelope interferences in the previous works. To enable application of this circuit for varying-envelope interferences in multimode transceivers, we proposed a new adaptation method which exploits the availability of the transmitted interference. We showed that the adaptation method can strongly suppress the interference such that it will normally be much smaller than the desired signal at the ADC input. We identified and analyzed the principal distortion products introduced by the NIS, namely Gain Variation Distortion (GVD) and Inter-Modulation (IM) leakage. The GVD increases when desired Signal to Interference power Ratio (SIR) at the NIS input increases. We determined a threshold on SIR below which the NIS offers a negligible degradation to the desired Signal to Noise power Ratio (SNR) at the demodulator input. As a rule of thumb, to limit the SNR degradation to less than 0.1 dB, we should stop using the NIS when the SIR [dB] $\geq$ ($-$SNR [dB]$-$7). For larger SIRs the linear receiver without the NIS can handle the interference with no or just a few additional ADC bits. Hence, with the proposed solution we can cover the whole range of possible input SIRs with no or just a few additional ADC bits. The IM leakage is only considerable for smallest frequency separation of the desired and interfering signals and it vanishes rapidly by increasing the frequency separation. Hence for most conditions of practical interest adequate interference suppression is achieved with negligible distortion of the desired signal. The analysis of power consumption shows that using the NIS in the multimode transceiver can reduce the power consumption by an order of magnitude.

Appendix I: Proof for required number of ADC bits

In this appendix we derive the number of additional ADC bits that is required to quantize a desired signal $d(t)$ in the presence of a large interferer $i(t)$. In the absence of any interference, number n_{b0} of ADC bits is chosen such that the maximum amplitude that the ADC can quantize would be about the maximum of $d(t)$:

$$2^{n_{b0}-1}\Delta \cong \max\{|d(t)|\}, \tag{3.25}$$

where Δ is quantization step of the ADC and $\cong$ denotes approximately equal. In the presence $i(t)$, to quantize $d(t) + i(t)$ without distortion, we should increase number of bits from n_{b0} to n_b such that:

$$2^{n_b-1}\Delta \cong \max\{|i(t)|\}. \tag{3.26}$$

By dividing (3.26) by (3.25) the number of additional bits is obtained as:

$$2^{n_b-n_{b0}}\Delta \cong \frac{\max\{|i(t)|\}}{\max\{|d(t)|\}}. \tag{3.27}$$

Crest factors r_d and r_i for $d(t)$ and $i(t)$ are defined as:

$$r_d = \frac{\max\{|d(t)|\}}{\sqrt{\mathrm{E}\left(d^2(t)\right)}}, \quad r_i = \frac{\max\{|i(t)|\}}{\sqrt{\mathrm{E}\left(i^2(t)\right)}}, \tag{3.28}$$

and can be used to translate the ratio of the maximum amplitudes in (3.27) to ratio of powers as:

$$2^{n_b-n_{b0}} \cong \frac{r_i}{r_m\sqrt{\mathrm{SIR}_d}}, \tag{3.29}$$

where $\mathrm{SIR}_d = \frac{\mathrm{E}(d^2(t))}{\mathrm{E}(i^2(t))}$ is the average SIR at the ADC input. Eq. (3.29) determines the number of required additional ADC bits due to the presence of the interference. According to (3.29), when $\mathrm{SIR}_d \ll 1$, for every 6 dB decrement of SIR_d, we have to add one additional ADC bit.

Appendix II: Proof for dependence of envelopes on ISIR

The NIS input can be written as:

$$x(t) = A_i(\cos\theta_i + \mathrm{ISIR}_x(t)\cos\theta_d). \tag{3.30}$$

By replacing (3.30) in (3.7) we obtain:

$$f(x(t)) = A_i f(\cos\theta_i + \mathrm{ISIR}_x(t)\cos\theta_d). \tag{3.31}$$

By replacing (3.31) in (3.10) we obtain:

$$A_{i,y}(A_i, A_d) = A_i A_{i,y}(\mathrm{ISIR}_x(t)), \tag{3.32}$$

where $A_{i,y}(\mathrm{ISIR}_x(t))$ is defined as:

$$A_{i,y}(\mathrm{ISIR}_x(t)) = \frac{1}{2\pi^2}\int_0^{2\pi}\int_0^{2\pi} f(\cos\theta_i + \mathrm{ISIR}_x(t)\cos\theta_i)\sin\theta_i d\theta_i d\theta_d. \tag{3.33}$$

In a similar manner we can obtain the following equations:

$$\begin{aligned} A_{d,y}(A_i, A_d) &= A_i A_{d,y}(\mathrm{ISIR}_x(t)) \\ A_{\mathrm{IM}}(A_i, A_d) &= A_i A_{\mathrm{IM}}(\mathrm{ISIR}_x(t)), \end{aligned} \tag{3.34}$$

where $A_{d,y}(\mathrm{ISIR}_x(t))$ and $A_{\mathrm{IM}}(\mathrm{ISIR}_x(t))$ are defined in a similar manner as (3.33). Using (3.34), one can easily verify that the quantities in (3.11)-(3.13) are fully determined by $\mathrm{ISIR}_x(t)$.

Appendix III: Proof for calculation of SDR

By replacing $A_{d,y}$ from (3.20) into (3.17), $\bar{g_d}$ is obtained as:

$$\bar{g_d} = \frac{\mathrm{E}(-\frac{1}{2}A_d^2 + \frac{A_d^4}{16A_i^2})}{\mathrm{E}(A_d^2)} \tag{3.35}$$

When $A_d \sim \mathrm{Rayleigh}(1)$, kth moment of A_d can be obtained as [28]:

$$\mathrm{E}\{A_d^k\} = \Gamma(\frac{k}{2} + 1), \tag{3.36}$$

where $\Gamma(.)$ is the Gamma function. By calculating the required moments in (3.35) using (3.36), $\bar{g_d}$ and the GVD power after the NIS are obtained as:

$$\bar{g_d} = -\frac{1}{2} + \frac{1}{8}\frac{\overline{P_d}}{\overline{P_i}}, \quad \mathrm{E}(A_e^2) = \frac{1}{128}\frac{\overline{P_d}^3}{\overline{P_i}^2} \tag{3.37}$$

The SDR can be calculated from (3.19) as:

$$\mathrm{SDR} = \frac{\overline{P_d}\Big(-\frac{1}{2} + \frac{1}{8}\frac{\overline{P_d}}{\overline{P_i}}\Big)^2}{\frac{1}{128}\frac{\overline{P_d}^3}{\overline{P_i}^2}} = 32\frac{(1 - 0.25\mathrm{SIR}_x)^2}{\mathrm{SIR}_x^2} \tag{3.38}$$

Chapter 4

Closed-loop Adaptation of a Nonlinear Interference Suppressor for multimode Transceivers[1]

4.1 abstract

In multimode transceivers, the transmitter for one communication standard may induce a large interference in the receiver for another standard, often exceeding the desired signal by many tens of dBs. To linearly suppress this interference, the receiver requires a very large linear dynamic range, resulting in excessive power consumption. In a recent paper, a nonlinear block, which requires an adaptation signal proportional to the envelope of the received interference, is used to strongly suppress the interference without excessive power consumption. In that work, the required adaptation signal for the nonlinear block is determined analytically. In this paper we quantify the required accuracy for the adaptation signal to properly suppress the interference while keeping the degradation to the receiver symbol error rate (SER) negligible. To provide the required accuracy, we propose a closed-loop method that calculates the adaptation signal based on a model, which describes the received interference in terms of the locally available baseband interference.

[1]This chapter is reproduced from the paper submitted as H. Habibi, E.J.G. Janssen, Wu Yan, P.G.M. Baltus, J.W.M. Bergmans, "Closed-loop Adaptation of a Nonlinear Interference Suppressor for multimode Transceivers", to *IEEE Transaction on Vehicular Technology.*

We propose a method to adapt this model during the operation of the transceiver such that the power of the residual interference at the output of the nonlinear block is minimized. Our analysis shows that the proposed method can strongly suppress the interference while a SER close to that of an exactly linear receiver is achieved. Simulation results for a practical scenario validate this analysis. The proposed nonlinear interference suppression method promises much smaller power consumption than for linear approaches.

4.2 Introduction

Nowadays, many handheld devices (smart phones and tablets) have become multimode transceivers. These support a multitude of wireless communications standards. From the users' point of view, simultaneous operation of these transceivers is highly desirable [3]. Owing to the small size of the handheld device, however, the Local Transmitter (LTX) of one standard induces an interference in the Local Receiver (LRX) of another standard [19], often several orders of magnitude stronger than the received desired signal. Active components of the receiver, like Low Noise Amplifier (LNA), have a linear dynamic range, in which they can process an input signal linearly. When the input signal exceeds this range, various undesirable nonlinear effects like intermodulation, cross-modulation distortion, or desensitization (excessive loss of gain) occur [21]. Digital compensation methods can be used to compensate for the cross-modulation and intermodulation distortion [13, 23, 48–53], if the desensitization is prevented by using a receiver with large enough dynamic range and ADCs with a large number of bits. Such a receiver will, however, have a high power consumption, which makes it unsuitable for mobile devices. Also some of the compensation methods use ADCs with high sampling rates [23] or multiple receiver branches [13, 48, 50].

By suppressing the interference at an early stage of the front-end the desensitization can be prevented. Typically a Band Pass Filter (BPF), implemented with a technology like Surface Acoustic Wave (SAW), is used to suppress the interference to some extent before the active components of the receiver. In the case that both standards share the same frequency band, like WLAN and Bluetooth, however, the BPF does not attenuate the interference. In the case of standards with small frequency separation, like WLAN and WiMAX, the suppression that can be achieved is limited to about 10 to 30 dB. Furthermore using SAW filters increases the cost, especially in multimode transceivers where multiple filters are required. Also it limits the flexibility of the receiver for multiband applications [54]. For example, consider a multimode scenario of a WLAN LRX (operating in the frequency range of 2400-2483 MHz) and a WiMAX LTX (operating in the frequency range of 2496-2690 MHz). Suppose that a 20 dBm transmitted WiMAX signal is coupled to the LRX antenna after 15 dB attenuation and is suppressed by the

SAW filter by about 25 dB. Then the WiMAX interference after the SAW filter can still be 60 dB stronger than the received WLAN signal which can be as small as -80 dBm. Increasing the receiver dynamic range to cover both the desired signal and the interference leads to an excessive power consumption [4] beyond the capability of handheld devices.

In multimode transceivers, the transmitted interference is available locally. Hence to cancel the interference, the transmitted interference can be used as a reference signal to generate a replica of the received interference and subtract it from the received signal [5–10, 55]. Accurate and adaptive generation of an RF signal (the replica), requires a high complexity and a large power consumption. Hence with the limited power and available space in mobile devices the replica cannot be constructed accurately, especially if the cancellation point is postponed till after the LNA and the BPF [5]. This significantly, limits the interference suppression that can be attained by cancellation.

An alternative approach to linear filtering and interference cancellation is to suppress the interference by passing the received signal through a special memoryless nonlinearity [16]. The Input-Output (IO) characteristic of this nonlinearity, which will be called Nonlinear Interference Suppressor (NIS), can be modeled as the combination of a hard limiter IO with an adaptable limiting amplitude $l(t)$ and a linear IO (with a gain of $-c$), as shown in Fig. 4.1. Theoretical and experimen-

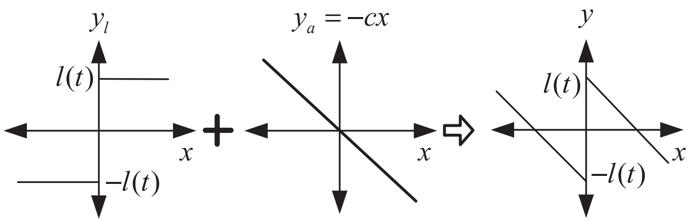

Figure 4.1: Realization of NIS input-output characteristic by combining an adaptable limiter and a linear amplifier.

tal results in [32] [56] [33] show that the NIS can be used to strongly suppress a constant-envelope interference. In [57], it is shown that for an interference with an arbitrary time-varying envelope $A_i(t)$ at the NIS input, there is an optimal adaptation signal $\tilde{l}(t)$:

$$\tilde{l}(t) = \frac{\pi}{4} c A_i(t), \tag{4.1}$$

which achieves the following goals:

- Goal 1: Suppressing the interference such that the power of unwanted components will be smaller than power of the desired signal at the NIS output.
- Goal 2: Introducing a negligible amount of nonlinear distortion.

In [57], the NIS approach is studied with the assumption that the optimal adaptation signal is known. To calculate the optimal adaptation signal according to (4.1), $cA_i(t)$ must be known. In the multimode transceiver a baseband version of the transmitted interference is locally available. Hence $cA_i(t)$ can be calculated based on a baseband model of the transmit-receive (TX-RX) path of the interference from the transmitted baseband interference to the received interference at the NIS input. We investigate the required accuracy for the adaptation signal to achieve a certain interference suppression. Based on this requirement, we analyze the required complexity of a Finite Impulse Response (FIR) filter for the baseband model of the TX-RX path.

The TX-RX path is subject to environmental changes, e.g. the presence of the user's hand can change the coupling between the LTX and the LRX antennas. Hence the path model must be continuously adapted during the transceiver's operation. We develop an adaptation method to adapt the path model such that the power of residual interference at the NIS output is minimized. The performance of this method, in achieving the first and second goals, is analyzed and the results are verified by simulation. The promising analysis and simulation results encourage an experimental elaboration and validation of the proposed method in the future works.

The rest of this paper is organized as follows. In Section 4.3, we describe the model of the receiver with the NIS. In Section 4.4, the accuracy requirements on the adaptation signal and the FIR modeling of the TX-RX path are studied. In Section 4.5, we develop an adaptation method for the FIR filter taps and analyze its performance. In Section 4.6, the simulation results are presented. Practical aspects are considered in Section 4.7 and the concluding remarks come in Section 4.8.

4.3 System model

In this section we describe the model of the multimode transceiver that uses the NIS. This model is used to analyze the effect of the NIS on the receiver operation and estimation of the adaptation signal.

4.3.1 Description of the signals received by the local RX

Fig. 4.2 shows a model of the multimode transceiver including the LTX, the LRX, and a remote transmitter. At the LRX, a desired signal transmitted by the remote TX is received in the presence of a part of the transmitted interference coupled

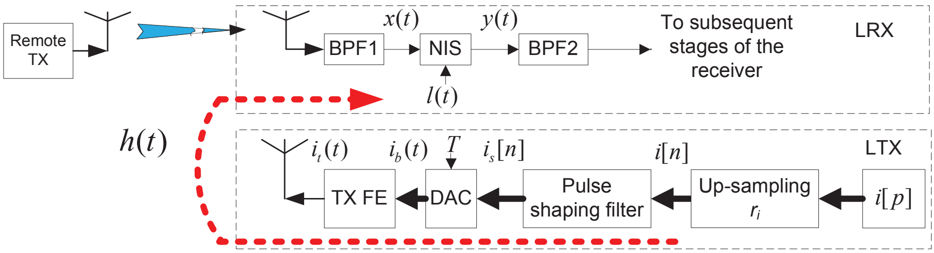

Figure 4.2: Multimode transceiver with NIS.

from the LTX. The combination of these two signals is passed through a Band Pass Filter (BPF1). Typically a SAW filter is used for BPF1. The desired signal is passed essentially unchanged through BPF1 and the interference is attenuated by BPF1. After BPF1, the NIS input $x(t)$ includes both a desired signal $x_d(t)$ and an interference $x_i(t)$ and can be written as:

$$x(t) = x_d(t) + x_i(t) = A_d(t)\cos(2\pi f_d t + \varphi_d(t)) + A_i(t)\cos(2\pi f_i t + \varphi_i(t)), \quad (4.2)$$

where A_d, φ_d, f_d, A_i, φ_i, and f_i are envelope, phase and center frequencies of the desired signal and interference after BPF1, respectively. The desired signal and interference are bandlimited to $[f_d - \frac{B_d}{2}, f_d + \frac{B_d}{2}]$ and $[f_i - \frac{B_i}{2}, f_i + \frac{B_i}{2}]$, where B_d and B_i are bandwidths of the desired signal and interference, respectively. The average powers of the desired signal and the interference are denoted by $P_d = \mathrm{E}(\frac{A_d^2}{2R})$ and $P_i = \mathrm{E}(\frac{A_i^2}{2R})$, where $R = 50\ \Omega$ is the reference impendence and E() denotes the statistical average.

The received signal at the NIS input also includes an additive noise component which is neglected in (4.2). This component is a combination of the circuits noise and channel noise. Typically the power of the additive noise is much smaller than P_d, which in turn is much smaller than P_i. Later we will see that in the estimation of the adaptation signal, the desired signal acts as a disturbing factor. Hence impact of the input noise in (4.2) on the NIS adaptation can be neglected compared to that of the desired signal. In the simulations in Section 4.6, to verify this argument we take into account the input noise by adding bandlimited Gaussian noise to $x(t)$.

After BPF1, $x(t)$ is passed through the NIS, which is adapted by an adaptation signal $l(t)$. Since the NIS has a strong nonlinear characteristics, high frequency harmonics (at frequencies around $3f_i$, $5f_i$, etc) are also generated at the NIS output. The power of the harmonics after the NIS is an order of magnitude smaller than P_i but still several orders of magnitude larger than P_d. Hence the harmonics must be filtered immediately after the NIS to prevent generation of nonlinear distortion in the subsequent blocks of the receiver. As these harmonics are far from f_d, they can be filtered out with a simple band pass filter (BPF2).

4.3.2 Adaptation signal

In this section we present a model that describes the required adaptation signal in terms of the baseband interference which is locally available. As shown in Fig. 4.2, the complex-valued baseband interference $i[p]$ with a baud rate $\frac{1}{T_i}$ is up-sampled by an integer factor r_i by inserting zeros between samples of $i[p]$ (complex-valued signals are shown with solid bold lines). The up-sampled signal $i[n]$ is passed through a transmit pulse shaping filter with a discrete-time frequency response $H_t(e^{j\omega})$, resulting in a signal $i_s[n]$. Typically a square root raised cosine filter is used for pulse shaping. A Digital to Analog Converter (DAC) with a conversion period of $T = \frac{T_i}{r_i}$ converts $i_s[n]$ to an analog baseband signal $i_b(t)$ with unit power. The LTX up-converts $i_b(t)$ to a center frequency f_i and transmits the signal $i_t(t) = \mathrm{Re}\left\{\sqrt{2P_t} i_b(t) e^{2\pi f_i t}\right\}$ with a power P_t. A part of $i_t(t)$ is coupled (modeled by a scaling factor α_p[2]) to the LRX and after passing through BPF1 is received at the NIS input. In this paper, we assume that a SAW filter with a frequency response $H_{\mathrm{SAW}}(f)$ is used for the BPF1.

In Fig. 4.2, the TX-RX path of the interference from $i[n]$ to $x_i(t)$ is shown with a dashed bold line. This path can be modeled as a linear system with a complex-valued baseband impulse response $h(t)$. Hence the optimal adaptation signal $\tilde{l}(t)$ is obtained as:

$$\tilde{l}(t) = \frac{\pi}{4} c A_i(t) = \frac{\pi}{4} c |x_i(t)| = \left| \sum_{m=-\infty}^{+\infty} i[m] h(t - mT) \right| . \tag{4.3}$$

In (4.3), the scaling factor $\frac{\pi}{4}c$ is considered as part of $h(t)$. To digitally generate $\tilde{l}(t)$ a discrete-time representation of $\tilde{l}(t)$ is required. Using the following notations for signals and impulse responses at time $t = nT$:

$$\tilde{l}[n] = \tilde{l}(nT), \qquad A_i[n] = A_i(nT), \qquad h_n = h(nT), \tag{4.4}$$

and considering the causality of h_n, we can obtain the discrete-time counterpart of (4.3) as:

$$\tilde{l}[n] = \frac{\pi}{4} c A_i[n] = |(h * i)[n]| = \left| \sum_{m=0}^{+\infty} i[n-m] h_m \right| \tag{4.5}$$

Here we assume that the sampling frequency $\frac{1}{T}$ is high enough so that $\tilde{l}(t)$ can be reconstructed from $\tilde{l}[n]$ with a negligible error. In Section 4.7.1, the impact of sampling frequency on this assumption is investigated.

[2]Since the propagation delay between the LTX and the LRX is much smaller than T_i, multipath effects are negligible. Such effects, however, could be absorbed as a part of frequency response of the TX-RX path.

The Discrete-time Fourier Transform (DFT) $H(e^{j\omega})$ of h can be linked to elements of the TX-RX path as:

$$H(e^{j\omega}) = \frac{\pi}{4} c\alpha_p \sqrt{2P_t} H_t(e^{j\omega}) H_{\mathrm{SAW}} \left(\left(\frac{\omega}{2\pi} \frac{1}{T} + f_i \right) \right), -\pi < \omega < \pi. \tag{4.6}$$

In (4.6), $\frac{\omega}{2\pi}\frac{1}{T} + f_i$ maps $H_{\mathrm{SAW}}(f)$ over $[f_i - \frac{1}{2T}, f_i + \frac{1}{2T}]$ to discrete-time frequency $-\pi < \omega < \pi$.

If we knew h_n, $l[n]$ could be calculated by using (4.5). Actually, we do not exactly require h to calculate $\tilde{l}[n]$. For example any set of filter taps $\tilde{h}_n$ as: $\tilde{h} = h_n e^{j\theta}$ results in the same adaptation signal $\tilde{l}[n]$, for any real-valued θ. In Appendix I, the relation between h_n and possible optimal taps $\tilde{h}_n$ that result in the same $\tilde{l}[n]$ is investigated. Our goal here is to determine a set of filter taps g_n such that the power of the residual interference at the NIS output would be minimized. These taps result in an estimate $\hat{l}[n]$ of the adaptation signal as:

$$\hat{l}[n] = |(g * i)[n]| = \left| \sum_{m=0}^{M-1} i[n-m] g_m \right|, \tag{4.7}$$

where M taps are used to realize g. A DAC converts $\hat{l}[n]$ to a continues-time signal $\hat{l}(t)$ which is applied as the estimated adaptation signal to the NIS.

4.3.3 Description of the signals at the NIS output

As shown in Fig. 4.1, the NIS output is the combination of the limiter and linear gain block outputs. Using the approximations for the bandpass limiter output [58] for $A_i > A_d$, one can obtain:

$$\begin{aligned} y(t) \simeq\ & A_{d,y}(t)\cos(2\pi f_d t + \varphi_d(t)) + A_{i,y}(t)\cos(2\pi f_i t + \varphi_i(t)) \\ & + A_{IM}(t)\cos(2\pi(2f_i - f_d)t + 2\varphi_i(t) - \varphi_d(t)), \end{aligned} \tag{4.8}$$

where $A_{d,y}$, $A_{i,y}$ and A_{IM} are envelopes of desired signal, interference and main Inter-Modulation (IM) components at the NIS output, respectively. It must be considered that (4.8) is valid when $f_i - f_d$, B_d and B_i are small compared to f_d and f_i, so that higher harmonics and other intermodulations of x_d and x_i do not have any spectral overlap with x_d and x_i. For $A_i > A_d$, by using a series expansion for the hard limiter output [42], one can obtain:

$$\begin{aligned} A_{i,y}(t) &\simeq \left(\frac{4l(t)}{\pi} - cA_i(t) \right) - \frac{l(t)}{\pi} \frac{A_d^2(t)}{A_i^2(t)} \\ A_{d,y}(t) &\simeq \left(\frac{2l(t)}{\pi A_i(t)} - c \right) A_d(t) + \frac{l(t)}{4\pi} \frac{A_d^3(t)}{A_i^3(t)}, \\ A_{\mathrm{IM}}(t) &\simeq -\frac{2A_d(t)}{\pi A_i(t)} l(t). \end{aligned} \tag{4.9}$$

For $l(t) = \tilde{l}(t) = \frac{\pi}{4} c A_i$, using (4.9) we obtain:

$$\tilde{A}_{i,y}(t) \simeq -\frac{c}{4}\frac{A_d^2(t)}{A_i(t)}, \quad \tilde{A}_{d,y}(t) \simeq -\frac{c}{2}A_d(t) + \frac{c}{16A_i^2(t)}A_d^3(t), \quad \tilde{A}_{\mathrm{IM}}(t) \simeq -\frac{c}{2}A_d(t). \tag{4.10}$$

According to (4.10), for $A_i \gg A_d$, $\tilde{A}_{i,y} \simeq 0$, $\tilde{A}_{d,y} = -\frac{c}{2}A_d$, and $\tilde{A}_{\mathrm{IM}} = -\frac{c}{2}A_d$. Hence when the interference is much stronger than the the desired signal, by applying the optimal adaptation signal the interference is nulled at the NIS output and the desired signal is amplified with a constant gain.

4.3.3.1 Interference suppression

We define the instantaneous Signal to Interference Ratio (SIR) at the NIS input and output as: $\mathrm{ISIR_x}(t) = \left(\frac{A_d(t)}{A_i(t)}\right)^2$ and $\mathrm{ISIR_y}(t) = \left(\frac{A_{d,y}(t)}{A_{i,y}(t)}\right)^2$ respectively. For $l(t) = \tilde{l}(t)$ using (4.10) we obtain:

$$\mathrm{ISIR_y}(t) \simeq 4 \ \ {\mathrm{ISIR_x}}^{-1}(t). \tag{4.11}$$

According to (4.11) the instantaneous SIR at the NIS output will be about 6 dB larger than inverse of the instantaneous SIR at the NIS input. Hence the local interference, which is stronger than the desired signal at the NIS input, is suppressed such that it would be weaker than the desired signal at the NIS output.

4.3.3.2 Distortion products

The instantaneous gain $g_d(t)$ of the desired signal can be defined as $g_d(t) = \frac{A_{d,y}(t)}{A_d(t)}$ and by using (4.10) we see that:

$$g_d(t) \simeq -\frac{c}{2} + \frac{cA_d^2(t)}{16A_i^2(t)} = -\frac{c}{2} + \frac{c}{16}\mathrm{ISIR_x}(t). \tag{4.12}$$

According to (4.12), $g_d(t)$ varies over time. This variation leads to in-band distortion of the desired signal. This Gain Variation Distortion (GVD) is a general form of cross-modulation distortion. According to (4.12) as $\mathrm{ISIR_x}$ decreases the gain approaches a constant value of $-\frac{c}{2}$. Hence the GVD is negligible when the average SIR ($\mathrm{SIR}_x = \frac{P_d}{P_i}$) at the NIS input is small. According to (4.10) an IM component with the same envelope as the desired signal will be present at the NIS output. Although the IM component is centered at $2f_i - f_d$, depending on the frequency separation $\Delta f = f_i - f_d$ of the desired signal and the interference, a part of the IM component may leak into the frequency channel of the desired signal. The IM leakage vanishes rapidly with increasing Δf and is negligible for most conditions of practical interest.

4.3.4 External interference

Now we consider the case that besides the local interference an external interference $x_e(t)$ is also present at the NIS input. The NIS input can be written as:

$$
\begin{aligned}
x(t) &= \underbrace{x_d(t) + x_e(t)}_{x_s(t)} + x_i(t) = A_d(t)\cos(2\pi f_d t + \varphi_d(t)) + \\
&\quad + A_e(t)\cos(2\pi f_e t + \varphi_e(t)) + A_i(t)\cos(2\pi f_i t + \varphi_i(t)) \\
&\quad = A_s(t)\cos(2\pi f_s t + \varphi_s(t)) + A_i(t)\cos(2\pi f_i t + \varphi_i(t)),
\end{aligned}
\tag{4.13}
$$

where A_s, φ_s, and f_s are obtained as:

$$
\begin{aligned}
f_s &= \frac{f_d + f_e}{2} \\
A_s(t) &= \sqrt{A_e^2 + A_d^2 + 2A_e A_d \cos(2\pi(f_d - f_e)t + \varphi_d - \varphi_e)} \\
\varphi_s(t) &= \tan^{-1}\left(\frac{A_d(t)\sin(\pi(f_d - f_e)t + \varphi_d(t)) + A_e(t)\sin(\pi(f_e - f_d)t + \varphi_e(t))}{A_d(t)\cos(\pi(f_d - f_e)t + \varphi_d(t)) + A_e(t)\cos(\pi(f_e - f_d)t + \varphi_e(t))}\right).
\end{aligned}
\tag{4.14}
$$

Since the BPF filters out any component with a large frequency separation from f_d, we can assume that f_e is close to f_d. Hence the bandwidth of $x_s(t)$ is much smaller than f_i and f_s. The distance of the LTX to the LRX is at least one order of magnitude smaller than that to any external interfering transmitter. Hence we can assume that the local interference is at least two orders of magnitude stronger than any nonlocal interference. Using these two assumptions we can use (4.8) and (4.9) to calculate the NIS output.

Two cases can be distinguished: 1- The more common case where $A_i \gg A_e$, $A_i \gg A_d$, and A_e and A_d have the same order of magnitude, 2- The extreme case where $A_i > A_e \gg A_d$. For the first case by using (4.8) and (4.9), for $l(t) = \tilde{l}(t)$, one can obtain:

$$
\begin{aligned}
y(t) \simeq &-\frac{c}{2}A_d(t)\cos(2\pi f_d t + \varphi_d(t)) - \frac{c}{2}A_e(t)\cos(2\pi f_e t + \varphi_e(t)) \\
&- \frac{c}{2}A_d(t)\cos(2\pi(2f_i - f_d)t + 2\varphi_i(t) - \varphi_d(t)) \\
&- \frac{c}{2}A_e(t)\cos(2\pi(2f_i - f_e)t + 2\varphi_i(t) - \varphi_e(t)).
\end{aligned}
\tag{4.15}
$$

According to (4.15) the NIS processes $x_s(t) = x_d(t) + x_e(t)$ linearly, with the exception of IM components generated from interaction of x_d with x_i and x_e with x_i. For the second case, since $A_e \gg A_d$ we can assume $A_s \simeq A_e$. Using (4.9), by replacing x_d with x_s, for $l(t) = \tilde{l}(t)$, one can obtain:

$$\begin{aligned} y(t) \simeq & -\frac{c}{2}\left(1+\frac{A_e^2(2)}{8A_i^2(t)}\right) A_d(t)\cos(2\pi f_d t + \varphi_d(t)) \\ & -\frac{c}{2} A_e(t)\cos(2\pi f_e t + \varphi_e(t)) - \frac{c}{4}\frac{A_e^2(t)}{A_i(t)}\cos(2\pi f_i t + \varphi_i(t)) \\ & -\frac{c}{2} A_d(t)\cos(2\pi(2f_i - f_d)t + 2\varphi_i(t) - \varphi_d(t)) \\ & -\frac{c}{2} A_e(t)\cos(2\pi(2f_i - f_e)t + 2\varphi_i(t) - \varphi_e(t)) \end{aligned} \tag{4.16}$$

According to (4.16), in the presence of an external interference with $A_e \gg A_d$, the interference suppression and GVD are determined by $\frac{A_e}{A_i}$. The stronger the external interference is, the more GVD and the less interference suppression are attained. A part of the energy of the IM product at $2f_i - f_e$ and the residual interference at f_i may leak into the frequency channel of the desired signal, depending on $f_e - f_i$ and $f_d - f_i$. A possible solution to mitigate this IM product is to use digital techniques to compensate for the intermodulation distortion [23].

4.4 Accuracy requirements for NIS adaptation

In this section, firstly, we study the impact of an error in the adaptation signal on the NIS performance. Then the relation between estimation error of the filter taps and error of the adaptation signal is analyzed. Finally, we find the required number of filter taps to model a SAW filter with the required accuracy. In this section and section IV we consider the practical case where $A_i \gg A_d$. Therefore we only consider the first order terms in (4.9). Also we assume that at the NIS input only the desired signal and the local interference are present.

4.4.1 Impact of adaptation signal errors on the NIS performance

When an estimate $\hat{l}(t)$ of $\tilde{l}(t)$ is used, using (4.9) the envelopes of dominant components at the NIS output are approximated by:

$$\begin{aligned}\hat{A}_{d,y}(t) &\simeq \left(\frac{2\hat{l}(t)}{\pi A_i(t)} - c\right) A_d(t) = \left(\frac{\hat{l}(t)}{2\tilde{l}(t)} - 1\right) cA_d(t),\\ \hat{A}_{i,y}(t) &\simeq \frac{4\hat{l}(t)}{\pi} - cA_i(t) = \frac{4}{\pi}\left(\hat{l}(t) - \tilde{l}(t)\right),\\ \hat{A}_{\mathrm{IM}}(t) &\simeq -\frac{2A_d(t)}{\pi A_i(t)}\hat{l}(t) = -\frac{\hat{l}(t)}{2\tilde{l}(t)} cA_d(t).\end{aligned} \tag{4.17}$$

According to (4.17), the impact of the adaptation error $(\hat{l}(t) - \tilde{l}(t))$ on the desired signal and intermodulation is a change of NIS gain for them. We use Normalized Adaptation Error (NAE) defined as:

$$\mathrm{NAE} = \frac{\mathrm{E}\left((\hat{l}(t) - \tilde{l}(t))^2\right)}{\mathrm{E}(\tilde{l}^2(t))}. \tag{4.18}$$

to gauge the estimation accuracy. As long as NAE is small (e.g. less than -40 dB), $\frac{\hat{l}(t)}{\tilde{l}(t)}$ will be very close to unity and hence the impact of adaptation error on the desired signal and the inter-modulation will be negligible.

The average Interference Suppression (IS) can be defined as the ratio of average SIR at the NIS output (SIR_y) to average SIR at the NIS input (SIR_x) and is related to NAE as:

$$\mathrm{IS} = \frac{\mathrm{SIR}_y}{\mathrm{SIR}_x} \simeq \frac{\frac{c^2\mathrm{E}(A_d^2)/4}{(\frac{4}{\pi})^2\mathrm{E}\left((\hat{l}-\tilde{l})^2\right)}}{\frac{\mathrm{E}(A_d^2)}{\mathrm{E}(A_i^2)}} = \frac{1}{4}\frac{(\frac{4}{\pi c})^2\mathrm{E}\left((\hat{l}-\tilde{l})^2\right)}{(\frac{4}{\pi c})^2\mathrm{E}(\tilde{l}^2)} = \frac{1}{4\mathrm{NAE}}, \tag{4.19}$$

where we assumed $\frac{\hat{l}(t)}{\tilde{l}(t)} \simeq 1$. The first impact of an adaptation error is that it limits the interference suppression (Goal 1). Hence the required interference suppression poses a first requirement on NAE. If we aim to suppress the interference below the desired signal then NAE should be 6 dB smaller than SIR_x. In practice, however, owing to implementation limitations such interference suppression may not be attainable [56]. Therefore a lower accuracy may be sufficient depending on the implemented NIS.

The second impact of an adaptation error is a bandwidth expansion of the residual interference $y_i(t) = \hat{A}_{i,y}(t)\cos(2\pi f_i t + \varphi_i(t))$. If $\hat{A}_{i,y}(t) = \frac{4}{\pi}(\hat{l}(t) - \tilde{l}(t))$ is proportional to $A_i(t)$ then $y_i(t)$ will be bandlimited to $[f_i - \frac{B_i}{2}, f_i + \frac{B_i}{2}]$. The adaptation

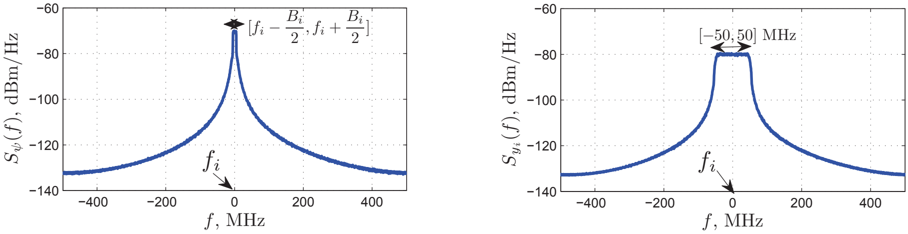

(a) $S_\psi(f)$ for $B_i = 10$ MHz.

(b) $S_{y_i}(f)$, assuming a unit power for $\varepsilon(t)$.

Figure 4.3: Interference leakage.

error or a part of it, however, can be uncorrelated with $A_i(t)$. Suppose that a part of the adaptation error denoted by $\varepsilon(t)$ is uncorrelated with $A_i(t)$. Power Spectral Density (PSD) $S_{y_i}(f)$ of $y_i(t)$ is the convolution of the PSD $S_\psi(f)$ of the phase-modulated signal $\psi(t) = \cos(\omega_i t + \varphi_i(t))$ and PSD $S_\varepsilon(f)$ of $\varepsilon(t)$. For an OFDM signal with a rectangular PSD over $[f_i - \frac{B_i}{2}, f_i + \frac{B_i}{2}]$ and $B_i = 10$ MHz, $S_\psi(f)$ is shown in Fig. 4.3a. The PSD is shown for the baseband equivalent signal. About 10% of the energy of $\psi(t)$ falls outside $[f_i - \frac{B_i}{2}, f_i + \frac{B_i}{2}]$. Outside of $[f_i - B_i, f_i + B_i]$, $S_\psi(f)$ is proportional to $\frac{1}{\left(\frac{f-f_i}{B_i}\right)^3}$ [43]. In this case the bandwidth of $y_i(t)$ can be much wider than B_i and a part of it may leak into the frequency channel $[f_d - \frac{B_d}{2}, f_d + \frac{B_d}{2}]$ of the desired signal .

The amount of leakage can not be quantified easily and depends on $S_\varepsilon(f)$, $\Delta f = f_i - f_d$ and B_d. To get insight into the amount of leakage and the required NAE we consider an example where ε has a unit power and a white spectrum over a bandwidth of $[-50, 50]$ MHz. This can be for example the result of the quantization noise of the DAC that converts $\hat{l}[n]$ to $\hat{l}(t)$. Then $S_{y_i}(f)$ will be a smoothed version of $S_\psi(f)$ as shown in Fig. 4.3b, for P_i=0 dBm. Suppose that $B_d = 10$ MHz. Based on Δf, two cases can be distinguished:
1-$[f_d - \frac{B_d}{2}, f_d + \frac{B_d}{2}]$ falls in $[f_i - 50, f_i + 50]$: then to bring the PSD of leakage x [dB] below the PSD of the desired signal we must have:
P_i [dBm]-80 [dBm/Hz] +NAE [dB] + x [dB] $<$ P_d [dBm]-6 [dB]-70 [dBm/Hz]
$\Rightarrow$ NAE [dB] $<$ SIR$_x$ [dB] + 4 [dB] $-$ x [dB].
For example if SIR$_x = -60$ dB and $x = 20$ dB then we must have NAE $<$ -76 dB.
2-$[f_d - \frac{B_d}{2}, f_d + \frac{B_d}{2}]$ falls outside $[f_i - 50, f_i + 50]$: the accuracy requirement for this case becomes more relaxed. For example for $\Delta f = 100$ MHz, SIR$_x = 60$ dB, and $x = 20$ dB, we require NAE $<$ -42 dB, which can be achieved easily.
By every doubling of Δf, the leakage decreases by 9 dB and the accuracy requirement on NAE becomes more relaxed.

For modulations of the interference with no envelope variations, the phase signal $\cos(2\pi f_i t + \varphi_i(t))$ is bandlimited to $[f_i - \frac{B_i}{2}, f_i + \frac{B_i}{2}]$. Also the estimated envelope

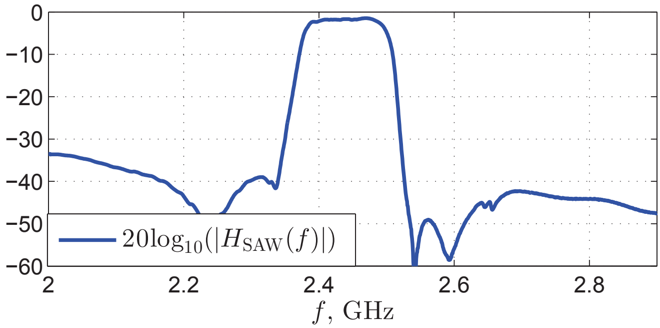

Figure 4.4: Frequency response $H_{\mathrm{SAW}}(f)$ of a SAW filter.

and hence $\varepsilon(t)$ have bandwidths much smaller than B_i. Hence the bandwidth expansion is much smaller than B_i and will be negligible.

4.4.2 Linear model of the TX-RX path

Main elements of the TX-RX path are the digital pulse shaping filter, the amplification in the LTX, the attenuation resulting from the coupling loss, and the SAW filter. The filter taps $h_{t,n}$ of the digital pulse shaping filter are known. Except for the SAW filter, the remaining unknown elements have a combined flat frequency response over the interference band $[f_i - \frac{B_i}{2}, f_i + \frac{B_i}{2}]$ and hence their combined impact on the interference can be modeled by a scaling and a delay. Fig. 4.4 shows the frequency response $H_{\mathrm{SAW}}(f)$ of a SAW filter [59]. We see that depending on f_i the interference suppression can change between 0 dB to 60 dB. When f_i is outside the passband or transition band of the SAW filter ([2.35,2.51] GHz in Fig. 4.4), the interference is suppressed by more than 30 dB. On the other hand, when f_i falls in [2.35,2.51] GHz a very small or even no interference suppression is provided by the SAW filter. In these regions, we can only rely on the NIS to suppress the interference, and hence an accurate estimation of the adaptation signal is required to achieve a large interference suppression by the NIS.

For narrow band interferences, $H_{\mathrm{SAW}}(f)$ over $[f_i - \frac{B_i}{2}, f_i + \frac{B_i}{2}]$ may be approximated by a constant complex number. Hence the unknown part of the TX-RX path can be modeled by a scaling factor. In this case, since the output $i_s[n]$ of the pulse shaping filter is known, $\hat{l}[n]$ can be calculated by estimating this scaling factor. On the other hand for wide-band interferences (B_i in the order of 10 MHz), the frequency response of the SAW filter can significantly vary over $[f_i - \frac{B_i}{2}, f_i + \frac{B_i}{2}]$ and a multi-tap FIR filter may be required.

4.4.3 Accuracy requirements of filter taps g_n

To find out when $H_{\mathrm{SAW}}(f)$ can be approximated by a scaling factor and when we require a multi-tap filter we need to study the impact of using M taps in (4.7) on NAE. Finding an analytical expression that links NAE to the errors of filter taps seems difficult. Based on the reverse triangle inequality:

$$(|(g*i)[n]| - |(h*i)[n]|)^2 \leq |((g-h)*i)[n]|^2 \tag{4.20}$$

an upper bound on NAE can be obtained as:

$$\mathrm{NAE} = \frac{\mathrm{E}\left((|(g*i)[n]| - |(h*i)[n]|)^2\right)}{\mathrm{E}(||(h*i)[n]|)^2} \leq \frac{\mathrm{E}(|((g-h)*i)[n]|^2)}{\mathrm{E}(|(h*i)[n]|^2)}. \tag{4.21}$$

Since $i[n]$ is assumed to be white we can obtain:

$$\begin{aligned} \mathrm{E}(|(h*i)[n]|^2) &= E\left(|i[n]|^2\right) \sum_{m=0}^{+\infty} |h_m|^2, \\ \mathrm{E}(|((h-g)*i)[n]|^2) &= E\left(|i[n]|^2\right) \sum_{m=0}^{+\infty} |h_m - g_m|^2. \end{aligned} \tag{4.22}$$

Using (4.21), (4.22) and Parseval's theorem, we obtain:

$$\mathrm{NAE} \leq \frac{\sum\limits_{m=0}^{+\infty} |h_m - g_m|^2}{\sum\limits_{m=0}^{+\infty} |h_m|^2} = \frac{\int\limits_{-\pi}^{+\pi} \left|H(e^{j\omega}) - G(e^{j\omega})\right|^2 d\omega}{\int\limits_{-\pi}^{+\pi} \left|H(e^{j\omega})\right|^2 d\omega}. \tag{4.23}$$

According to (4.23), NAE is bounded from above by the normalized Mean Square Error (MSE) between $G(e^{j\omega})$ and $H(e^{j\omega})$. We use (4.23) in the next section to find out the required number of taps to model the SAW filter such that NAE will be sufficiently small.

4.4.4 Required number of filter taps for modelling the SAW filter

To find out the number of taps N required to the model the SAW filter we calculate the Minimum of the MSE (MMSE) between $G(e^{j\omega})$ and $H(e^{j\omega})$ as:

$$\mathrm{MMSE}(N, f_i, B_i) = \min_{G_{\mathrm{SAW}}} \frac{\int\limits_{-\pi}^{+\pi} \left|H(e^{j\omega}) - G_{\mathrm{SAW}}(e^{j\omega}) H_t(e^{j\omega})\right|^2 d\omega}{\int\limits_{-\pi}^{+\pi} \left|H(e^{j\omega})\right|^2 d\omega}, \tag{4.24}$$

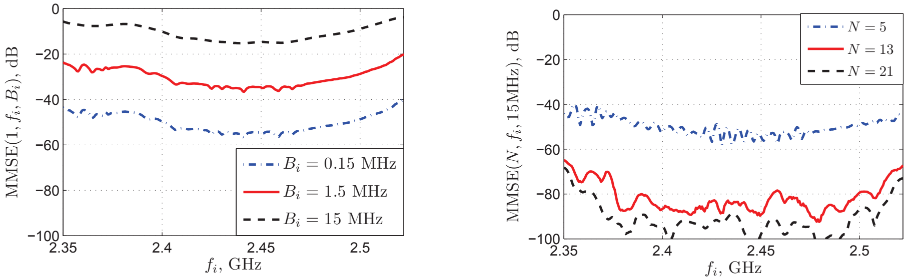

(a) MMSE$(1, f_i, B_i)$ for $B_i = 0.15, 1.5, 15$ MHz.

(b) MMSE$(N, f_i, 15MHz)$ for $N = 5, 13, 21$ and $B_i = 15$ MHz.

Figure 4.5: MMSE(N, f_i, B_i).

where N taps are used to realize $G_{\mathrm{SAW}}(e^{j\omega})$, and $H()$ is calculated according to (4.6). We use the frequency response of the SAW filter in Fig. 4.4 as an example.

We assume an up-sampling ratio $r_i = 2$ and $\beta = 0.5$. Hence $B_i = \frac{1.5}{T_i}$. First we study the accuracy of modeling the SAW filter by a scaling factor, i.e. $G_{\mathrm{SAW}}(e^{j\omega}) = G_{\mathrm{SAW}}$ in (4.24). For f_i from 2.35 GHz to 2.52 GHz, and $B_i = 0.15, 1.5, 15$ MHz, MMSE$(N = 1, f_i, B_i)$ is found and shown vs. f_i in Fig. 4.5a. For an interference with B_i =0.15 MHz, MMSE and hence NAE is below -40 dB. Hence even a single tap filter as the path model results in a significant interference suppression. On the other hand for the 15 MHz interference, MMSE can be as large as -5 dB. Hence a multi-tap filter is required for wide-band interferences.

Now we use an N-tap FIR filter to construct $G_{\mathrm{SAW}}(e^{j\omega})$. For f_i from 2.35 GHz to 2.52 GHz, MMSE$(N, f_i, B_i = 15$ MHz$)$ is found and is plotted in Fig. 4.5b for $N = 5, 13, 21$. We see that for $N = 13$ the MMSE can be brought down to about -65 dB.

To determine N, $H_{\mathrm{SAW}}(f)$ must be known. This can be obtained from the manufacturer's datasheet before implementing the system. In practice the frequency response of each filter may be slightly different or it may drift over time or with temperature. The required order, however, depends mainly on the overall shape of the frequency response and does not change due to these slight variations. This can be inferred from Fig. 4.4 and Fig. 4.5b. In Fig. 4.4 although $H_{\mathrm{SAW}}(f)$ varies with f over 2.35 GHz to 2.52 GHz, the MMSE in Fig. 4.5b does not change substantially with f_i for a certain value of N. A cautious designer, however, would use a filter with a slightly higher order than what is predicted based on $H_{\mathrm{SAW}}(f)$ from the manufacturer's datasheet to take into account practical variations and to guarantee the accuracy during the operation.

4.5 Closed-loop adaptation of the NIS

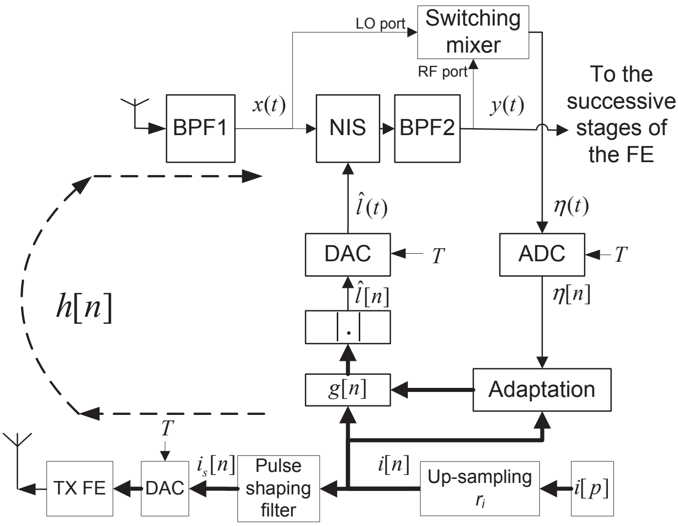

Figure 4.6: NIS adaptation.

As we saw by using an FIR filter g the adaptation signal in (4.7) can be generated. Since g depends on the environmental changes, it must be adapted to track these changes. We propose a closed-loop adaptation method for the NIS, as shown in Fig. 4.6, that measures the envelope $A_{i,y}$ of the residual interference at the NIS output and adapts the filter taps g such that $\mathrm{E}(A_{i,y}^2)$ is minimized. By measuring $A_{i,y}$ the changes in the NIS parameter c is also taken into account. As shown in Fig. 4.6, $A_{i,y}$ is measured using a switching mixer, as will be explained in Section 4.5.1. The mixer output $\eta(t)$ is approximately proportional to $A_{i,y}(t)$ and is sampled by an ADC with sampling rate of $\frac{1}{T}$. To adapt $g[n]$ we process $\eta[n]$ and the up-sampled baseband interference $i[n]$ together such that $\mathrm{E}(\eta^2)$ is minimized, as will be explained in Section 4.5.2. Such reference aided adaptation provides us with a fast and robust method to estimate g. Both $i[n]$ and $i_s[n]$ can be used as the input signal for g and the adaptation block. Using $i[n]$ instead of $i_s[n]$ as the input has two advantages: 1- $i[n]$ is a white signal. Hence the adaptation converges with a single mode of convergence. 2- $i[n]$ is quantized with fewer bits compared to $i_s[n]$ and $\frac{r_i-1}{r_i}$ of its samples are zero. This simplify the adaptation, computationally. On the other hand, when $i[n]$ is used as the input, a larger number of taps is required. Since g should also model the pulse shaping filter. In the rest of this paper we will use $i[n]$ instead of $i_s[n]$. The developed adaptation method however, can be also used with $i_s[n]$ as the input. Finally, the estimated envelope of the received interference $\hat{l}[n] = |(g * i)[n]|$ is calculated and converted to an analog signal using a DAC with conversion period of T.

4.5.1 Extraction of error signal

As shown in Fig. 4.6, to measure $A_{i,y}$ we propose to down-convert $y(t)$ using a switching mixer with $x(t)$ as its Local Oscillator (LO) port and $y(t)$ as its Radio Frequency (RF) port. The advantage of this method is that because $x(t)$ is much stronger than $y(t)$, we can use a passive switching mixer with zero power consumption, low complexity and small DC-offset. A switching mixer changes the sign of its RF input based on its LO input as:

$$\eta(t) = \begin{cases} y(t) & x(t) > 0, \\ 0 & x(t) = 0, \\ -y(t) & x(t) < 0. \end{cases} \tag{4.25}$$

In Appendix II, we prove that for $A_d \ll A_i$:

$$\eta(t) \simeq \frac{2}{\pi} A_{i,y}(t) + v(t) \simeq \frac{8}{\pi^2}\left(\hat{l}(t) - \tilde{l}(t)\right) + \nu(t) = \frac{8}{\pi^2}\left(|g(t) * i(t)| - \tilde{l}(t)\right) + \nu(t), \tag{4.26}$$

where

$$\nu(t) = \frac{2}{\pi}\left(\frac{\hat{l}(t)}{2\tilde{l}(t)} - 1\right) cA_d(t)\cos(2\pi(f_d - f_i)t + \varphi_d(t) - \varphi_i(t)) \tag{4.27}$$

acts as a disturbance term in the estimation of h. It is proved in Appendix II, that $\nu(t)$ is uncorrelated with the information bearing part of $\eta(t)$, i.e. $\mathrm{E}\left(\nu(t)A_{i,y}\right) = 0$. Hence by minimizing $\mathrm{E}(\eta^2(t))$, the power $\mathrm{E}(A_{i,y}^2(t))$ of the residual interference at the NIS is minimized.

4.5.2 adaptation algorithm

To minimize $\mathrm{E}(\eta^2(t))$ we sample $\eta(t)$ as:

$$\begin{aligned} \eta[n] &= \frac{8}{\pi^2}\left(|(g * i)[n]| - \tilde{l}[n]\right) + \nu[n] \\ &= \frac{8}{\pi^2}\left(\left|\sum_{m=0}^{M-1} g_m i[n-m]\right| - \tilde{l}[n]\right) + \nu[n] \\ &= \frac{8}{\pi^2}(|\mathbf{g}^T \mathbf{i}[n]| - \tilde{l}[n]) + \nu[n] \end{aligned} \tag{4.28}$$

where column vectors $\mathbf{g}$ and $\mathbf{i}[n]$ are defined as:

$$\begin{aligned} \mathbf{g} &= [g_0, g_1, \ldots, g_{M-1}]^T, \\ \mathbf{i}[n] &= [i[n], i[n-1], \ldots, i[n-M+1]]^T, \end{aligned} \tag{4.29}$$

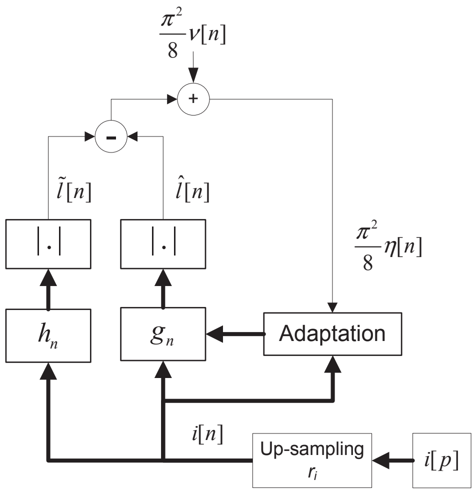

Figure 4.7: Simplified model of the NIS adaptation.

and the superscript T denotes the transpose operation. According to (4.28) the adaptation loop in Fig. 4.6 can be approximated by the discrete-time adaptation loop in Fig. 4.7. The loop adapts the filter taps g_n to minimize a cost function defined as:

$$J(\mathbf{g}) = \mathrm{E}\left(\left(\frac{\pi^2}{8}\eta(t)\right)^2\right) = \mathrm{E}\left((|\mathbf{g}^T\mathbf{i}[n]| - \tilde{l}[n])^2\right) + \mathrm{E}\left(\frac{\pi^4}{64}\nu^2[n]\right) \tag{4.30}$$

The steepest decent algorithm can be used to minimize $J(\mathbf{g})$ [60]. To use this algorithm the complex-valued gradient vector $\nabla_{\mathbf{g}} J(\mathbf{g})$ of the cost function is required which is obtained in Appendix III as:

$$\nabla_{\mathbf{g}} J(\mathbf{g}) = 2\mathrm{E}\left\{\eta[n]\frac{\mathbf{g}^T\mathbf{i}[n]}{|\mathbf{g}^T\mathbf{i}[n]|}\mathbf{i}^*[n]\right\}, \tag{4.31}$$

where * denotes complex conjugate. Approximating the expected value in (4.31) by its instantaneous value results in the stochastic version of the steepest decent algorithm as:

$$\mathbf{g}[n+1] = \mathbf{g}[n] - \mu\eta[n]\frac{\mathbf{g}^T[n]\mathbf{i}[n]}{|\mathbf{g}^T[n]\mathbf{i}[n]|}\mathbf{i}^*[n], \tag{4.32}$$

where $\mathbf{g}[n]$ denotes the filter taps at time instat n and μ is a positive real number called step-size.

Notes:

- $\frac{\mathbf{g}^T\mathbf{i}[n]}{|\mathbf{g}^T\mathbf{i}[n]|}$ is a complex-valued scalar with unit amplitude.

- For a one-tap filter ($M = 1$), we can assume that the only tap g_0 is a real positive number. In this case the adaptation update equation simplifies to $g_0[n+1] = g_0[n] - \mu\eta[n]|i[n]|$. If we consider the constant modulus case, then $|i[n]| = 1$ and we get the same solution as we developed for narrow-band constant envelope interferences [32].

4.5.3 Convergence of the adaptation algorithms

Generally the presence of local minima in a cost function disrupts the convergence of the steepest decent algorithm to its global minima. In Appendix III the second derivative (also called Hessian) of $J(\mathbf{g}[n])$ is obtained as:

$$\nabla^2_{\mathbf{g}}(J(\mathbf{g}[n])) = 2\mathrm{E}\left(\left(2 - \frac{\tilde{l}[n]}{\hat{l}[n]}\right)\mathbf{i}[n]\mathbf{i}^H[n]\right). \tag{4.33}$$

According to (4.33) the cost function is not convex and the second derivative becomes zero when $\hat{l}[n] = \frac{1}{2}l[n]$. The cost function for $M = 1$ and $h_0 = 0.5 + 0.5i$ is shown in Fig.4.8. The x axis and the y axis show the real and imaginary parts of g_0, and z axis shows $J(g_0)$. Although $J(\mathbf{g})$ is not convex there is no local minimum. The global minimum occurs for all the points that have the same amplitude as h_0. There is one local maximum at $g_0 = 0$. Since there is no local minimum the adaptation algorithm converges to the global minimum.

For $M > 1$ we have no proof for the convergence to the global minimum. As we will see in the next section, the cost function becomes approximately convex after an initial convergence. Owing to the small distance between the LTX and LRX, the change in the frequency response of the TX-RX path are small. Hence we can be sure that we always start from an initial point close to the steady state value of the adaptation.

4.5.4 Speed of the adaptation loop

Because of the nonlinear update equation (4.32) analyzing the transient behavior of the adaptation would be very complex. After proper initial convergence $\hat{l}[n]$ will be close to $l[n]$. In this situation, which is called the tracking mode of the adaptation loop, the Hessian matrix in (4.33) can be approximated by:

$$\nabla^2_{\mathbf{g}}(J(\mathbf{g}[n])) \simeq 2\mathrm{E}\left(\mathbf{i}[n]\mathbf{i}^H[n]\right) = 2\mathrm{E}\left\{|i[n]|^2\right\} I_{M\times M} = \frac{2}{r_i} I_{M\times M} \tag{4.34}$$

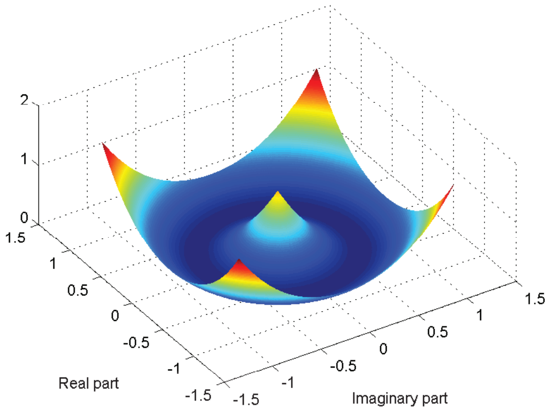

Figure 4.8: Cost function for $M = 1$.

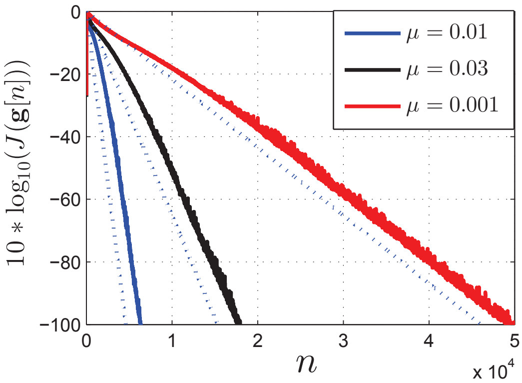

Figure 4.9: Learning curves of the adaptation based on Fig. 4.7.

where $I_{M\times M}$ is the $M \times M$ identity matrix. In (4.34), we used the assumption that $i[n]$ is obtained by r_i times up-sampling of the white and unit power signal $i[p]$.

The Hessian of the quadratic cost function $J_{\mathrm{qd}}(\mathbf{g}[n]) = E(\left|\mathbf{g}^T[n]\mathbf{i}[n] - \mathbf{h}^T[n]\mathbf{i}[n]\right|^2)$ can be obtained as: [60]
$\nabla^2_{\mathbf{g}}(J_{\mathrm{qd}}(\mathbf{g}[n])) \simeq 4\mathrm{E}\left(\mathbf{i}[n]\mathbf{i}^H[n]\right)$.
For $J_{\mathrm{qd}}(\mathbf{g}[n])$, because of the constant second derivative, the first derivative decays with a constant rate which results in an exponential decay of $J_{\mathrm{qd}}(\mathbf{g}[n])$ with a discrete-time time constant of $\frac{r_i}{2\mu}$ [60].

In the tracking mode of adaptation, the Hessian of $J(\mathbf{g}[n])$ in (4.34) is half of the Hessian of $J_{\mathrm{qd}}(\mathbf{g}[n])$. Hence $J(\mathbf{g}[n])$ also should decay exponentially with a discrete-time time constant of $\tau_d = \frac{r_i}{\mu}$. A simulation is done based on the simplified model shown in Fig. 4.7 to measure τ_d. In this simulation a random i.i.d Gaussian signal is used as $i[p]$, and $\nu[n]$ is neglected. In Fig. 4.9, the learning curves of $J(\mathbf{g}[n])$ are shown versus n for different values of μ. The dotted lines show the lines corresponding to $e^{-\frac{n}{\tau_d}}$ and follow the learning curves closely.

The discrete-time time constant τ_d translates into the analog time constant $\tau = T\tau_d = \frac{T_i}{\mu}$. Hence the 3-dB bandwidth of the adaptation loop will be $\frac{1}{2\pi\tau} = \frac{\mu}{2\pi}\frac{1}{T_i}$. The bandwidth of the adaptation loop must be large enough to track variations of $h(t)$, which originate from the environmental changes such as the presence of the user hand or temperature. The frequency of these changes is assumed to be well below a few tens of Hertz. Hence a 3-dB bandwidth of 0.5 KHz is amply large enough to track environmental changes. Moreover μ should be small enough to suppress the disturbance term $\nu(t)$ in (4.26) and also to make the excess mean square error of estimating h small enough. In Section 4.6.3, an appropriate value for μ is chosen based on SER simulations for several values of μ.

4.6 Simulation Results

4.6.1 Simulation setup

In this section, simulation results for a multimode scenario of a WLAN LRX with a local WiMAX LTX are presented. The simulation parameters are listed in Table. 4.1. We assume that there is -10 dB coupling between the LTX and the LRX. The

Table 4.1: Simulation parameters.

	LRX	LTX
Standard	WLAN	WiMAX
Center frequency	f_d=2460 MHz	f_i =2510 MHz
Baudrate	20 MSPS	10 MSPS
Modulation	OFDM	OFDM
Number of sub carriers	64 sub carrier	64 sub carrier
Modulation of each sub carriers	16 QAM	16 QAM
Power (50 Ω system)	minimum 10^{-11} W (-70 dBm)	Maximum 0.1 W (20 dBm)

SAW filter suppresses the WiMAX interference at f_i by 10 dB. Hence SIR_x can be as low as -70 dB. The NIS performance is mainly determined by the probability distribution function of the envelopes and average powers of the interference and desired signal. An OFDM signal approximately has a Circularly Symmetric

Complex-valued Gaussian (CSCG) distribution. The distribution remains CSCG when the OFDM signal passes through a multipath or frequency selective channel. Hence the only impact of a fading channel for the desired signal on the NIS performance is a change of P_d. Therefore for the desired signal only an Additive White Gaussian Noise (AWGN) channel is considered. With the AWGN channel, the SER performance of a linear receiver depends only on the desired Signal to Noise power Ratio (SNR), with the noise power measured in the frequency channel of the desired signal. The SNR is chosen such that it results in an un-coded SER of 10^{-3} for an exactly linear RX, which leads to an error free reception after forward error correction in the WLAN LRX. The required SNR for the 16QAM modulation is 17.6 dB [44]. Root raised cosine pulse shaping with a roll-off-factor of 0.5 is used for both interference and desired signal. In all simulations $c = 1$ and the signals are represented by floating point numbers.

4.6.2 Interference suppression

Fig. 4.10a shows magnitude response $|H(e^{j\omega})|$of the TX-RX path. Fig. 4.10b shows the PSD of the signal at the NIS input. The X-axis shows the frequency in MHz with reference to f_i. In Fig. 4.10b, the interference is centered at zero frequency and the desired signal is centered at $f_d - f_i = -50$ MHz. SIR_x is -60 dB in this simulation. The input channel noise is filtered by the SAW filter and is centered at about -50 MHz. The impact of the SAW filter on the interference can be seen in Fig. 4.10b.

Fig. 4.11 shows NAE for $\mu = 0.0003$ and $r_i = 20$. The adaptation is started from $\mathbf{g}[0] = \mathbf{0}$. NAE decreases exponentially and reaches the steady state of -90 dB. NAE can be decreased further by decreasing μ. In Fig. 4.12a, magnitude of the DFT $|G(e^{j\omega})|$ of $\mathbf{g}$ after reaching the steady state is shown. Although the loop has converged to filter taps g_n which are not equal to h_n, NAE has become sufficiently small as shown in Fig. 4.11.

Fig. 4.12b shows the PSD of the signal at the NIS output after reaching the steady state condition, corresponding to the input with the PSD shown in Fig. 4.10b. We see that the interference at zero frequency is suppressed below the noise floor and hence it is not visible in the figure. The IM component is present at +50 MHz ($2f_i - f_d$) with the same power as that of the desired signal.

4.6.3 Distortion products and SER of the RX

Fig. 4.13a and Fig. 4.13b show Signal to Noise plus Distortion Ration (SNDR) and the un-coded SER versus SIR_x for the optimal adaptation signal based on (4.1)

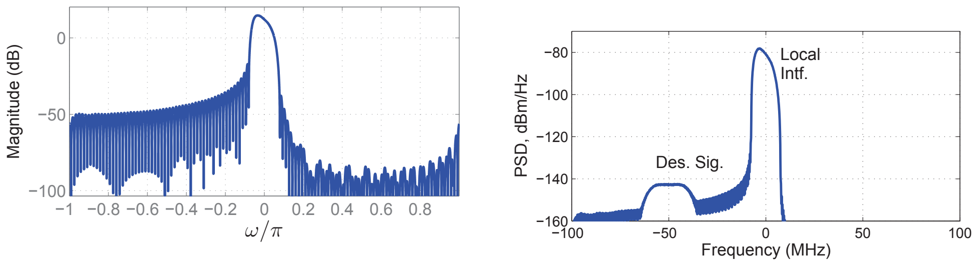

(a) $|H(e^{j\omega})|$ (b) PSD of $x(t)$

Figure 4.10: frequency response of the TX-RX path and PSD of NIS input signal $x(t)$.

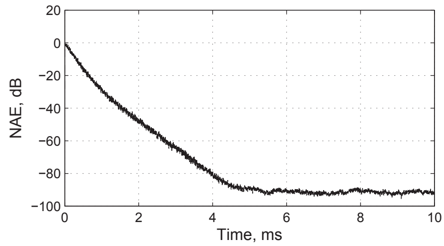

Figure 4.11: NAE versus time.

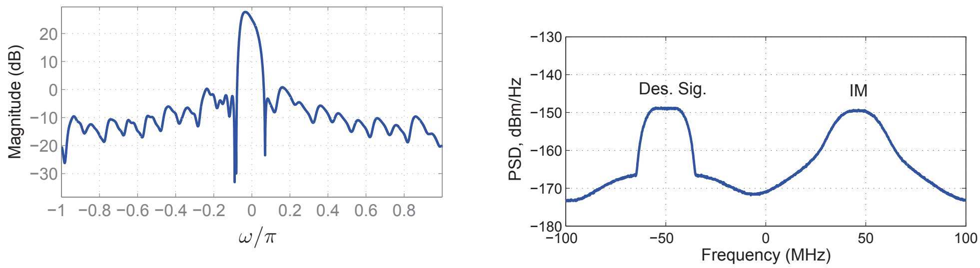

(a) $|G(e^{j\omega})|$ (b) PSD of $y(t)$

Figure 4.12: $|G(e^{j\omega})|$ and PSD of NIS output signal $y(t)$.

as well as the closed-loop adaptation method. For the exactly linear receiver an SNDR of 17.6 dB is obtained after the matched filtering, resulting in an un-coded SER of 10^{-3}. For the closed-loop method, the SNDR and the SER are measured after reaching the steady state. The adaptation is performed with two values of μ (0.0001 and 0.0003), which are equivalent to 3-dB bandwidth of 160 Hz and 480 Hz for the adaptation loop, respectively. For the receiver with the NIS, owing to the distortion products, the SNDR is less than 17.6 dB. When SIR decreases SNDR increases and eventually reaches a constant level. For the optimal adaptation

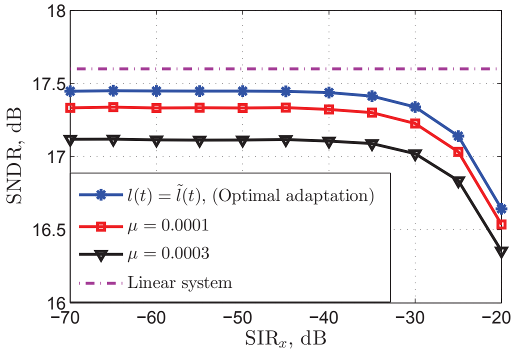

(a) SNDR.

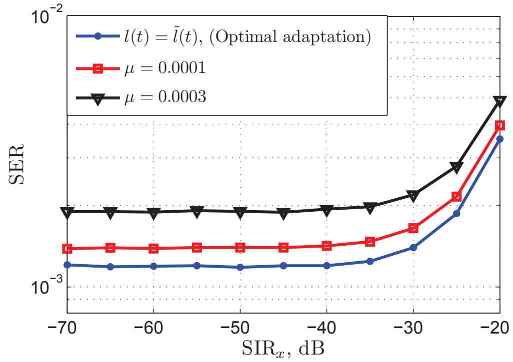

(b) SER.

Figure 4.13: SER and SNDR vs. SIR$_x$ for OFDM modulation, SER of the baseline RX: 10^{-3}.

the SNDR degradation is only because of GVD and the IM leakage. The SNDR degradation because of GVD becomes negligible for SIR$_x$ $<$ -30 dB. For SIR$_x$ $<$ -30 dB, the degradation to SNDR originates from the IM leakage. For the closed-loop method the disturbance component $\nu(t)$ in (4.26), causes a random adaptation error $\hat{l}(t) - \tilde{l}(t)$, whose power increases when μ increases. The adaptation error as discussed in Section 4.4.1 causes the interference leakage which degrades the SNDR and the SER compared to the optimal adaptation. For a sufficiently small μ, which still affords a practical adaptation speed, this degradation tends to be negligible.

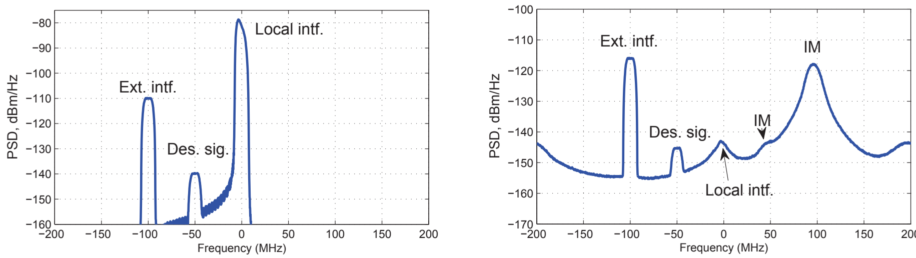

(a) PSD of $x(t)$

(b) PSD of $y(t)$

Figure 4.14: PSD of $x(t)$ and $y(t)$ in the presence of an external interference.

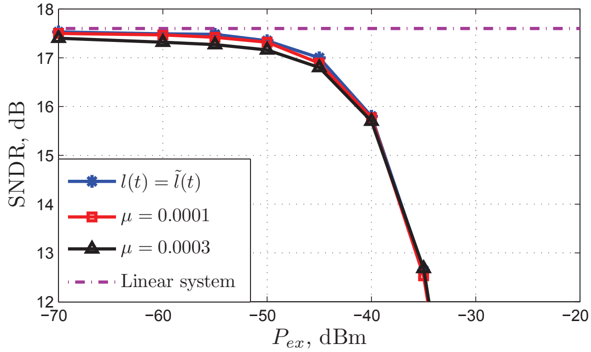

Figure 4.15: SNDR versus power P_{ex} of the external interference, for P_d =-60 dBm, P_i =0 dBm.

4.6.4 External Interference

In this section we assume that an external interference is present besides the local interference. Fig. 4.14a shows the NIS input with an external interference 30 dB weaker than the local interference and 30 dB stronger than the desired signal. Fig. 4.14b shows the NIS output after convergence of the adaption algorithm to its steady state solution. The external interference and desired signal are seen at the NIS output after 6 dB attenuation ($c = 1$). The residual interference is observed at zero frequency after about 66 dB attenuation as predicted by (4.16). Two IM components are seen at 50 MHz ($2f_i - f_d$) and 100 MHz ($2f_i - f_e$), with the same power as the desired signal and the external interference at the output.

Fig. 4.15 shows the SNDR for $P_d = -60$ dBm, $P_i = 0$ dBm, and the power of the external interference P_{ex} is swept from -70 dBm to -20 dBm. An SNR of 17.6 dB is chosen as in Section 4.6.3. The SNDR approaches that of a linear receiver as P_{ex} is about or less than P_i. When P_{ex} increases, distortion products emerge. These are a combination of interference leakage, GVD and IM leakage. For the common case where P_{ex} and P_d have the same order of magnitude, the degradation of SNDR is negligible. For the extreme case where $P_{ex} \gg P_d$, the distortion products decrease the SNDR substantially. In both cases, however, a large interference suppression is attained. For the second case a possible solution would be to use the NIS to substantially suppress the interference and use digital compensation methods to mitigate nonlinear distortion products.

4.7 Implementation aspects of the adaptation loop

4.7.1 Conversion rate of the DAC

To reconstruct $\hat{l}(t) \simeq \frac{\pi}{4} c A_i(t)$ from its sample $\hat{l}(n)$, the sampling rate $\frac{1}{T} = \frac{1}{r_i T_i}$ must be larger than twice the bandwidth of $A_i(t)$. For many modulation schemes the bandwidth of $A_i(t)$ can be several times larger than B_i. For example consider an OFDM modulated interference with a rectangular PSD over $[f_i - \frac{B_i}{2}, f_i + \frac{B_i}{2}]$. Then $A_i(t)$ has an approximately triangular PSD over $[-B_i, B_i]$ with a spike at the zero frequency (because of the DC component in $A_i(t)$). Outside of $[-B_i, B_i]$, the PSD of $A_i(t)$ at frequency f, decays approximately proportional to $\frac{1}{f^5}$ for $f \gg B_i$ [43]. In Table 4.2, NAE is shown as a function of r_i for an OFDM interference. The OFDM signal is pulse shaped by the root raised cosine filtering with $\beta = 0.1$. The amount of energy of $A_i(t)$ outside $[-10B_i, 10B_i]$ is 62 dB less than $\mathrm{E}\{A_i^2\}$. Hence by choosing $r_i = 20$ we will have NAE=-62 dB. (Because of $\frac{1}{f^5}$ decay, every doubling of r_i decreases NAE by about 15 dB.)

Table 4.2: NAE vs. r_i for various modulations of the interference.

r_i	2	4	6	8	10	20
NAE	-23 dB	-35 dB	-42 dB	-46 dB	-50 dB	-62 dB

4.7.2 Number of DAC and ADC bits

In Fig. 4.6, the DAC that converts $\hat{l}[n]$ to $\hat{l}(t)$, introduces a quantization error which leads to an adaptation error $\hat{l}(t) - \tilde{l}(t)$. For a DAC with n_b bits, the power of the quantization error will be $6n_b$ [dB] smaller than $\mathrm{E}\{l^2(t)\}$ [61]. For the extreme example in Section 4.4.1, we require NAE $<$ 76 dB, which is satisfied with a 13 bit DAC.

The number of bits for the ADC that digitizes $\eta(t)$ has a minor impact on the adaptation algorithm. The algorithm converges to a correct solution even if sign($\eta(t)$) - equivalent to a single bit ADC- is used. For the extreme case of a single bit ADC, however, the algorithm converges to the solution with a linear rate, similar to what is observed in the sign-LMS algorithm [62]. For a fixed μ, the misadjustment in NAE increases as the number of ADC bits is decreased. The misadjustmen can be decreased by decreasing μ [62].

4.7.3 Power consumption of the NIS approach

The NIS approach includes analog and digital circuits. The analog circuits include the NIS circuit, DAC and ADC. The power consumption of a realization of the NIS circuit, which can suppress an interference as large as 11 dBm, is 35 mW [33]. The power consumption of a 14 bit 100 MSPS DAC is 16 mW [63]. The power consumption of a 6 bit 100MSPS ADC is 5 mW [15]. The digital part of the NIS adaptation includes the adaptation block, filtering by the complex-valued filter taps g and calculating the envelope. The complexity of the digital part of NIS adaptation is much smaller than that of digital blocks of modern receivers. A more detailed analysis of the digital part of the NIS adaptation can be found in [46] which results in 10 mW for $\frac{1}{T} = 100$ MHz. As a result the total power consumption of the NIS method would be about 66 mW.

A typical WLAN RX front-end with a 1 dB compression point (P1dB) of -27 dBm consumes about 82 mW [47]. The power consumption of active circuits is proportional to their linearity (e.g. P1dB) [4]. In the WiMAX LTX and WLAN LRX scenario we may encounter WiMAX interferences as large as 0 dBm. To handle such a large interference by increasing the linearity of the RX, the power consumption must be increased by 3 orders of magnitude which is impossible. Accordingly the NIS method can suppress the interference with a much smaller power consumption.

4.8 Conclusion

In multimode transceivers, the interference induced by a local transmitter can be several orders of magnitude stronger than the received desired signal, even after partial suppression by analog filters. Hence a linear receiver requires an excessive linear dynamic range to process the desired signal in the presence of such a large interference, leading to an unreasonable power consumption. Alternatively a memoryless nonlinear circuit which is adapted to track the envelope of the received interference can suppress the interference without excessive power consumption. In this paper we analyzed the accuracy requirement on the adaptation signal such that the interference is sufficiently suppressed and at the same time a symbol error rate (SER) close to that of the linear receiver is achieved. To provide the required accuracy we proposed a closed-loop method based on an adaptive model of the transmit-receive path of the interference. This model is adapted during the operation of the transceiver such that the power of the residual interference at the output of the nonlinear circuit is minimized. The analysis and simulations for a practical multimode scenario shows that the proposed method can suppress the interference to a level below that of the desired signal. For most conditions of practical interest the nonlinear suppressor introduces a negligible amount of nonlinear distortion products. It is found that presence of an external interference much stronger than the desired signal can introduce substantial distortion products. Digital compensation methods may be used in future works to mitigate these products. The power consumption of the proposed nonlinear interference suppression approach is estimated based on the state of the art components and tends to be much smaller than that of linear suppression approaches.

Appendix I : Possible Solutions for filter tap h_n

In this appendix we study all possible filter taps $\tilde{h}_n$ that lead to the same envelope signal in (4.5). We see that except r_i arbitrary phase shifts in the form of $e^{j\theta_i}$, $i = 1, .., r_i$ the taps are unique. The equality of envelopes:

$$|(h * i)[n]| = |(\tilde{h} * i)[n]| \tag{4.35}$$

is equivalent to:

$$|(h * i)[n = r_i p + k]| = |(\tilde{h} * i)[n = r_i p + k]|, \qquad k = 0, 1, ..., r_i - 1, \tag{4.36}$$

which should hold for all samples of $i[n]$. Considering that $i[n]$ is obtained by inserting $r_i - 1$ zeros between independent and identically distributed symbols of $i[p]$, in (4.36) equations for different values of k are independent from each other. Hence without loss of generality we can investigate the possible solutions for one equation $k = 0$ and then construct all possible solutions by combing the solutions for different ks. We first investigate the possible solutions for two taps as:

$$\tilde{l}[p] = |h_0 i[p] + h_{r_i} i[p-1]| = |\tilde{h}_0 i[p] + \tilde{h}_{r_i}[p-1]|. \tag{4.37}$$

The generalization to more than two taps can be achieved by induction. The solution for $\tilde{h}_0$ and $\tilde{h}_{r_i}$ is not unique. By multiplying both taps by a unit amplitude complex number $e^{j\theta}$ the equality in (4.37) still holds. Hence all the taps in the form of $[\tilde{h}_0, \tilde{h}_{r_i}] = [e^{j\theta_0} h_0, e^{j\theta_0} h_{r_i}]$ are solutions. By factoring $\tilde{h}_0$, (without loss of generality we can assume $|\tilde{h}_0| \neq 0$.), we obtain:

$$|h_0 i[p] + h_{r_i} i[p-1]| = \alpha |i[p] + \beta_1 i[p-1]|. \tag{4.38}$$

A sufficient condition for (4.38) to hold is that :

$$\alpha = |h_0| \text{ and } \beta_1 = \frac{h_{r_i}}{h_0}. \tag{4.39}$$

Now we prove that for most practical communication signals $i[p]$, the conditions in (4.39) are necessary too. To this end we can prove that (4.38) results in a unique solution for β_1. Since $i[p]$ is a communication signal, it should take at least two different values i_0 and i_1. Also these values are transmitted randomly. Hence all the 4 combinations of i_0 and i_1 in (4.38) occur. Suppose that the 4 combinations occur for time instants p_1,...,p_4 Hence we have at least 4 equation as:

$$\begin{aligned} |i_0 + \beta_1 i_0| &= \frac{\tilde{l}[p_1]}{\alpha} \\ |i_0 + \beta_1 i_1| &= \frac{\tilde{l}[p_2]}{\alpha} \\ |i_1 + \beta_1 i_0| &= \frac{\tilde{l}[p_3]}{\alpha} \\ |i_1 + \beta_1 i_1| &= \frac{\tilde{l}[p_4]}{\alpha}, \end{aligned} \tag{4.40}$$

which must hold, simultaneously. The first and forth equations in (4.40) are identical. The first three equations can be written as:

$$\begin{aligned}
|1+\beta_1| &= \frac{\tilde{l}[0]}{\alpha|i_0|} = R_0 \\
|\frac{i_0}{i_1}+\beta_1| &= \frac{\tilde{l}[1]}{\alpha|i_1|} = R_1 \\
|\frac{i_1}{i_0}+\beta_1| &= \frac{\tilde{l}[2]}{\alpha|i_2|} = R_2.
\end{aligned} \tag{4.41}$$

The possible solutions for first equation in (4.41) are shown in Fig. 4.16a. Since $|1+\beta_1|$ is the amplitude of the sum of two vectors (from -1 to 0 and from 0 to a point with coordinate β_1 in the complex plane), the locus of solutions is a circle with radius R_0 and center of -1, in the complex plane. As shown in Fig. 4.16b, the locus for solutions of second and third equations in (4.41) are circles with centers $-\frac{i_0}{i_1}$ and $-\frac{i_1}{i_0}$ and radii of R_1 and R_2. Two circles with different centers collide at most 2 points (here circles collides at least 1 point, i.e. β_1). Hence by using the first and second equations in (4.41), the possible solutions are limited to two points. Using the third equation gives us a unique answer, i.e. β_1. The only case that three circles may have two intersections is when the centers are on the same line, as shown in Fig. 4.16c. For three points (z_0,z_1,z_3) to be on the same line in the complex plane we must have : $(z_3 - z_2) = a(z_2 - z_1)$, where a is real number, which occurs only when $\frac{i_0}{i_1} = a$. This ratio can be real for PAM modulations. In this case both β_1 and β_1^* can solve (4.41). However the solution for phase or frequency modulations, QAM modulations and OFDM modulations will be unique. Hence all solutions for (4.37) are in the form of $[\tilde{h}_0, \tilde{h}_{r_i}] = e^{j\theta}[h_0, h_{r_i}]$.

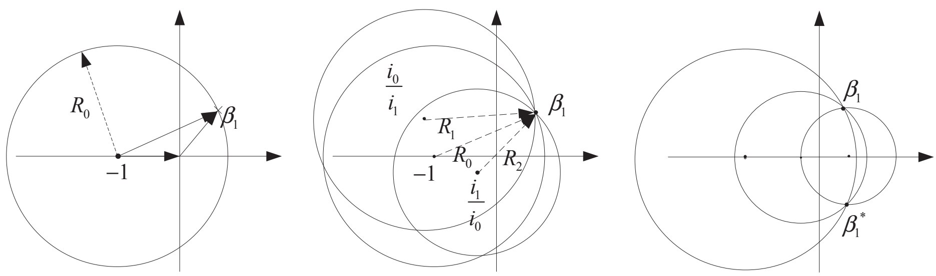

Figure 4.16: Possible solutions of (4.41).

Now all solutions of (4.36) can be obtained by combing the solutions of (4.37) for $k = 0, 1, ..., r_i - 1$ as:

$$\begin{aligned}
&[\tilde{h}_0, \tilde{h}_1, ..., h_{r_i-1}, \tilde{h}_{r_i}, \tilde{h}_{r_i+1}, ..., \tilde{h}_{2r_i-1}] = \\
&[e^{j\theta_0}h_0, e^{j\theta_1}h_1, ..., e^{j\theta_{r_i-1}}h_{r_i-1}, e^{j\theta_0}h_{r_i}, e^{j\theta_1}h_{r_i+1}, ..., e^{j\theta_{r_i-1}}h_{2r_i-1}],
\end{aligned}$$

where θ_i are independent real numbers.

For more than two taps, the result for two tap can be recursively used to arrive at all possible solutions. For example for three taps the equation:
$\tilde{l}[n] = \alpha|i[p] + \beta_1 i[p-1] + \beta_2 i[p-2]|$
can be written as:
$\tilde{l}[n] = \alpha|i[p] + \beta_1(i[p-1] + \frac{\beta_2}{\beta_1} i[p-2])| = \alpha|i[p] + \beta_1(i'[p-1])|$,
where $i'[p-1] = i[p-1] + \frac{\beta_2}{\beta_1} i[p-2]$. Using the proof for two taps we deduce that β_1 is unique. The same procedure can be performed for β_2.

Appendix II: Derivation of the error signal

In this appendix the extraction of the error signal for the adaptation loop in Fig. 4.6 is analyzed. The switching mixing described in (4.25) is equivalent to multiplying $y(t)$ by $x_L(t) = \mathrm{sign}(x(t)) = \{1, x(t) > 0; 0, x(t) = 0; -1, x(t) < 0\}$. Equivalently $x_L(t)$ can be obtained by passing $x(t)$ through a hard limiter. Using the analysis in [58] for a bandpass limiter when $A_i(t) >> A_d(t)$, $x_L(t)$ is obtained as:

$$\begin{aligned} x_L(t) \simeq \frac{4}{\pi}\Bigg(& \cos(2\pi f_i t + \varphi_i(t)) + \frac{A_d(t)}{2A_i(t)}\cos(2\pi f_d t + \varphi_d(t)) \\ & - \frac{A_d(t)}{2A_i(t)}\cos(2\pi(2f_i - f_d)t + 2\varphi_i(t) - \varphi_d(t))\Bigg) \\ & + \text{high frequency components around } 3f_d, 3f_i,\ 5f_d,\ 5f_i, .., \ 2f_i \pm f_i, ... \end{aligned} \tag{4.42}$$

The BPF2 in Fig. 3 filters out the high frequency components of $y(t)$ in (4.8) such that only the components around f_d and f_i remain. Thus it is sufficient to only consider the component of $x_L(t)$ around f_i and f_d. The mixer output $\eta(t)$ is obtained as:

$$\begin{aligned} \eta(t) \simeq x_L(t)y(t) = \frac{2}{\pi}\Bigg(& A_{i,y}(t) + A_{d,y}(t)\frac{A_d(t)}{2A_i(t)} - A_{\mathrm{IM}}(t)\frac{A_d(t)}{2A_i(t)} \\ & + \left(A_{d,y}(t) + A_{i,y}(t)\frac{A_d(t)}{2A_i(t)}\right)\cos(2\pi(f_d - f_i)t + \varphi_d(t) - \varphi_i(t)\Bigg) \\ & + \text{high frequency components around } 2f_d, \\ & , 2f_i, 2f_i - 2f_d, 2(2f_i - f_d), f_i + f_d, 3f_i \pm f_d, .. \ . \end{aligned} \tag{4.43}$$

Because of the low-pass nature of the feedback loop we can neglect the high frequency components of $\eta(t)$. Also the component at $f_d - f_i$ which has an envelope of $A_{i,y}(t)\frac{A_d(t)}{2A_i(t)}$ can be neglected, since $A_{i,y}(t)\frac{A_d(t)}{2A_i(t)} \ll A_{d,y}(t)$. By neglecting these components we obtain:

$$\begin{aligned} \eta(t) \simeq x_L(t)y(t) = \frac{2}{\pi}\Bigg(& A_{i,y}(t) + A_{d,y}(t)\frac{A_d(t)}{2A_i(t)} - A_{\mathrm{IM}}(t)\frac{A_d(t)}{2A_i(t)} \\ & + A_{d,y}(t)\cos(2\pi(f_d - f_i)t + \varphi_d(t) - \varphi_i(t)\Bigg). \end{aligned} \tag{4.44}$$

Using (4.17) and (4.44), $\eta(t)$ is simplified to:

$$\eta(t) \simeq K(\hat{l}(t) - \tilde{l}(t)) + \nu(t) \simeq K(|g(t) * i(t)| - |h(t) * i(t)|) + \nu(t), \tag{4.45}$$

where

$$K = \frac{8}{\pi^2}\left(1 + \frac{1}{2}\frac{A_d^2(t)}{A_i^2(t)}\right), \tag{4.46}$$

and

$$\begin{aligned}\nu(t) &= \frac{2}{\pi}A_{d,y}(t)\cos(2\pi(f_d - f_i)t + \varphi_d(t) - \varphi_i(t)), \\ &= \frac{2}{\pi}\left(\frac{\hat{l}(t)}{2l(t)} - 1\right)cA_d(t)\cos(2\pi(f_d - f_i)t + \varphi_d(t) - \varphi_i(t)), \\ &\simeq \frac{1}{\pi}cA_d(t)\cos(2\pi(f_d - f_i)t + \varphi_d(t) - \varphi_i(t)). \end{aligned} \tag{4.47}$$

Now we prove that the information-bearing part of $\eta(t)$, i.e. $|g(t)*i(t)|-|h(t)*i(t)|$, and $\nu(t)$ are uncorrelated.

$$\mathrm{E}((|g(t)*i(t)| - |h(t)*i(t)|)\nu(t)) \simeq \frac{1}{\pi}c\mathrm{E}((|g(t)*i(t)| - |h(t)*i(t)|)\nu(t)) \tag{4.48}$$

$$= \frac{1}{\pi}c\mathrm{E}\begin{pmatrix} (|g(t)*i(t)| - |h(t)*i(t)|)\,A_d(t)\cos(2\pi f_d t + \varphi_d(t))\cos(2\pi f_i t + \varphi_i(t)) \\ +\,(|g(t)*i(t)| - |h(t)*i(t)|)\,A_d(t)\sin(2\pi f_d t + \varphi_d(t))\sin(2\pi f_i t + \varphi_i(t)) \end{pmatrix}$$

Since the desired signal and interference are uncorrelated and $\mathrm{E}\left(A_d(t)\cos(2\pi f_d t + \varphi_d(t))\right) = \mathrm{E}\left(A_d(t)\sin(2\pi f_d t + \varphi_d(t))\right) = 0$, we obtain:

$$\mathrm{E}((|g(t)*i(t)| - |h(t)*i(t)|)\nu(t)) = 0 \tag{4.49}$$

Appendix III: Derivation of the gradient

In this appendix the first and second derivative of the cost function are obtained. The complex-valued gradient vector $\nabla_{\mathbf{g}}$ is defined as [60]:

$$\nabla_{\mathbf{g}} = \left[\frac{\partial}{\partial g_0}, .., \frac{\partial}{\partial g_p}, .., \frac{\partial}{\partial g_{M-1}}\right]^T \tag{4.50}$$

where g_p is a complex-valued variable:

$$g_p = x_p + jy_p, \tag{4.51}$$

and the complex-valued derivative $\frac{\partial}{\partial g_p}$ is defined as:

$$\frac{\partial}{\partial g_p} = \frac{\partial}{\partial x_p} + j\frac{\partial}{\partial y_p} \tag{4.52}$$

It can be easily proved that:

$$\frac{\partial}{\partial g_p} g_p = 0, \qquad \frac{\partial}{\partial g_p} g_p^* = 2, \qquad \frac{\partial}{\partial g_p} |g_p|^2 = 2g_p \tag{4.53}$$

The derivative of the cost function with respect to g_p is obtained as:

$$\frac{\partial}{\partial g_p} J(\mathbf{g}) = 2\mathrm{E}\left(\eta[n]\left(\frac{\partial}{\partial g_p}|\mathbf{g^T i}[n]|\right)\right). \tag{4.54}$$

We define u and v as:

$$\begin{aligned} u &= \sum_{\substack{m=0 \\ m\neq p}}^{M-1} i[n-m]g_m \\ v &= i[n-p], \end{aligned} \tag{4.55}$$

then $\mathbf{g^T i}[n] = u + g_p v$ and

$$\begin{aligned} \frac{\partial}{\partial g_p}|\mathbf{g^T i}[n]| &= \frac{\partial}{\partial g_p}(|u+g_p v|) = \frac{\partial}{\partial g_p}(\sqrt{|u+g_p v|^2}) \\ &= \frac{\partial}{\partial g_p}(\sqrt{(u+g_p v)(u^* + g_p^* v^*)}) = \frac{2uv^* + 2g_p v v^*}{2\sqrt{|u+g_p v|^2}} = \frac{u+g_p v}{|u+g_p v|}v^* \end{aligned} \tag{4.56}$$

and hence

$$\frac{\partial}{\partial g_p}|\mathbf{g}^T\mathbf{i}[n]| = \frac{\mathbf{g}^T\mathbf{i}[n]}{|\mathbf{g}^T\mathbf{i}[n]|} i^*[n-p]. \tag{4.57}$$

The same derivation holds for other elements (taps) of $\mathbf{g}$ and the gradient vector is obtained as:

$$\begin{aligned}\nabla_{\mathbf{g}}|\mathbf{g}^T\mathbf{i}[n]| &= \frac{\mathbf{g}^T\mathbf{i}[n]}{|\mathbf{g}^T\mathbf{i}[n]|}\mathbf{i}^*[n] \\ \nabla_{\mathbf{g}}J(\mathbf{g}) &= \mathrm{E}\left(\eta[n]\frac{\mathbf{g}^T\mathbf{i}[n]}{|\mathbf{g}^T\mathbf{i}[n]|}\mathbf{i}^*[n]\right)\end{aligned} \tag{4.58}$$

The second derivative of the cost function is obtained as:

$$\begin{aligned}\frac{\partial}{\partial g_k^*\partial g_p}(J(\mathbf{g})) &= 2\mathrm{E}\left(\frac{\partial}{\partial g_k^*}\left(\eta[n]\left(\frac{\partial}{\partial g_p}|\mathbf{g}^T\mathbf{i}[n]|\right)\right)\right) \\ &= 2\mathrm{E}\left(\frac{\partial}{\partial g_k^*}\left(\eta[n]\frac{\mathbf{g}^T\mathbf{i}[n]}{|\mathbf{g}^T\mathbf{i}[n]|}i^*[n-p]\right)\right) \\ &= 2\mathrm{E}\left(i^*[n-p]\frac{\partial}{\partial g_k^*}\left(\eta[n]\frac{\mathbf{g}^T\mathbf{i}[n]}{|\mathbf{g}^T\mathbf{i}[n]|}\right)\right),\end{aligned} \tag{4.59}$$

and $\frac{\partial}{\partial g_k^*}\left(\eta[n]\frac{\mathbf{g}^T\mathbf{i}[n]}{|\mathbf{g}^T\mathbf{i}[n]|}\right)$ can be obtained as:

$$\frac{\partial}{\partial g_k^*}\left(\eta[n]\frac{\mathbf{g}^T\mathbf{i}[n]}{|\mathbf{g}^T\mathbf{i}[n]|}\right) = \frac{\partial}{\partial g_k^*}(\eta[n])\frac{\mathbf{g}^T\mathbf{i}[n]}{|\mathbf{g}^T\mathbf{i}[n]|} + \frac{\partial}{\partial g_k^*}\left(\frac{\mathbf{g}^T\mathbf{i}[n]}{|\mathbf{g}^T\mathbf{i}[n]|}\right)\eta[n]. \tag{4.60}$$

Similar to (4.56) it can be shown that:

$$\frac{\partial}{\partial g_k^*}(\eta[n]) = \frac{\left(\mathbf{g}^T\mathbf{i}[n]\right)^*}{|\mathbf{g}^T\mathbf{i}[n]|}i[n-k]. \tag{4.61}$$

Now we define u' and v' as:

$$u' = \sum_{\substack{m=0\\ m\neq k}}^{M-1} i[n-m]g_m, \qquad v' = i[n-k], \tag{4.62}$$

then

$$\begin{aligned}\frac{\partial}{\partial g_k^*}\left(\frac{\mathbf{g}^T\mathbf{i}[n]}{|\mathbf{g}^T\mathbf{i}[n]|}\right) &= \frac{\partial}{\partial g_k^*}\left(\frac{u'+g_kv'}{|u'+g_kv'|}\right) = \frac{\partial}{\partial g_k^*}\left(\sqrt{\frac{u'+g_kv'}{(u'+g_kv')^*}}\right) \\ &= \frac{1}{2}\frac{\frac{2v'\left(u'+g_kv'\right)^*}{\left(u'^*+g_k^*v'^*\right)^2}}{\sqrt{\frac{u'+g_kv'}{(u'+g_kv')^*}}} = \frac{v'}{|u'+g_kv'|} = \frac{i[n-k]}{|\mathbf{g}^T\mathbf{i}[n]|}\end{aligned} \tag{4.63}$$

Using (4.61) and (4.63), (4.60) can be simplified as:

$$\begin{aligned}\frac{\partial}{\partial g_k^*}\left(\eta[n]\frac{\mathbf{g}^T\mathbf{i}[n]}{|\mathbf{g}^T\mathbf{i}[n]|}\right) &= \frac{\left(\mathbf{g}^T\mathbf{i}[n]\right)^*}{|\mathbf{g}^T\mathbf{i}[n]|}i[n-k]\frac{\mathbf{g}^T\mathbf{i}[n]}{|\mathbf{g}^T\mathbf{i}[n]|} + \eta[n]\frac{i[n-k]}{|\mathbf{g}^T\mathbf{i}[n]|} \\ &= i[n-k]\left(1+\frac{\eta[n]}{|\mathbf{g}^T\mathbf{i}[n]|}\right) = i[n-k]\left(2-\frac{l[n]}{|\mathbf{g}^T\mathbf{i}[n]|}\right) \\ &= i[n-k]\left(2-\frac{\tilde{l}[n]}{\hat{l}[n]}\right) \end{aligned} \tag{4.64}$$

By substituting (4.64) in (4.59) we obtain:

$$\frac{\partial}{\partial g_k^* \partial g_p}(J(\mathbf{g})) = 2\mathrm{E}\left(i^*[n-p]i[n-k]\left(2-\frac{\tilde{l}[n]}{\hat{l}[n]}\right)\right). \tag{4.65}$$

Hence the Hessian matrix $\nabla^2_{\mathbf{g}}(J(\mathbf{g}[n]))$ of the cost function is obtained as:

$$\nabla^2_{\mathbf{g}}(J(\mathbf{g})) = 2\mathrm{E}\left(\left(2-\frac{\tilde{l}[n]}{|\mathbf{g}^T\mathbf{i}[n]|}\right)\mathbf{i}[n]\mathbf{i}^H[n]\right) = 2\mathrm{E}\left(\left(2-\frac{\tilde{l}[n]}{\hat{l}[n]}\right)\mathbf{i}[n]\mathbf{i}^H[n]\right). \tag{4.66}$$

Chapter 5

Experimental evaluation of an Adaptive Nonlinear Interference Suppressor for Multimode Transceivers[1]

5.1 abstract

In multimode transceivers, the transmitter for one communication standard may induce a strong interference in the receiver for another standard. Using linear filtering techniques to suppress this interference requires a receiver with a very large dynamic range, leading to an excessive power consumption. A much more power efficient approach suppresses the interference using an adaptive Nonlinear Interference Suppressor (NIS). In previous work an ideal model was used to derive an adaptation method and study the receiver performance afforded by the NIS. In this paper, we present experimental results of a receiver that uses an implementation of the NIS, fabricated in 140 nm CMOS technology. Main imperfections that limit the NIS performance are identified, simple models are developed that explain the experimental results, and for the key imperfections, low-complexity digital compensation and calibration methods are proposed. These digital meth-

[1]This chapter is reproduced from the paper published as H. Habibi, E.J.G. Janssen, Wu Yan, D. Milosevic, P.G.M. Baltus, J.W.M. Bergmans, "Experimental evaluation of an Adaptive Nonlinear Interference Suppressor for Multimode Transceivers", *IEEE Journal on Emerging and Selected Topics in Circuits and Systems, Dec. 2013.*

ods permit the use of lower-performance analogue circuits, thus further reducing the transceiver cost and power consumption. The experimental results show that the NIS can achieve a substantial interference suppression at attractive complexity and power dissipation.

5.2 Introduction

Modern mobile phones include multimode transceivers, which combine several transceivers that may be active at the same time [2, 3, 19]. Owing to the small size of the phone, the local Transmitter (TX) of one standard induces a large interference in the local Receiver (RX) of another standard, often many orders of magnitude stronger than the desired received signal.

Current filtering techniques cannot sufficiently suppress this large interference directly after the receive antenna [64]. An interference with no spectral overlap with the desired signal can in theory be filtered out after down-conversion by the receiver Front-End (FE). The receiver FE, however, in practice has a limited linear dynamic range and the large local interference desensitizes the receiver FE [21], resulting in a severe loss in receiver sensitivity. Increasing the linear dynamic range to avoid desensitization leads to an unacceptable increase in power consumption [4].

A much more power efficient approach suppresses the interference by passing the received signal through a special memoryless nonlinearity [16, 65]. This Nonlinear Interference Suppressor (NIS) can be built by adding outputs of a linear amplifier (with gain of $-c$) and a limiter with an adaptable limiting amplitude $l(t)$ as shown in Fig. 5.1. At the NIS input there is a strong interference at a frequency f_i and a weak desired signal at a frequency f_d. When these two signals pass though the limiter, owing to its compressive nature, the weak signal at f_d will be suppressed relative to the strong one at f_i. The amplifier, on the other hand, has the same gain ($-c$) for both signals. By adapting $l(t)$ proportional to the envelope of the strong signal, the gain of the limiter for the strong signal can be made equal to c. As a result no interference will be left at the output of the NIS, whereas a net desired signal component remains. As seen in Fig. 5.1, owing to the limiter nonlinear characteristic, an Inter-Modulation (IM) product of the interference and the desired signal is also generated. The IM, however, is located at a different frequency than f_d and can be filtered out in later stages.

In the multimode transceiver, the baseband transmitted interference is available locally. Using a baseband model of the interference coupling path, from the transmitted interference to the received interference at the NIS input, the adaptation signal can be obtained digitally. Since the coupling path is subject to environmen-

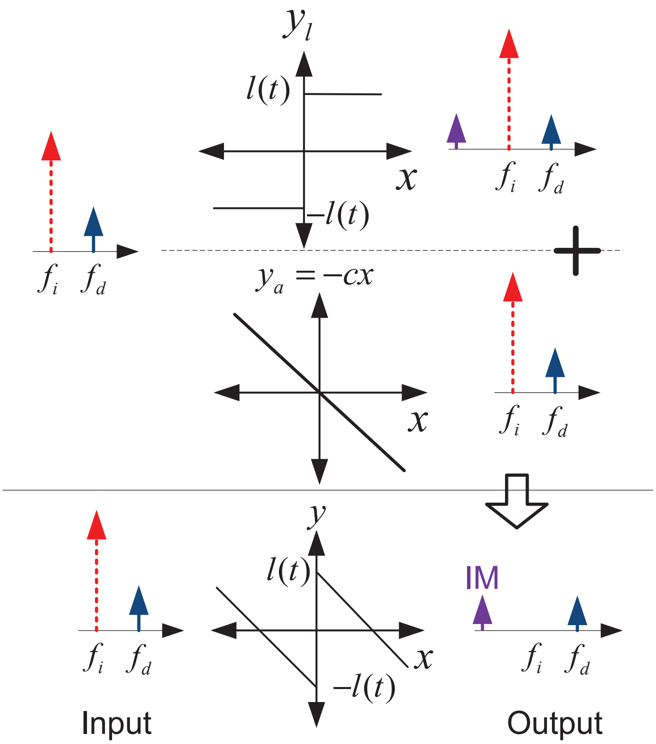

Figure 5.1: NIS input-output characteristic.

tal changes, the path model should be adapted to track these changes. In [65], a closed-loop adaptation method is proposed to adapt the path model such that the residual interference at the NIS output is minimized. In previous work [32, 65], the ideal model of Fig. 5.1 was used to analyze the receiver performance with the NIS. It was found that both constant and varying-envelope interferences can be substantially suppressed with a negligible degradation to the symbol error rate compared to that of an exactly linear receiver [65].

In [33], an implementation of the NIS circuit, fabricated in 140 nm CMOS technology, is presented. In [56], early experimental results for constant-envelope interference were presented. In this paper, we present experimental results of a multimode transceiver testbed that uses a mixed-signal NIS implementation for suppression of constant and varying-envelope interferences. Based on these experiments, we identify key deviations of the NIS implementation from the ideal model and present simple models to explain them. The key deviations are:
1-*Phase misalignment between limiter and amplifier*: This originates from memory effects in the circuit and limits the interference suppression. A model is developed to explain this effect and a method is proposed to measure the phase misalign-

ment accurately, which in principle can be used for automatic calibration of the alignment.
2-*The finite slope of the implemented limiter at the origin*: This firstly limits the weakest interference that the NIS can suppress, and secondly causes the gain of the desired signal to depend on the envelope of the interference. This dependency results in a nonlinear distortion of the desired signal.
3-*DC offset in the adaptation loop*: This limits interference suppression.
4-*AM-PM distortion of the desired signal*: This originates from a combination of nonlinear effects and short-term memory effects.
We propose and evaluate simple schemes to digitally compensate for the distortions at baseband and calibrate for the DC offset. To account for these practical imperfections, the closed-loop adaptation methods in [32, 65] are modified and are validated using the transceiver testbed. The measurement results show that a significant interference suppression and an acceptable modulation error ratio can be achieved. This suggests that the proposed method is promising for practical applications.

The problem that a local interference causes to a local receiver is encountered in a number of other applications like Frequency Division Duplex (FDD) transceivers [5], co-located base station transceivers [10], FMCW radar [66], and RFID Gen 2 readers [67]. The NIS approach can also be considered as a potential solution for such applications.

The rest of the paper is organized as follows. In Section 5.3 we describe the multimode transceiver and the NIS. In Section 5.4 the multimode transceiver testbed is described. In Section 5.5 the measurement results for Single Tone (ST) signals are presented and compared with numerical results based on the proposed NIS models. By considering these measurement results a practical closed-loop adaptation method is proposed. In Section 5.6 the experimental results for constant-envelope interference are presented. In Section 5.7, the numerical and experimental results for varying envelope interferences using the closed-loop adaptation method are presented. Section 5.8 compares the NIS approach with a cancellation approach and gives a summary of pros and cons of using the NIS. The concluding remarks come in Section 5.9.

5.3 System model

5.3.1 Multimode Transceiver with NIS

The multimode transceiver including the NIS is shown in Fig. 5.2. A Local RX (LRX) is meant to receive a desired signal, transmitted by a Remote TX (RTX). At the same time, the Local TX (LTX) Front-End (FE) up-converts the baseband

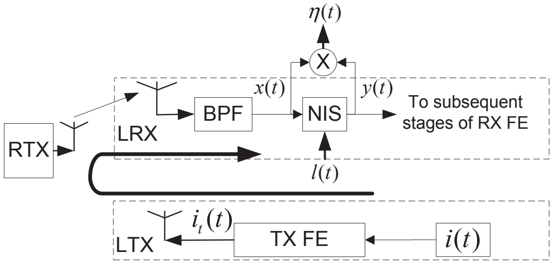

Figure 5.2: Multimode transceiver with NIS.

interference $i(t)$ and transmits it as $i_t(t)$. A part of $i_t(t)$ is received by the LRX after a coupling loss [19], inducing an interference. The combination of the received desired signal and the interference is passed through a Band Pass Filter (BPF). After the BPF, the NIS input $x(t)$ includes both the desired signal and interference as:

$$x(t) = A_d(t)\cos(2\pi f_d t + \varphi_d(t)) + A_i(t)\cos(2\pi f_i t + \varphi_i(t)), \tag{5.1}$$

where A_d, φ_d, f_d, A_i, φ_i, and f_i are envelope, phase and center frequencies of the desired signal and interference at the NIS input, respectively.

The NIS output $y(t)$ is a nonlinear function $f(\cdot)$ of $x(t)$ as: $y(t) = f(x(t))$. The high-frequency components of $y(t)$ around $3f_i$ and higher harmonics must be sufficiently attenuated immediately at the NIS output, otherwise they can saturate the NIS output, or generate nonlinear distortion products in the subsequent stages. The current NIS circuit uses an embedded LC tank to suppress the harmonics, which is sufficient, owing to the large frequency separation of the harmonics from f_d. By considering only the components around f_d and assuming a memoryless nonlinearity, $y(t)$ can be written as [58]:

$$\begin{aligned} y(t) \simeq\ & A_{d,y}(t)\cos(2\pi f_d t + \varphi_d(t)) + A_{i,y}(t)\cos(2\pi f_i t + \varphi_i(t)) \\ & + A_{IM}(t)\cos(2\pi(2f_i - f_d)t + 2\varphi_i(t) - \varphi_d(t)), \end{aligned} \tag{5.2}$$

where $A_{i,y}$, $A_{d,y}$, and A_{IM} are envelopes of the interference, desired signal and the main intermodulation at the NIS output. For $A_d \ll A_i$ one can obtain [68]:

$$\begin{aligned} A_{i,y} &= F(A_i), \\ A_{d,y} &= \frac{1}{2}A_d\left(\frac{\partial F(A_i,l)}{\partial A_i} + \frac{F(A_i,l)}{A_i}\right), \\ A_{\mathrm{IM}} &= \frac{1}{2}A_d\left(\frac{\partial F(A_i,l)}{\partial A_i} - \frac{F(A_i,l)}{A_i}\right), \end{aligned} \tag{5.3}$$

where $F(\cdot)$ is the baseband model of the RF nonlinearity $f(\cdot)$ and can be obtained as:

$$F(A) = \frac{1}{\pi} \int_{0}^{2\pi} f(A\cos(\theta))\cos(\theta)d\theta. \tag{5.4}$$

5.3.2 Adaption of the NIS

For the NIS there is an optimal adaptation signal $\tilde{l}(t)$ that minimizes $\mathrm{E}(A_{i,y}^2)$, where E() denotes the expected value. For the hard-limiter (HL) NIS, shown in Fig. 5.1, we have: $f_{\mathrm{HL}}(x,l) = l \cdot \mathrm{sign}(x) - cx$. Using (5.4) one can obtain: $A_{i,y} = F_{\mathrm{HL}}(A_i, l) = \frac{4}{\pi} l - cA_i$. For the HL NIS, $A_{i,y}$ can be zeroed by adapting the NIS according to:

$$\tilde{l}_{\mathrm{HL}}(t) = \frac{\pi}{4} c A_i(t). \tag{5.5}$$

For the HL NIS according to (5.3), we obtain:

$$A_{d,y} = -\frac{c}{2} A_d, \qquad A_{\mathrm{IM}} = A_{d,y}. \tag{5.6}$$

Thus the voltage gain of the HL NIS limiter for the weak desired signal will be half the gain $(-c)$ of the amplifier.

In a multimode transceiver $i(t)$ is available locally so that $A_i(t)$ and hence $\tilde{l}_{\mathrm{HL}}(t)$ can be computed from $i(t)$, if the characteristics of the coupling path (shown in Fig. 5.2 with the bold line) are known. These characteristics can be described via a linear baseband model. Since the coupling path is subject to environmental changes, the model parameters must be adapted during receiver operation. A closed-loop adaptation method is proposed in [65], which generates a discrete-time estimation $\hat{l}[n]$ of $\tilde{l}(t)$ using a finite impulse response model $g[n]$ of the path. The model $g[n]$ is adapted during the transceiver operation based on the output $\eta(t)$ of the switching mixer in Fig. 5.2 such that $\mathrm{E}(A_{i,y}^2)$ is minimized.

In principle, the NIS can be used to suppress any interference, if the envelope of the received interference is accurately tracked. For an external interference, however, this requires an auxiliary receiver tuned to the interference. Moreover, a receiver inevitably introduces a significant delay. Thus the NIS input $x(t)$ must be also delayed to synchronize it with the adaptation signal. Besides the required analogue complexity, implementing such delay would be a challenging task.

The following notations are used in the rest of the paper. The instantaneous powers of the desired signal and interference at the NIS input and output are denoted by $P_d(t) = \frac{A_d^2(t)}{2R}$, $P_i(t) = \frac{A_i^2(t)}{2R}$, $P_{d,y}(t) = \frac{A_{d,y}^2(t)}{2R}$, and $P_{i,y}(t) = \frac{A_{i,y}^2(t)}{2R}$, where $R = 50\ \Omega$ is the reference impedance. The NIS power gains for the desired

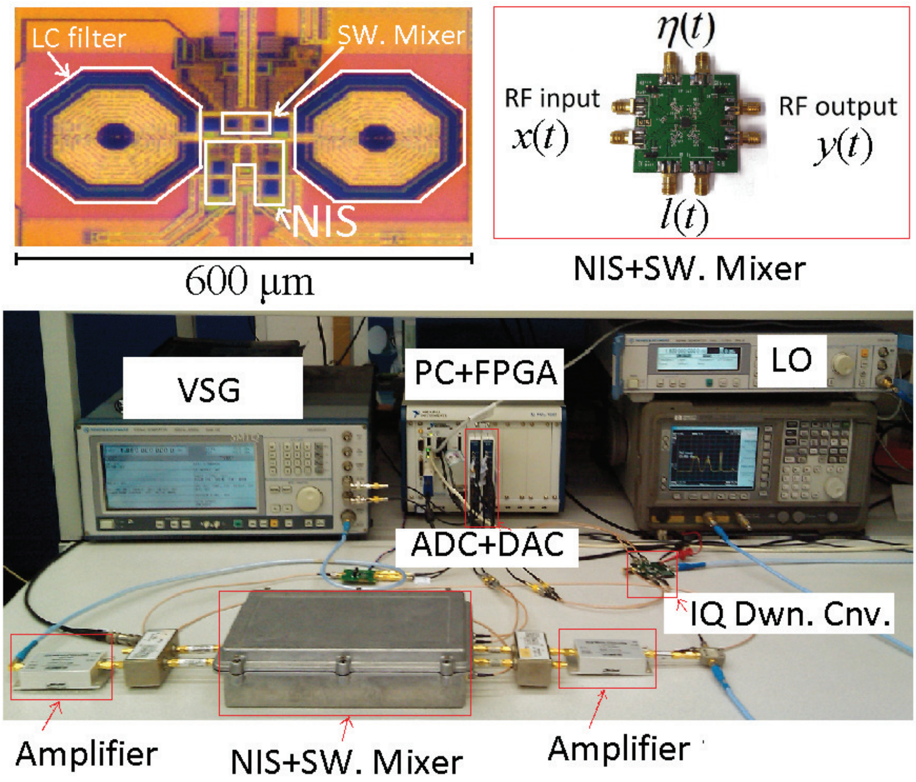

Figure 5.3: Multimode transceiver testbed.

signal and interference are defined as:

$$g_d = \frac{P_{d,y}}{P_d}, \quad g_i = \frac{P_{i,y}}{P_i}. \tag{5.7}$$

The average powers of the desired signal and interference at the NIS input and output are denoted by $\overline{P_d}$, $\overline{P_i}$, $\overline{P_{d,y}}$, and $\overline{P_{i,y}}$, which are the expected values of the corresponding instantaneous powers.

5.4 Multimode Transceiver Testbed

A testbed, as shown in Fig. 5.3, is developed to characterize the NIS circuit and investigate the NIS performance in the receiver. The NIS and the switching mixer (SW. Mixer) are fabricated as one chip in 140 nm CMOS technology. A micrograph of the chip is shown in Fig. 5.3. The circuit schematic and a detailed circuit analysis

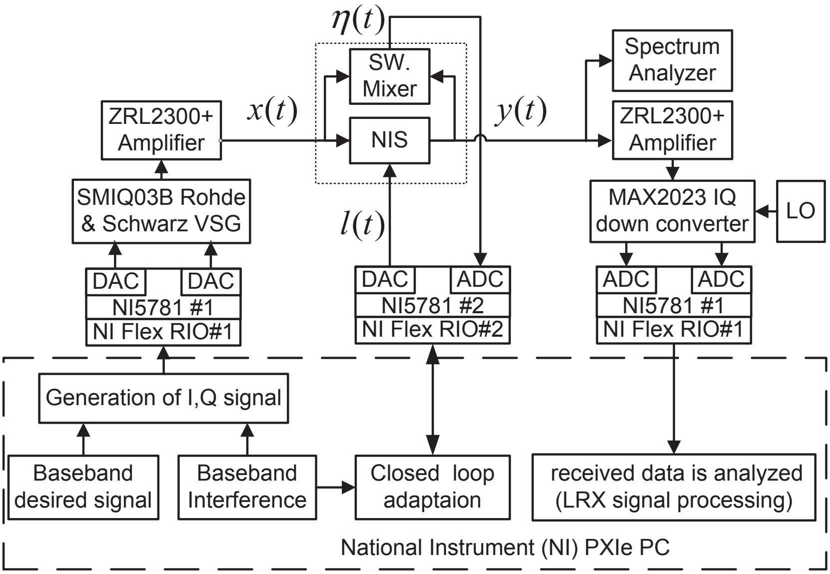

Figure 5.4: Block diagram of the testbed, including LTX, RTX, and LRX with the NIS.

can be found in [33]. The chip is packaged and mounted on a PCB and the PCB is enclosed in a Faraday cage to shield the circuit electromagnetically.

The block diagram of the testbed is shown in Fig. 5.4. The baseband desired signal and interference are generated in a PC. They are combined digitally, uploaded to a National Instruments (NI) Flex RIO FPGA module (#1), converted to analog IQ signals by NI5781 module (#1), and up-converted by a Vector Signal Generator (VSG). The output of the VSG includes the interference (f_i=1.85 GHz) and the desired signal (f_d=1.87 GHz). The VSG output is amplified by a ZRL-2300+ from Minicircuit, which has a 1dB compression point of 23 dBm. The amplified VSG output is connected to the NIS input by a coaxial cable. The NIS output signal is amplified and then is down-converted by a commercial IQ down converter, digitized using the adapter module #1, and sent to the PC by the FPGA module #1 for further processing. A video recording of the working setup can be found at http://www.youtube.com/realtimeNIS.

Flex RIO#2 and NI5781 module#2 are used to generate $l(t)$ from $l[n]$ and digitize $\eta(t)$ to $\eta[n]$. The model $g[n]$ of coupling path of the interference is adapted such that $\mathrm{E}(\eta^2[n])$ is minimized. Except for the measurements in Section 5.7.4, the adaptation is done via the PC. To increase the adaptation speed, in Section 5.7.4 the closed-loop adaptation is implemented in Flex RIO#2 FPGA module.

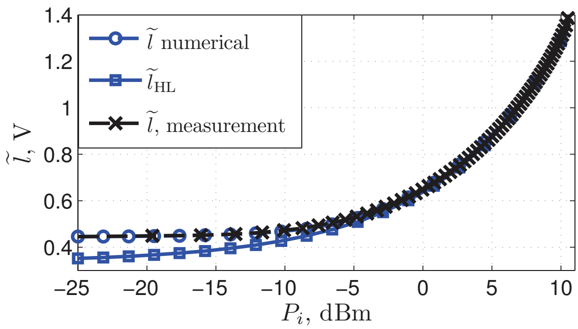

Figure 5.5: Optimal adaptation signal, measured and numerical evaluation.

5.5 Measurement and analysis for Single Tone (ST) signals

In this section we use Single Tone (ST) signals to characterize the NIS circuit and analyze the imperfections of the circuit compared to the memoryless hard-limiter model shown in Fig. 5.1. At the end of the section, Table 5.1 summarizes the imperfections being faced in the NIS circuit.

5.5.1 Adaptation Signal

Using a ST for the interference, we find the optimal adaptation signal $\tilde{l}$ that minimizes $P_{i,y}$ by sweeping $l(\cdot)$. Fig. 5.5 shows the measured $\tilde{l}$ vs. P_i. When P_i is large, the relation between $\tilde{l}$ and P_i approaches that of the HL NIS ($\tilde{l}_{\mathrm{HL}}$ according to (5.5)). As P_i decreases, (5.5) does not accurately describe $\tilde{l}(P_i)$. This is due to the fact that a practical limiter, unlike the hard-limiter, has a finite slope at the origin. This limited slope makes the HL model increasingly inaccurate when P_i is small. To account for this effect, the following model of a CMOS limiter is used [33]:

$$y_l(x) = \begin{cases} -l(t) & x < -\sqrt{\frac{l(t)}{k}} \\ kx\sqrt{\frac{2l(t)}{k} - x^2} & |x| \leq \sqrt{\frac{l(t)}{k}} \\ l(t) & x > \sqrt{\frac{l(t)}{k}} \end{cases}, \tag{5.8}$$

where k is a constant related to the channel width and length of the transistors. For the model in (5.8), $\tilde{l}$ is evaluated numerically and is shown in Fig. 5.5. The numerical results matches the measurement results. The measured $\tilde{l}$ versus A_i, described as $\tilde{l} = L(A_i)$, is stored in a look-up table, and is used to obtain $\hat{l}(t) = L(\hat{A}_i(t))$, as we will see in Section 5.5.7.

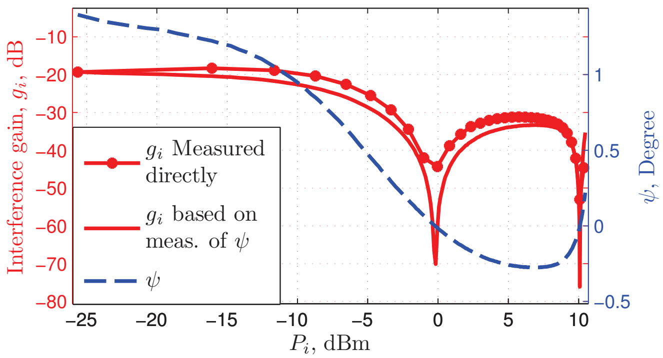

Figure 5.6: Measurement of g_i, ψ.

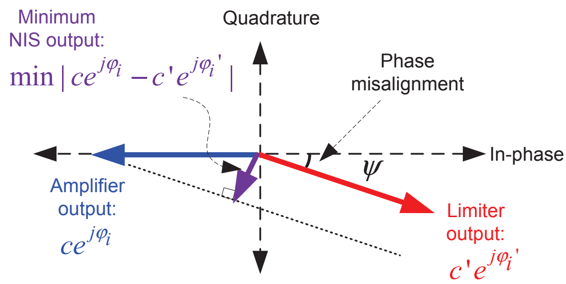

Figure 5.7: Phasor diagram illustrating impact of ψ on g_i.

5.5.2 Phase Misalignment Between Amplifier and Limiter

Fig. 5.6 shows measured g_i versus P_i when $l = \tilde{l}(P_i)$. Unlike what is predicted for a memoryless NIS, g_i is not zero and depends on P_i. A possible explanation is that the circuit blocks exhibit short term memory effects which lead to phase misalignment of the amplifier and the limiter. Fig. 5.7 considers that the output $-c\cos(\omega t + \varphi_i)$ of the amplifier and the output $c'(l)\cos(\omega t + \varphi_i')$ of the limiter have a phase misalignment $\psi = \varphi_i - \varphi_i'$ and hence $A_{i,y} = \left|c'(l)e^{j\varphi_i'} - ce^{j\varphi_i}\right| = \left|c'(l) - ce^{j\psi}\right|$. If $\psi = 0$ then by changing l, $c'(l)$ can be made equal to c, and hence $g_i = 0$ is obtained. If $\psi \neq 0$, the interference cannot be suppressed completely. As seen in Fig. 5.7, the minimum g_i is achieved for $c' = c\cos(\psi)$ which results in $g_i = (c\sin(\psi))^2$.

The phase misalignment ψ should be measured for $l = \tilde{l}(P_i)$, where a Single Tone (ST) with power of P_i is applied to the NIS input. When the interference is significantly suppressed at the NIS output (e.g. at P_i =0 dBm and 10 dBm as seen in Fig. 5.5), an accurate measurement of its phase is problematic. To solve

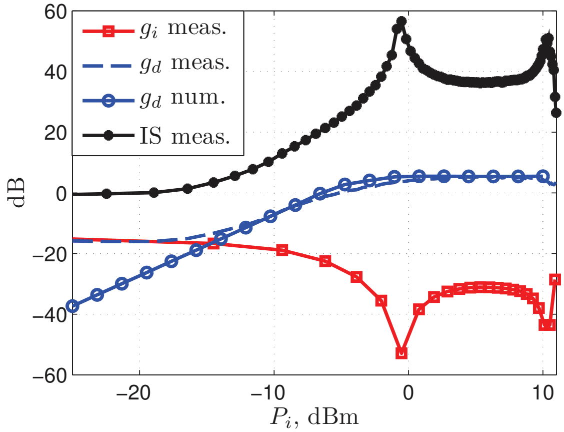

Figure 5.8: g_i and g_d in the presence of the desired signal.

this problem, l is swept linearly in the vicinity of $\tilde{l}(P_i)$ and $ce^{j\varphi_i} - c'(l)e^{j\varphi_i'}$ (as shown in Fig. 5.7) is measured using the IQ downconverter in Fig. 5.4. By fitting a line to $ce^{j\varphi_i} - c'(l)e^{j\varphi_i'}$, $\psi = \varphi_i - \varphi_i'$ can be measured accurately. The result is shown in Fig. 5.6 and varies between -0.25 to 1.25 degrees. We see that ψ depends on P_i and at two points becomes zero. Based on the measured ψ, the interference power gain g_i is calculated as $g_i = (c\sin(\psi))^2$. The calculated g_i based on the measurement of ψ is shown and compared with g_i measured directly by minimizing $P_{i,y}$. The good agreement between the two results pinpoints the phase misalignment as the main factor that limits the minimum of g_i. The two nulls in g_i coincide with the point where an exact phase alignment occurs. Even with the current phase misalignment, a significant interference suppression is achieved. The phase misalignment originates from the mismatch between input capacitance of the limiter and amplifier. Since the capacitance has a slight dependence on P_i, ψ depends on P_i. In the current NIS circuit, by changing a bias voltage of the amplifier, ψ can be manually tuned. One possibility to achieve an even larger suppression is to control this bias voltage digitally during the operation.

5.5.3 Measurements of g_i and g_d in the presence of the desired signal

To measure the impact of the NIS on the desired signal, the small signal gain g_d must be measured in the presence of a large signal. To this end, we use a ST for the interference and another ST for the desired signal, 50 dB smaller than the interference, and set $l = \tilde{l}(P_i)$. Also g_i is measured in the presence of the desired signal. The Interference Suppression (IS) is defined as IS= $\frac{g_d}{g_i}$ and equals the amount of improvement in Signal to Interference Ratio (SIR) from the NIS input to output. The measurement results are shown in Fig. 5.8.

Ideally, we like to amplify the desired signal with a constant gain. An approximately constant g_d is achieved for 0 dBm $< P_i <$ 11 dBm. When P_i drops below 0 dB, g_d drops. When P_i becomes small, the soft limiter behaves like an amplifier. The interference is merely attenuated by subtracting the outputs of two linear amplifiers, which have the same gain for the interference and the desired signal. Hence both weak and strong signals are attenuated equally and IS becomes 0 dB. To extend the range of constant g_d to smaller P_i, a limiter with a steeper slope at the origin can be used so that the smaller signals also experience a limiting effect. We see that the measurement results and numerical evaluation of g_d using (5.3) are in agreement. This validates the soft limiter model in (5.8). An IS of more than 35 dB is observed for -2 dBm $< P_i <$ 11 dBm. The upper range of the input power that the NIS can handle is determined by the rail-to-rail supply voltage, which is 0-1.8 V. For $P_i >$ 9 dBm, the input voltage already exceeds the supply voltage. For $P_i >$ 11 dBm, both the amplifier and the limiter start to show the same clipping behavior. Thus the difference between gain of the weak and the strong signal in amplifier and limiter starts to vanish.

For a varying-envelope interference, dependency of g_d on $P_i(t)$ leads to transfer of interference amplitude modulation to amplitude modulation of the desired signal. This is called cross-modulation and its impact on the desired signal will be analyzed in Section 5.7.1. In Section 5.7.3, a method is proposed to digitally compensate for this distortion.

5.5.4 AM-PM distortion

According to (5.2), which is valid for a memoryless nonlinearity, the phase of the weak desired signal at the NIS output is independent of A_i (the phase is measured with reference to the NIS input). The NIS, however, exhibits short-term memory effects, which leads to a dependency of the phase of the weak desired signal at the NIS output on $A_i(t)$. Hence the amplitude modulation of the interference is transferred to the phase of the desired signal. This is called AM-PM distortion [69]. The desired signal component at the NIS output will be $A_{d,y}(t)\cos(2\pi f_d t + \varphi_d(t) + \varphi_{d,y}(A_i(t)))$. For a constant envelope interference, this has little impact on the desired signal. For a varying envelope interference, however, variation of $\varphi_{d,y}(A_i(t))$ over time leads to a distortion of the desired signal. The measurement results for $\varphi_{d,y}(P_i)$ vs. P_i are shown in Fig. 5.9. We observe that $\varphi_{d,y}(P_i)$ remains approximately constant for 0 dBm $< P_i <$ 11 dBm and decreases when P_i decreases. Hence for $P_i(t) <$ 0 dBm, variations of $P_i(t)$ leads to distortion of the weak desired signal. We will see in Section 5.7.3 that this distortion can be digitally compensated with low complexity.

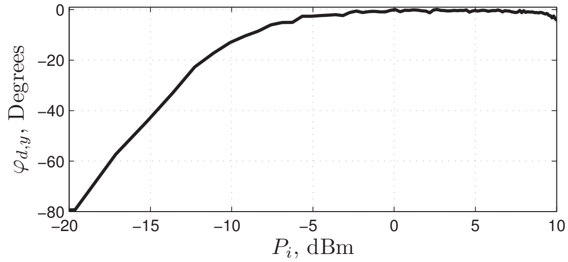

Figure 5.9: AM-PM Distortion.

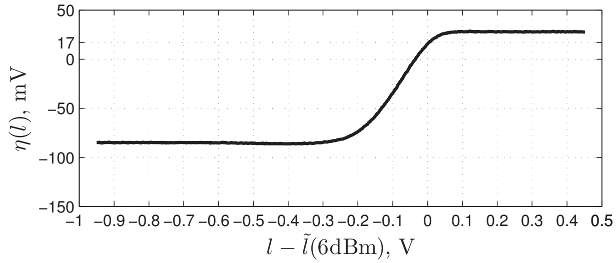

Figure 5.10: Mixer output $\eta(l)$ versus $l - \tilde{l}(P_i)$ for $P_i = 6$ dBm.

5.5.5 Characteristics of the switching mixer

The closed-loop adaptation of the NIS relies on the output $\eta(t)$ of the switching mixer, shown in Fig. 5.2, to estimate the model $g[n]$ of the coupling path. Assuming $A_{i,y} \ll A_i$, the output $\tilde{\eta}(t)$ of an ideal switching mixer would be [65]:

$$\tilde{\eta}(t) \simeq \frac{8}{\pi^2}\left(l(t) - \tilde{l}(t)\right) + \nu(t), \tag{5.9}$$

where $\nu(t)$ is a random zero-mean error uncorrelated to $l(t)$. Hence $\tilde{\eta}(t)$ indicates the error of the applied adaptation signal $l(t)$ with respect to $\tilde{l}(t)$. The output $\eta(l)$ for the switching mixer, which is implemented in the NIS package, versus l is measured and shown in Fig. 5.10 for $P_i = 6$ dBm. When l is around the optimal value $\tilde{l}(P_i = 6 \text{ dBm}) \simeq 0.95$ V, the interference is substantially suppressed ($A_{i,y} \ll A_i$). Thus $\eta(l)$ is linear with respect to $(l(t) - \tilde{l}(t))$. For $l \gg \tilde{l}$ and $l \ll \tilde{l}$, $A_{i,y}$ has about the same amplitude as A_i. Thus the mixer saturates and $\eta(l)$ only conveys the sign of $(l(t) - \tilde{l}(t))$. By using only the sign, the adaptation algorithm can still minimize $\mathrm{E}\left((l(t) - \tilde{l}(t))^2\right)$ [62]. The convergence, however, will be at a linear rate, instead of an exponential one. After an initial convergence, in the tracking mode of the adaptation, l would be close to $\tilde{l}$. Hence $A_{i,y} \ll A_i$ and tracking at an exponential rate is achieved.

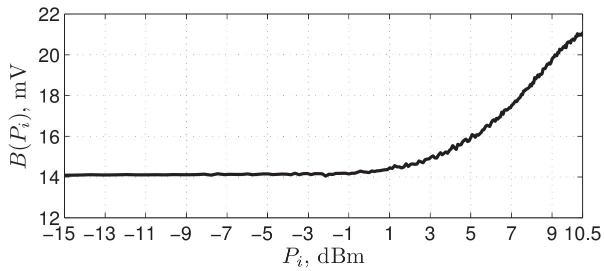

Figure 5.11: Mixer DC offset.

5.5.6 DC Offset of the switching mixer

Another imperfection of the switching mixer in Fig. 5.2, is an additive DC offset $B(A_i)$ in its output. In Fig. 5.10, we see that for $l = \tilde{l}$, $\eta \neq 0$, instead:

$$\eta(t) = S\left(l(t) - \tilde{l}(t)\right) + \nu(t) + B(A_i), \tag{5.10}$$

where $S()$ is the function shown in Fig. 5.10 minus the offset, i.e. $S(0) = 0$. To make $\eta(t)$ zero when $P_{i,y}$ is minimized, $B(P_i)$ can be subtracted from $\eta(t)$. The DC offset $B(P_i)$ is measured and is shown in Fig. 5.11.

It is seen that $B(P_i)$ is a function of P_i. Hence for a varying envelope interference, $B(A_i(t))$ is time varying and must be synchronized to $\eta(t)$ before subtraction. Calculation of $B(A_i)$ requires both $B()$ and A_i. While the function $B()$ can be measured beforehand, P_i is not known initially. Instead we can use the estimate of A_i to correct for the DC offset as: $\hat{\eta}[n]$ as: $\hat{\eta}[n] = \eta[n] - B(\hat{A}_i[n])$.

In the following we analyze the required condition for which $\hat{l}$ converges to $\tilde{l}$, when the estimated DC offset is subtracted from $\eta[n]$. Suppose that at the m^{th} iteration of the adaptation $\hat{l}[m]$ is close to $\tilde{l}$. In the n^{th} iteration, where $n > m$, we make $\hat{\eta}[n] = 0$ by choosing a value for $\hat{l}[n]$ such that:

$$\hat{\eta}[n] = S(\hat{l}[n] - \tilde{l}) + b(\tilde{l}) - b(\hat{l}[m]) = 0, \tag{5.11}$$

where $b(l) = B(L^{-1}(l))$. Assuming that $B(A_i)$ is small enough so that $\hat{l} - \tilde{l}$ is in the linear range of $S()$, then by solving (5.11) we obtain:

$$\hat{l}[n] - \tilde{l} = \frac{b'(\tilde{l})}{S'(0)}(\hat{l}[m] - \tilde{l}), \tag{5.12}$$

where $S'(0) = \frac{dS(l)}{dl}|_{l=0}$ is the slope of $S()$ in its linear range. Consequently, subject to the condition $\left|\frac{b'(\tilde{l})}{S'(0)}\right| < 1 \Rightarrow \left|b'(\tilde{l})\right| < |S'(0)|$, $\hat{l}_n$ converges to $\tilde{l}$. For the current design the condition $\left|b'(\tilde{l})\right| < |S'(0)|$ is satisfied.

Table 5.1: Summary of the imperfections.

Imperfection	Impact	Mitigation method
Finite slope of limiter	$\tilde{l}(t) \neq \frac{\pi}{4} c A_i(t)$	Calibration: $\tilde{l}(t) = L(A_i)$
	Cross-modulation distortion (AM to AM)	Digital compensation
	Limits the lower range that IS>0	Increasing the slope of limiter
Phase misalignment between amplifier and limiter	Limits interference suppression	Measurement and possible calibration
AM-PM distortion	Cross-modulation distortion (AM to PM)	Digital compensation
DC offset of the switching mixer	Limits interference suppression	Digital offset tracking

5.5.7 Closed-loop adaptation for varying-envelope interferences

The closed-loop adaptation method for varying envelope interferences proposed in [65] was designed based on the HL model of the NIS and without considering the offset of $\eta[n]$. To account for these imperfections a slightly modified method, shown in Fig. 5.12, is used. Complex-valued signals are shown with thick lines, and the additional blocks compared to [65] are shown with double-line squares. Using samples of the interference $i[n]$, a discrete-time estimate $\hat{A}_i[n]$ of the envelope $A_i(t)$ of the received interference at the NIS input, is calculated. The adaptation signal $\hat{l}[n]$ is calculated based on $\hat{A}_i[n]$ according to $\hat{l} = L(\hat{A}_i[n])$, as described in Section 5.5.1. The time varying DC offset $B(\hat{A}_i[n])$ of the mixer, as described in Section 5.5.6, is subtracted from $\eta[n]$. The filter taps $g[n]$ are adapted by processing $i[n]$ and $\hat{\eta}[n] = \eta[n] - B(\hat{A}_i[n])$ as:

$$\mathbf{g}[n+1] = \mathbf{g}[n] - \mu\hat{\eta}[n]\frac{\mathbf{g}^T[n]\mathbf{i}[n]}{|\mathbf{g}^T[n]\mathbf{i}[n]|}\mathbf{i}^*[n], \tag{5.13}$$

where vectors $\mathbf{g}[\mathbf{n}]$ and $\mathbf{i}[n]$ are defined as:

$$\mathbf{g}=[g_0[n], ..., g_{M-1}[n]]^T, \mathbf{i}[n] = [i[n], ..., i[n-M+1]]^T,$$

where the superscript T denotes the transpose operation, and μ is a positive real number called step-size. A derivation of (5.13) can be found in [65].

5.6 Measurement results for constant-envelope interference

Beyond the ST interference, a constant-envelope interference is the simplest form of interference that can be suppressed by the NIS. The adaptation signal is essentially a DC signal which varies slowly as $\overline{P_i} = P_i$ changes. Hence there is enough time to extract the adaptation signal by integrating $\hat{\eta}(t)$ as described in [32]. For the interference a GMSK modulation and for the desired signal a QPSK modulation is used with bandwidths of 0.5 MHz and 7.5 MHz, respectively. Fig. 5.13 shows the NIS input spectrum. The SIR at the NIS input is -40 dB and $P_i = +10$ dBm. The closed-loop adaptation method that is described in [32] is modified as in Fig. 5.12 and is used to adapt the NIS. Fig. 5.14 shows the NIS output spectrum after convergence of the adaptation loop to the steady state value. A 43 dB improvement in SIR is observed. Also the intermodulation component is seen at the image frequency of the desired signal with respect to the interference. A Modulation Error Ratio (MER) of 30 dB for the QPSK signal is measured, where the error is dominated by VSG noise. The above achieved MER can be used as a

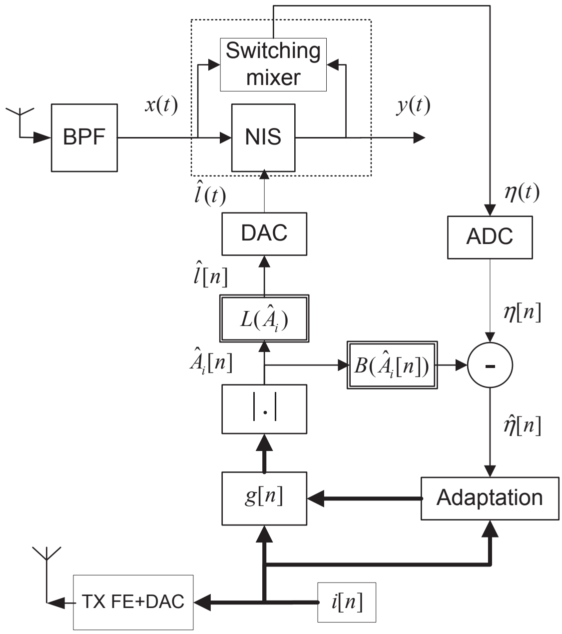

Figure 5.12: NIS adaptation with digital calibration.

reference point to be compared with the MER achieved for the varying envelope interferences in the next section. The QPSK signal is decoded with no errors.

5.7 Analysis and measurement results for varying envelope interferences

The measurement results of Section 5.5 are used to numerically predict the interference suppression of the NIS and the MER of the desired signal. The closed-loop adaption method is used to adapt the NIS for a varying envelope interference and the measurement results are compared with the numerical predictions. Finally, a method is proposed and evaluated to compensate for the distortion of the desired signal so as to bring the MER of the desired signal to an acceptable range.

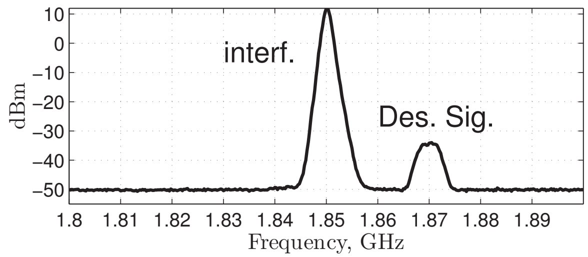

Figure 5.13: NIS input spectrum.

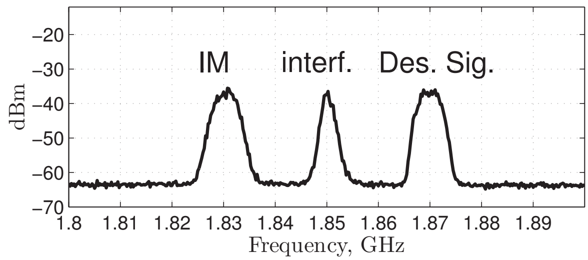

Figure 5.14: NIS output spectrum.

5.7.1 Numerical results

For a varying envelope interference, the instantaneous power $P_i(t)$ varies and hence the minimum obtainable $g_i(t)$ varies as shown in Fig. 5.8. Assuming that $l(t) = \tilde{l}(t)$, then the minimum of $g_i(P_i(t))$ is achieved for every value of $P_i(t)$. The minimum average power of the interference, at the NIS output, is obtained as:

$$\overline{P_{i,y}} = \int_0^\infty P_i g_i(P_i) f_{P_i}(P_i) dP_i, \tag{5.14}$$

where $f_{P_i}(P_i)$ is the Probability Density Function (PDF) of P_i and $g_i(P_i)$ is shown in Fig. 5.8. For $l(t) = \tilde{l}(t)$ the average power of the desired signal and average interference suppression ($\overline{\text{IS}}$) are obtained as:

$$\overline{P_{d,y}} = \overline{P_d} \int_0^\infty g_d(P_i) f_{P_i}(P_i) dP_i, \tag{5.15}$$

$$\overline{\text{IS}} = \frac{\text{SIR}_{\text{out}}}{\text{SIR}_{\text{in}}} = \frac{\frac{\overline{P_{d,y}}}{\overline{P_{i,y}}}}{\frac{\overline{P_d}}{\overline{P_i}}}. \tag{5.16}$$

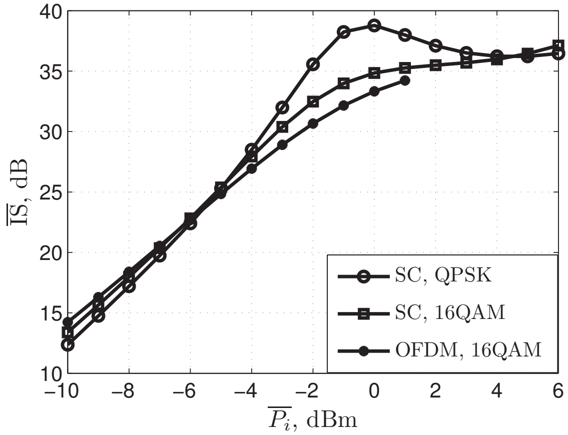

Figure 5.15: Numerical evaluation of the average Interference Suppression ($\overline{\text{IS}}$).

According to (5.14) to (5.16), $\overline{\text{IS}}$ is a function of $f_{P_i}(P_i)$ and depends on the modulation of the interference. Based on a numerical analysis $\overline{\text{IS}}$ is calculated using (5.16). The results are shown in Fig. 5.15 for Single Carrier (SC) QPSK, SC 16 QAM and OFDM (Orthogonal Frequency Division Multiplexing) modulations of the interference. Root raised cosine filtering with a roll-off of 0.5 is applied to the signals. For these modulations the PDF of the envelope $f_{A_i}(P_i)$ versus P_i in dBm is shown in Fig. 5.16 for $\overline{P_i} = 0$ dBm. SC QPSK, SC 16QAM, and OFDM 16 QAM have a peak to average power ratio of 3.3 dB, 5.7 dB and 11.5 dB. The maximum $\overline{P}_i$ for each modulation is chosen such that its peak power does not exceed 11 dBm, which is the maximum power that the current NIS circuit can handle. We see that a significant interference suppression can be achieved for these modulations. The similarity between $\overline{\text{IS}}$ and IS in Fig. 5.8 originates from the fact that $\overline{\text{IS}}$ is essentially an average of IS weighted by $f_{P_i}(P_i)$. Compared to the other modulations, for OFDM the smallest $\overline{\text{IS}}$ is achieved. This is so because, as observed in Fig. 5.16, with a larger probability, $P_i(t)$ is in the range for which a small IS is obtained (range of $P_i(t) < -2$ dBm).

For a varying envelope interference, $g_d(P_i(t))$ varies over time, which leads to distortion of the desired signal. Also we saw in Section 5.5.4 that the phase of the desired signal at the NIS output with reference to the NIS input, depends on $P_i(t)$. Hence the desired signal experiences time varying gain and phase changes when it is passed through the NIS. The amount of distortion experienced depends on $f_{P_i}(P_i)$ and the resulting MER can be evaluated numerically. Fig. 5.17 shows the MER for a SC 16QAM modulation of the desired signal, assuming that $l(t) = \tilde{l}(t)$. The MER is smaller for interferences with more envelope variations. For simple modulation of the interference, the MER is large enough for most modulations of the desired signal to achieve a sufficiently small Symbol Error Rate (SER). For

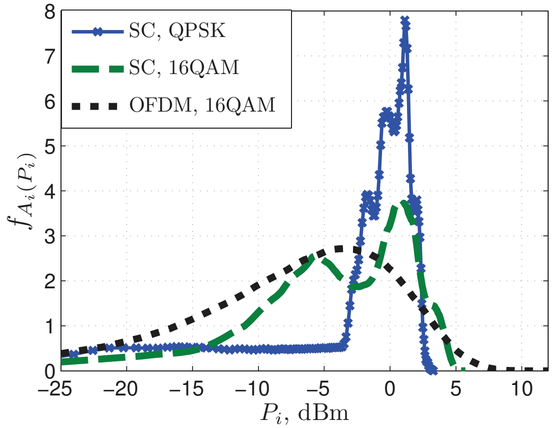

Figure 5.16: PDF of A_i versus P_i for $\overline{P_i} = 0$ dBm.

example 16QAM modulation requires an MER of 17.6 dB to achieve an SER of 10^{-3}, which is attainable here for the QPSK interference. For modulations with more envelope variations, however, the attainable MER can be so small that an acceptable SER is unattainable, even for the simplest modulations of the desired signal. This small MER can be significantly improved by digital compensation of the distortion as we will see in Section 5.7.3.

5.7.2 Measurement results for closed-loop adaptation

A SC 16 QAM modulation is used for both the interference and the desired signal, with raised cosine pulse shaping with a roll-off factor of 0.5. A symbol rate of 1 MSPS is used for both signals, resulting in a bandwidth of 1.5 MHz . The average interference suppression ($\overline{\text{IS}}$) after convergence of the adaptation loop is measured and shown in Fig. 5.18.

We see that the experimental results closely match the numerical results calculated in Section 5.7.1. The reason for the smaller $\overline{\text{IS}}$ compared to numerical results for $\overline{P_i} >$ -2 dBm is not identified yet. Over the range of -4 to 6 dBm the achieved $\overline{\text{IS}}$ is larger than 30 dB, which makes the interference suppression of the NIS comparable to the achievable interference suppression by SAW filters.

The constellation diagram of the received signal is shown in Fig. 5.19 for $\overline{P_i}$ =4 dBm. Owing to the dependency of g_d and $\varphi_{d,y}$ on $A_i(t)$, a distortion of the desired signal is observed. In Section 5.7.3, we propose a method to compensate for this distortion. The MER is measured and is shown in Fig. 5.20 versus $\overline{P_i}$. The experimental results match the numerical results of Section 5.7.1. This confirms

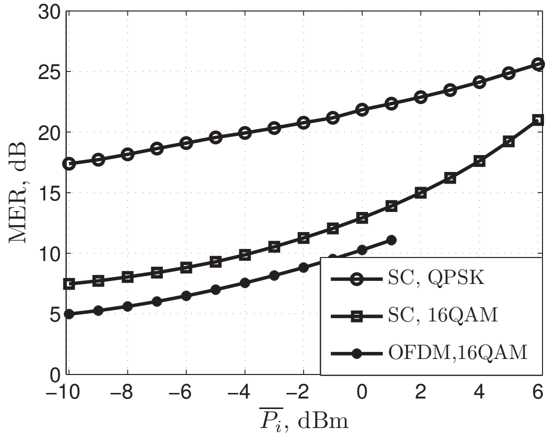

Figure 5.17: Numerical evaluation of MER for various modulations of the interference.

Table 5.2: Interference suppression versus B_i.

B_i, MHz	0.75	1.5	3	6	7.5	9.3750	15
$\overline{\text{IS}}$, dB	34.2	34	33.1	32.1	32	32	31

that the closed-loop adaptation method extracts an adaptation signal $\hat{l}(t)$ which is very close to $\tilde{l}(t)$, and validates the methodology of Section 5.7.1 for predicting the performance of the receiver with the NIS.

To investigate the interference suppression for interferences with a larger bandwidth, measurement were performed for $\overline{P_i} = 4$ dBm and SC 16QAM modulation of the interference. Table 5.2 shows $\overline{\text{IS}}$ versus bandwidth B_i of the interference. Although for larger bandwidths $\overline{\text{IS}}$ decreases slightly, still a significant suppression is achieved.

5.7.3 Digital compensation of distortion

As we saw the MER of the received desired signal $d_r[n]$, when the interference has large envelope variations, was too small to achieve an acceptable SER for complex modulations of the desired signal. The distortion, however, can be compensated by applying inverse of square root of the power gain $\sqrt{g_d}$ and the interference dependent phase $\varphi_{d,y}$, as measured in Fig. 5.8 and Fig. 5.9, respectively. The

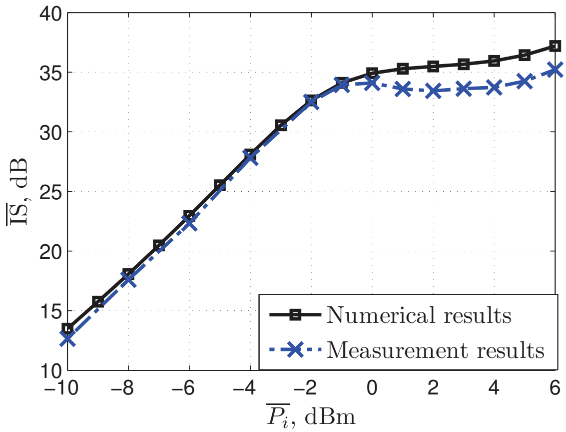

Figure 5.18: Measurement results for $\overline{\mathrm{IS}}$.

distortion-compensated desired signal $d_c[n]$ is obtained as:

$$d_c[n] = d_r[n] \frac{1}{\sqrt{g_d(\hat{A}_i[n])}} e^{-j\varphi_{d,y}(\hat{A}_i[n])}. \tag{5.17}$$

Since $\hat{A}_i[n]$ is already estimated for the NIS adaptation, $\frac{1}{\sqrt{g_d(\hat{A}_i[n])}} e^{-j\varphi_{d,y}(\hat{A}_i[n])}$ is easily calculated using a look-up table.

The constellation diagram of the desired signal after compensation is shown in Fig. 5.21 for $\overline{P_i}$ =4 dBm. We see that the distortion is significantly decreased compared to Fig. 5.19. The MER after compensation is shown in Fig. 5.22 and is compared to the MER before compensation. We see a considerable improvement in the MER after compensation, which enables reception of complex modulations with an acceptable un-coded SER. For example, for a 16 QAM modulation of the desired signal, an SER better than 10^{-3} is achieved for $\overline{P_i} > -7$ dBm.

Although in Fig. 5.21 the MER has increased significantly, still a residual distortion is observed. It is likely that this originates from small long-term memory effects. Since the compensator relies on a static AM-AM/PM distortion model, it cannot compensate for these effects. A more accurate modeling is required to identify the source of this residual distortion and accordingly one might improve the compensator by including nonlinear memory terms.

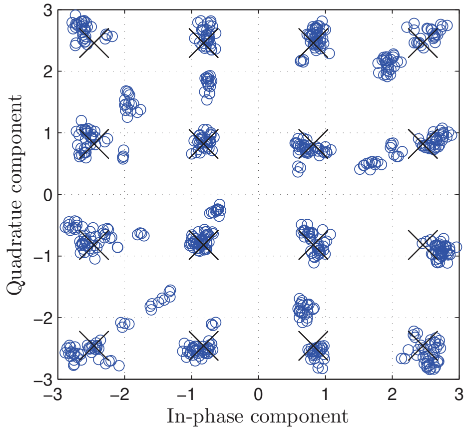

Figure 5.19: Constellation diagram of the received signal.

5.7.4 Real time adaptation

It takes several seconds to reach the steady state of the adaptation when it is done via the PC. To increase the adaptation speed such that changes in the environment can be tracked, the adaptation is implemented in the FPGA module. The same signals as in Section 5.7.2 are used for the interference and the desired signal. The interference at the NIS input is 4 dBm and the desired signal is 40 dB weaker that the interference. A 32-tap filter ($\mathbf{g}$) is initialized from zero and $P_{i,y}$ is measured and is shown versus time in microseconds, for two values of the adaptation step size ($\mu = \mu_0,\ 8\mu_0,.$) At the start of the adaptation a constant value for $P_{i,y}$ is observed, owing to the saturation of the LRX in the testbed. We see that depending on the step size the adaptation converges to its steady state condition after 1.5 or 8 milliseconds. The amount of measured $\overline{\mathrm{IS}}$ is 31 and 33 dB for μ_0 and $8\mu_0$, respectively.

As a practical test, the coax cable connection between the LTX and the LRX is replaced by two monopole antennas with a distance of about 6 cm. Objects are moved in the near field of the antennae. This results in a significant change in the interference coupling path, such that when the adaptation of the filter coefficients is disabled, no interference suppression is achieved. The adaptation algorithm for both the step sizes is fast enough to track the changes such that no change in the interference suppression is observed, when the objects are moved. A video recording of this experiment is available at:
www.youtube.com/RealTimeNIS.

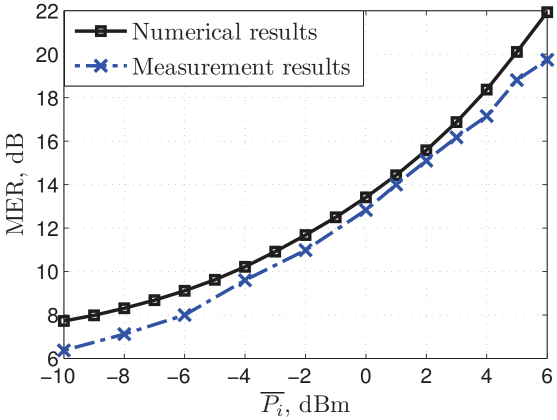

Figure 5.20: Measurement results for MER.

5.7.5 Calibration

The adaptation method requires a measurement and storage of $L(A_i)$ and $B(A_i)$ to utilize the potential interference suppression that the NIS circuit can provide. To correct the distortion, the functions $g_d(A_i)$ and $\varphi_{d,y}(A_i)$ also must be measured. All these functions can be measured during a calibration stage, by using the LTX as the exciter and the LRX as the calibrating receiver. All the calibrations are automatically performed in our testbed, which is built with commercially available components. This suggests the practicality of the proposed approach.

5.7.6 Power consumption of the NIS approach

The NIS approach includes analog and digital circuits. The analog circuits include the NIS circuit, DAC and ADC. The power consumption of the current realization of the NIS circuit is proportional to P_i and increases from 5 mW to 35 mW for $P_i =$ -5 dBm to 11 dBm. The power consumption of a 14 bit 100 MSPS DAC is 16 mW [63]. The power consumption of a 6 bit 100 MSPS ADC is 5 mW [15]. The digital part of the NIS adaptation includes the adaptation block, filtering by the complex-valued filter taps g and calculating the envelope. The complexity of the digital part of NIS adaptation is much smaller than that of digital blocks of modern receivers. A more detailed analysis of the digital part of the NIS adaptation can be found in [46], which results in 10 mW when the adaptation is run at a 100 MHz clock. The total power consumption of the NIS method then would be about 66 mW. It must be noted that: firstly, these numbers are loose upper bounds, secondly, power consumption of the ADC, DAC and digital processing decreases

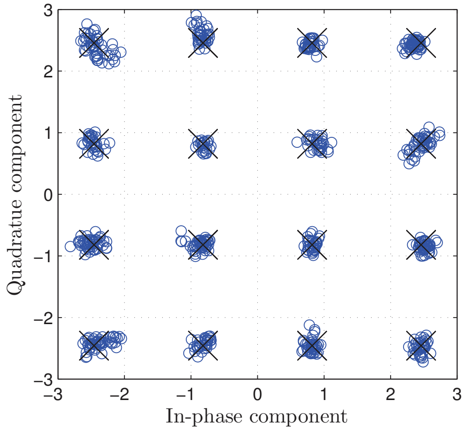

Figure 5.21: Constellation diagram after compensation.

as bandwidth of the interference decreases, thirdly, power consumption of the digital part can be reduced by further optimization of the adaptation algorithms.

5.8 Comparison and summary

In this section, firstly, we compare the NIS approach with analogue cancellation of the interference, a method which is widely explored with a similar motivation as the NIS approach. Secondly, we present a brief summary of strengths and weaknesses of the NIS approach.

5.8.1 Comparison to analogue cancellation

As shown in Fig. 5.24, a replica of the received interference at the LRX can be generated based on a linear model of the interference coupling path, with the transmitted interference as the input of this model. By subtracting this replica from the received signal in the analogue domain the local interference can be cancelled. Variations of this method are widely explored [5–8, 10]. To cancel the interference, the model should be accurate over the bandwidth of the interference. Hence a model with several branches is required. In practice, however, even a single-branch model requires a significant analog complexity and power consumption. Especially, implementing long delays (in the order of several nanoseconds) in an integrated circuit can be difficult. Hence several variants of the cancellation method are being explored to improve the cancellation and decrease the complex-

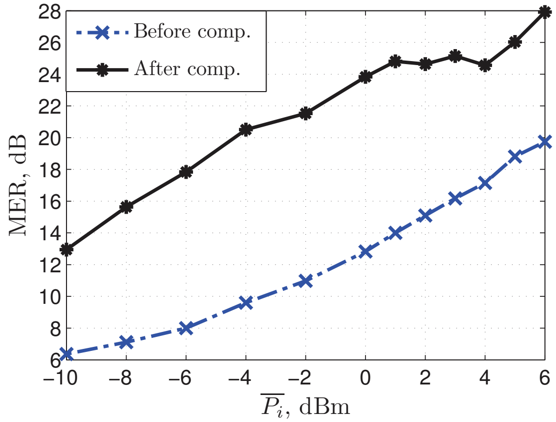

Figure 5.22: MER after compensation of distortion.

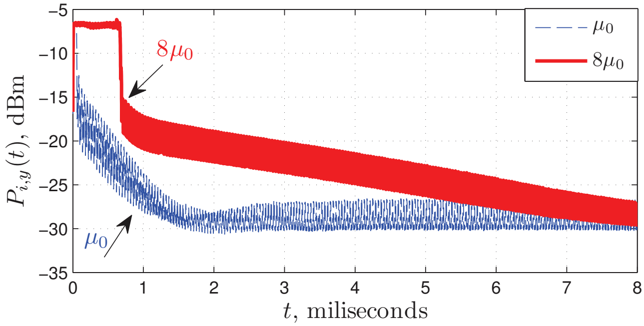

Figure 5.23: NIS output power $P_{i,y}$ measured during adaptation by FPGA.

ity, for example emulating the coupling path by a bandpass filter or collecting the input of the model by an antenna. These two methods, however, are not suitable for mobile devices as they increase the number of external components and also are not flexible (must be physically modified for each design). A summary of cancellation methods is gathered in Table 5.3, indicating the cancellation technique, the amount of cancellation achieved, and the bandwidth of the cancellation. In comparison, the NIS approach can achieve 30 dB to 43 dB of interference suppression depending on the interference modulation.

Another limitation of the analog cancellation method is difficulty of its adaptation. For a reference-aided adaptation, analog circuits must be implemented to correlate the transmitted interference with the residual interference after the cancellation point [5]. Such an adaptation would increase the complexity further. Hence in [7] a search method over a_1 is used to minimize the energy of the residual

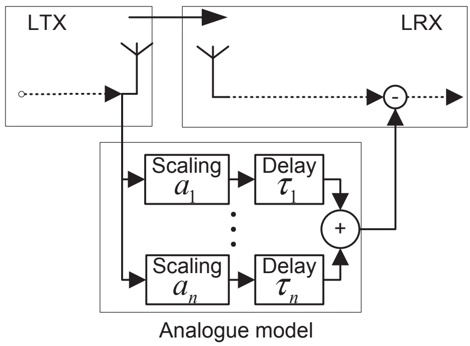

Figure 5.24: Interference cancellation using an adaptive analogue model.

Table 5.3: Interference cancellation state of the art.

Reference	Cancellation technique	Cancellation	Bandwidth
[6]	Double-branch with delay	46 dB	5 MHz
[7]	Single-branch with bandpass emulation filter	25-30 dB	5 MHz
[5]	single-branch without delay	10.8-28 dB	1.5 MHz
[8]	Double-branch with delay	20 dB	2 MHz
[10]	Single-branch with	25-46 dB	10 kHz
	auxiliary antenna	25-46 dB	10 kHz
[11]	Single-branch without delay	20-30 dB	4 MHz

interference. Such a search method, however, becomes increasingly slow when the number of paths increases. For the NIS, by comparison, a fast reference-aided digital adaptation method can be used with low implementation complexity.

5.8.2 Strengths and Weaknesses of the NIS

Key strengths of the NIS approach can be summarized as:
1-Significant interference suppression,
2-Low complexity and power consumption.

In return for these strengths, using the NIS leads to the following undesired effects:
1-Spectral mirroring: All the components around $2f_i - f_d$ at the NIS input are mapped to f_d at the NIS output. This leads to a fundamental 3 dB floor on the noise figure of the NIS. This necessitates using a BPF before the NIS to suppress this component.

2-Added noise figure: The NIS circuit will have a Noise Figure (NF) higher than a Low Noise Amplifier (LNA). Using an LNA before the NIS is not preferred since the LNA cannot handle a strong interference. Hence it is desirable that the NIS is implemented with a small NF.
3-Harmonic generation: Owing to the strong nonlinear effects in the NIS, higher-order harmonics of the interference are generated. These harmonics are far away from f_i and can be filtered out easily. They must be, however, be filtered out immediately to prevent saturation of the NIS. To this end, the current implementation of the NIS circuit has an embedded bandpass filter.

5.9 Conclusion

In this paper we presented experimental results of a multimode transceiver testbed which uses a Nonlinear Interference Suppressor (NIS) to alleviate local interference. Firstly, experiments were performed to obtain models that explain the main imperfections of the NIS circuit, implemented in 140 nm CMOS technology, with respect to the ideal model. Four key imperfections were identified, namely phase misalignment between limiter and amplifier, the limited slope of the adaptable limiter, a DC offset in the adaptation loop, and AM-PM distortion. The phase misalignment limits the maximum interference suppression that can be achieved. The limited slope of the limiter firstly leads to a certain minimum interference power where sufficient interference suppression can be achieved, and secondly to a dependency of gain of the desired signal gain on the envelope of the interference. Simple models are presented that explain the imperfections and methods are developed to compensate and calibrate for them. In principle the analogue imperfections could be mitigated by improving the circuit blocks. Such an improvement, however, generally leads to an increase in cost and power consumption of circuits [23, 52, 70, 71]. The less costly and power hungry approach, which we used in this paper, uses digital signal processing methods to calibrate and compensate for the imperfections.

A closed-loop adaptation method, which was developed in previous work, was implemented after slight modifications to account for the NIS imperfections. An interference suppression of up to 43 dB is attained for GMSK interference. For varying-envelope interferences, at least 30 dB-40 dB of interference suppression is achieved over the range of -3 to 6 dBm of interference average power. The upper limit of this range originates from the limitation of the supply voltage. The lower limit originates from the phase misalignment and the limited slope of the limiter. Both limits can be extended in future designs. The experiments show that the adaptation method can track rapid variations in the environment, as induced, for example, by moving objects between the local transmit and receive antennae. The distortion products, present in the case of a varying envelope interference, are successfully compensated to obtain an acceptable Modulation Error Ratio (MER). The experimental results suggest that the NIS with the proposed adaptation method can be used to substantially suppress the strong interference with a modest penalty to the quality of the desired signal.

Chapter 6

Conclusions and future work

6.1 Conclusions

Modern handheld devices such as mobile phones and tablets, have become multimode transceivers. These transceivers support multiple wireless standards to enable various communication functionalities. It is often required that two of these transceivers can work simultaneously. Owing to the proximity of the transceivers, dictated by the size of the device, the local transmitter of one communication standard induces a strong interference in the local receiver of another standard. This strong interference exceeds the linear dynamic of the local receiver, causing undesired nonlinear effects like desensitization and generation of in-band nonlinear distortion products. State-of-the-art approaches attempt to mitigate these effects by techniques like linear filtering and analogue cancellation. These techniques, unfortunately cannot sufficiently suppress the interference or require a high complexity and power consumption, so that they are unsuitable for handheld devices.

The main goal of this thesis and the companion thesis [17] was to develop a power-efficient and low-complexity method to mitigate the strong local interference in multimode transceivers. We showed that this goal can be achieved through a hybrid approach that meticulously combines the benefits of Digital Signal Processing (DSP) techniques and analogue design. We proposed to use an adaptive Nonlinear Interference Suppressor (NIS) early in the analogue front-end of the receiver to substantially suppress the interference, and to use DSP techniques to adapt the NIS and digitally compensate for the distortion products that are caused by the NIS. The main result of this thesis and [17] is the successful design, development, and experimental validation of the NIS approach. This approach is unique and promising in several respects:

- It can strongly suppress a local interference even with a small frequency separation to the desired signal. Frequency-domain linear filtering, by comparison, cannot sufficiently suppress interferences with a small separation, even with high-quality-factor filters. It must be noted that these filters are expensive external components with fixed stop-bands, making their application in multiband transceivers very cumbersome.

- It is a hybrid approach where the analogue NIS circuit is digitally adapted, resulting in a lower complexity compared to that of the adaptive analogue cancellation, where most of the adaptation must be done in the analogue domain. Moreover, the highly accurate adaptation of the NIS -made possible by DSP techniques- yields an interference suppression superior to that of analogue cancelation.

- Although at the first sight the NIS may seem similar to analogue cancellation, it is a fundamentally different approach. In fact it can be better categorized as an envelope filter (or an amplitude domain filter) as opposed to common frequency-domain filters. The difference can be understood by considering that both envelope and phase must be known to perform cancellation. For the NIS, however, knowledge of the envelope of the interference suffices. The NIS with a fixed adaptation signal is akin to a notch-filter tuned to a certain envelope. By changing the adaptation signal, the notch is moved to track changes of the envelope for a varying-envelope interference. This reasoning suggests that only a small part of the potential of this approach has been uncovered yet. For example, by combining multiple envelope notches it might be possible to achieve broader stop regions in the envelope domain.

The development of DSP techniques related to the NIS, as presented in this thesis, is carried out in three stages. In Chapter III, a system study is performed on the application of the NIS in the receiver, based on simple mathematical models. An optimal adaptation signal is derived which permits sufficient interference suppression and negligible nonlinear distortion. The promising results of the system study are followed in Chapter IV by an analysis of the required accuracy for the adaptation signal to achieve a sufficient interference suppression and negligible degradation to the receiver performance. A closed-loop adaptation method is developed to produce the adaptation signal and achieve the required accuracy. Simultaneously, the NIS circuit is designed, fabricated in CMOS 140 nm technology, and delivered as a module [17]. Chapter V presents the experimental results of integration of the NIS module in a testbed multimode transceiver. Successful operation of the NIS and the proposed adaptation method in a practical setting concludes our work and promises an interference suppression method with low complexity and power consumption, suitable for handheld devices.

There is a regime where the interference is not so strong as to cause significant loss of the receiver gain. The analysis of this regime in Chapter II shows that the Cross-Modulation (CM) distortion is the key factor degrading the receiver performance. Subsequently, a fully digital method is proposed to compensate for the CM distortion and improve the receiver performance significantly.

From the research carried out in this thesis and in [17], we concluded that for a hybrid approach that combines DSP techniques and analogue circuits a closed cycle of modelling- design-implementation-experiment is required to develop a truly practical approach.

In the following sections the conclusions of each chapter are described in more detail.

6.1.1 Digital compensation of Cross-Modulation (CM)

In Chapter II, we focus on the regime where the interference is not so strong as to cause significant loss of the receiver gain. In this weakly nonlinear regime, nonlinear distortion products are the key factor degrading the receiver performance. Cross-Modulation (CM) distortion is identified as the key distortion product, motivating us to develop a digital compensation method for the CM distortion. To this end a discrete-time model that describes the CM distortion is required. A third-order polynomial, which is suitable for the weakly nonlinear regime, is used to model the nonlinear Front-End (FE) and the transmit-receive path of the interferer is modelled by a time delay and attenuation. Based on these models a discrete-time nonlinear model for the CM distortion is developed, which includes two priori unknown parameters, namely a time delay and an amplitude. We propose estimators for these two parameters. Based on these estimated values and by using baseband transmitted interferer the CM distortion is compensated. The simulation results show the effectiveness of this method to improve the receiver's Symbol Error Rate (SER) in the presence of a strong interferer. For example for 64QAM modulation an improvement of 16 dB in signal-to-distortion ratio is observed, which is equivalent to 8 dB improvement of the receiver Input third-order Intercept Point (IIP3). An important aspect of the proposed compensation method is that it does not require any major modification to the receiver FE or the digital stages of the receiver after the CM compensator. This method, however, is limited to the weakly nonlinear regime. In the case that the interference is so strong as to cause desensitization, it must be mitigated in the analogue domain.

6.1.2 Nonlinear interference suppressor, Principle of operation

In Chapter III, we introduced the NIS, modelled by a combination of a hard-limiter with adaptable limiting amplitude and an amplifier with a constant gain. An optimal adaptation signal for the NIS was derived that leads to complete suppression of the interference in the absence of the desired signal. This adaptation signal was shown to be proportional to the envelope of the received interference at the NIS input. For the case that the optimal adaptation signal is exactly known, we performed a system study to analyze the performance of the NIS in the presence of the desired signal on two aspects: interference suppression, and generation of nonlinear distortion products. Firstly, we showed that the NIS can strongly suppress the interference to a level below that of the desired signal at the NIS output. Secondly, we identified and analyzed the principal distortion products introduced by the NIS, namely Gain Variation Distortion (GVD) and Inter-Modulation (IM) leakage. The GVD increases when the Signal to Interference power Ratio (SIR) at the NIS input increases. We determined a threshold on SIR below which the NIS offers a negligible degradation to the Signal to Noise power Ratio (SNR) at the demodulator input. As a rule of thumb, to limit the SNR degradation to less than 0.1 dB, we should stop using the NIS when the SIR [dB]>(-SNR [dB]-7). For larger SIRs the linear receiver without NIS can handle the interference without requiring an excessive dynamic range. Hence, with the proposed solution we can cover the whole range of possible input SIRs. The IM leakage is only considerable when frequency separation between the desired and the interference is below a few times the bandwidth of the interference. IM leakage vanishes rapidly with increasing frequency separation. Hence for most conditions of practical interest adequate interference suppression is achieved with negligible distortion of the desired signal.

6.1.3 Nonlinear interference suppressor, closed loop adaptation

In Chapter III, it was assumed that the optimal adaptation signal was exactly known. In the multimode transceiver the baseband interference is available locally. In Chapter IV, we developed a method to produce the adaptation signal that exploits the fact that in the multimode transceiver the baseband interference is available locally, thus allowing us to estimate a baseband model of the interference transmit-receive path from the baseband interference to the NIS input. To identify the required accuracy for the adaptation signal the impact of adaptation errors with respect to the optimal adaptation signal was studied. The interference suppression was found to be inversely proportional to the mean square error of the adaptation signal. The impact of adaptation errors on the quality of the desired signal was studied for a practical scenario. We proposed to use a Finite Impulse

Response (FIR) filter for the path model. The required length of the FIR filter was analyzed based on practical specification of the front-end components to achieve a specific accuracy for the adaptation signal. It was found that depending on the bandwidth of the interference a filter length of 1 to about 20 taps is required. The transmit-receive path is subject to environmental changes. To track these changes we proposed a closed-loop adaptation scheme that adapts the path model such that the residual interference at the NIS output is minimized. The convergence properties of the closed-loop scheme were analyzed and it was shown that the closed-loop scheme can:

1. attain the required accuracy for the adaptation signal,

2. track the dynamic changes in the path with a sufficient speed.

Finally, to verify our analysis, simulations for a practical multimode scenario were performed, showing that the proposed method can suppress the interference to a level below that of the desired signal while introducing negligible degradation to Symbol Error Rate (SER) of the receiver.

6.1.4 Nonlinear interference suppressor, Experimental results

A theoretical foundation for NIS adaptation was developed based on an ideal system model in the previous chapter. In Chapter V, we presented experimental results of a transceiver testbed with the NIS implemented in 140 nm CMOS technology. Firstly, experiments were performed to obtain models that explain the main imperfections of the NIS circuit with respect to the ideal model. Two key imperfections were identified, namely phase misalignment between limiter and amplifier, and the limited slope of the adaptable limiter. The phase misalignment depends on the interference power and limits the maximum interference suppression that can be achieved for a certain interference power. The limited slope of the limiter firstly leads to a certain amplitude range where sufficient interference suppression can be achieved, and secondly to a dependency of the desired signal gain on the envelope of the interference. This dependency induces CM distortion of the desired signal. The closed-loop adaptation method, which was developed in Chapter IV, was implemented after slight modifications to account for the NIS imperfections. An interference suppression of up to 43 dB is attained for GMSK interference. For varying-envelope interferences, at least 30 dB of interference suppression is achieved over the range of -3 to 6 dBm of interference average power. The upper limit of this range originates from the limitation of the supply voltage. The lower limit originates from the phase misalignment and the limited slope of the limiter and can be extended in future designs. The experiments show that the adaptation method can track rapid variations in the environment, as induced, for example, by moving objects between the local transmit and receive antennae. The CM distortion, present in the case of varying envelope interferences, has a different characteristic compared to the CM distortion that was encountered in Chapter II. To obtain an acceptable SER a method is proposed and successfully implemented to compensate for this distortion. The experimental results of this chapter suggest that the NIS with the proposed adaptation method can be used to substantially suppress the strong interference with a modest penalty to the quality of the desired signal.

6.2 Future work

6.2.1 Improvements and explorations for the NIS

Although the NIS can achieve unprecedented frequency-independent interference suppression with a low power consumption and cost, in certain respects it can be improved. In the following paragraphs some directions for possible improvements and explorations are suggested.

1) *Mitigation of spectral mirroring*: Owing to the spectral mirroring effect of the NIS, discussed in Section 3.4.5, unwanted components at the mirror frequency of the desired signal with respect to the interference frequency are translated into the desired signal frequency channel. By using a BandPass Filter (BPF) before the NIS, this problem can be mitigated if the mirror frequency falls into the stop band of the BPF. In some scenarios, however, the mirror frequency falls into the passband of the BPF. Although implementing a relatively wideband notch filter to sufficiently suppress the mirror component might be possible, it is not a desirable solution, since it requires dedicating a large chip area for inductors and capacitors. To solve the mirroring effect, digital compensation methods can be investigated.

2) *Decreasing the bandwidth of the adaptation signal*: The required adaptation signal for the NIS is proportional to the envelope of the interference. To accurately reconstruct the envelope of most communication signals, e.g. OFDM modulated signals, from discrete samples, a sample rate 4 to 10 times higher that the sample rate of the baseband interference is required. This over-sampling has two negative impacts:

1. It increases the complexity of the required digital and mixed-signal electronics.
2. Any added noise, e.g. quantization noise and noise of the digital electronic circuits, to the adaptation signal is upconverted to the frequency of the interference and may leak into the frequency channel of the desired signal.

The wider the bandwidth of this noise, the more problematic will be the leakage. To filter the noise a lowpass filter can be used to filter the adaptation signal after the DAC that converts the discrete-time adaptation signal to the continuous-time signal. A large bandwidth for the adaptation signal means a high cut-off frequency of the low-pass filter, thus increasing the bandwidth of the added noise.

On the other hand, the bandwidth of the square of the envelope is only twice the bandwidth of the baseband interference. Based on these observations, a useful improvement can be to redesign the NIS such that the adaptation signal would be proportional to the square of the envelope instead of the envelope itself. For this improved design the adaptation method in Chapter IV must be slightly modified to take into account the change from the envelope to the square of the envelope.

3) *Increasing the Interference suppression*: The interference suppression of the current NIS circuit is limited mainly because of the phase misalignment between the limiter and amplifier. One might try to achieve a better alignment by improving the circuit design. A more attractive approach, however, would be to digitally adapt the circuit such that a better alignment is attained. For the current NIS circuit the alignment can be manually tuned using a bias point to some extent. Future research can aim at an adaptation method for this bias point.

4) *Exploring alternative nonlinearities*: To adapt the NIS, complete knowledge of the interference envelope is required. This more or less limits the application of this method to local interferences, where the envelope of the received interference at the NIS input can be accurately estimated based on the transmitted baseband information. Different input-output characteristics for the NIS can be explored, with a goal that less information of the interference, e.g. only the average power, would be required.

6.2.2 Improving the digital compensation method

The digital compensation method in Chapter II was only evaluated using simulations. Although these indicate an improvement in the receiver performance, further investigation should be done on a practical transceiver to determine the extent of applicability of this approach. This investigation should start with careful measurement and modeling of a practical front-end, followed by refining the compensation methods based on these models.

6.2.3 Application of the NIS for FMCW radar

Similar to the multimode transceiver, Frequency Modulated Continuous Wave (FMCW) radar suffers from a leakage of its own transmitter [72, 73]. The isolation that is achieved by current techniques is proved to be insufficient [66]. Hence adaptive analogue cancellation methods have been proposed to mitigate this leakage [66, 74, 75], despite their problems described in Section 1.3.3. The NIS seems to be a very suitable approach to mitigate the transmitter leakage for commercial FMCW radars. Also the NIS adaptation for constant-envelope interferences, here the transmitted FMCW signal, is very simple. Using the NIS, however, may create new problems for this application. For example, owing to the spectral mirroring effect in the NIS, the sign of the Doppler frequency of the scatter from a moving object would be ambiguous; objects that are approaching will show the same Doppler shift as the objects that are departing. This ambiguity, however, might be resolved by further processing of the received scatter.

6.2.4 Application of the NIS for RFID readers

In Radio Frequency Identification (RFID) systems a transceiver, called reader, powers and communicates with tags that are within range. To maintain the flow of power from the reader to tags and enable communication with multiple tags the reader operates in full duplex. Owing to insufficient isolation between the transmitter (TX) and receiver (RX) of the reader, the transmitted signal by the TX induces interference in the RX that is many orders of magnitude stronger than the signal reflected by the tags. Currently, to maintain the RX sensitivity in the presence of such strong interference, a receiver with a large dynamic range and intricate automatic gain control is used. A technique like the NIS, which can substantially mitigate the TX leakage, can potentially decrease the RX complexity and power consumption.

Bibliography

[1] J.J. Gavan and M.B. Shulman. Effects of desensitization on mobile radio system performance, part ii: Quantitative analysis. *IEEE Transactions on Vehicular Technology*, 33(4):291 – 300, Nov 1984.

[2] IEEE Std 802.15.2TM. Coexistence of wireless personal area networks with other wireless devices operating in unlicensed frequency bands.

[3] 3GPP. Tr 36.816: Evolved universal terrestrial radio access (E-UTRA); study on signaling and procedure for interference avoidance for in-device coexistence.

[4] Wenjun Sheng, A. Emira, and E. Sanchez-Sinencio. CMOS RF receiver system design: a systematic approach. *IEEE Transactions on Circuits and Systems I: Regular Papers*, 53(5):1023 – 1034, May. 2006.

[5] V. Aparin, G.J. Ballantyne, C.J. Persico, and A. Cicalini. An integrated LMS adaptive filter of TX leakage for CDMA receiver front ends. *IEEE Journal of Solid-State Circuits*, 41(5):1171 – 1182, May 2006.

[6] S. Kannangara and M. Faulkner. Adaptive duplexer for multiband transreceiver. In *Proceedings of Radio and Wireless Conference(RAWCON)*, pages 381–384, 2003.

[7] A. Raghavan, E. Gebara, E.M. Tentzeris, and J. Laskar. Analysis and design of an interference canceller for collocated radios. *IEEE Transactions on Microwave Theory and Techniques*, 53(11):3498 – 3508, Nov. 2005.

[8] T. O'Sullivan, R.A. York, B. Noren, and P.M. Asbeck. Adaptive duplexer implemented using single-path and multipath feedforward techniques with bst phase shifters. *IEEE Transactions on Microwave Theory and Techniques*, 53(1):106–114, 2005.

[9] A. Roussel, C.W.T. Nicholls, and J.S. Wight. Frequency agile rf feedforward noise cancellation system. In *IEEE Radio and Wireless Symposium*, pages 109–112, 2008.

[10] S. Ahmed and M. Faulkner. Optimized interference canceling for colocated base station transceivers. *IEEE Transactions on Vehicular Technology*, 60(9):4175 –4183, Nov. 2011.

[11] Jung Il Choi, Mayank Jain, Kannan Srinivasan, Phil Levis, and Sachin Katti. Achieving single channel, full duplex wireless communication. In *Proceedings of the sixteenth annual international conference on Mobile computing and networking*, pages 1–12. ACM, 2010.

[12] G.E. Moore. Cramming more components onto integrated circuits. *Electronics*, 38(8), April 1965.

[13] Qiyue Zou, M. Mikhemar, and A.H. Sayed. Digital compensation of cross-modulation distortion in software-defined radios. *IEEE Journal of Selected Topics in Signal Processing*, 3(3):348 –361, Jun. 2009.

[14] M. Valkama, A. Shahed hagh ghadam, L. Anttila, and M. Renfors. Advanced digital signal processing techniques for compensation of nonlinear distortion in wideband multicarrier radio receivers. *IEEE Transactions on Microwave Theory and Techniques*, 54(6):2356 –2366, Jun. 2006.

[15] Junho Moon, Seunghwi Jung, Sanghoon Hwang, and Minkyu Song. A 6b 100MS/s 0.28mm^2 5mW 0.18um CMOS F/I ADC with a novel folder reduction technique. In *13th IEEE International Conference on Electronics, Circuits and Systems, 2006. ICECS '06.*, pages 140 –143, Dec. 2006.

[16] N.M. Blachman. Optimum memoryless bandpass nonlinearities. *IEE Proceedings Communications, Speech and Vision*, 140(6):436 –444, Dec. 1993.

[17] E.J.G. Janssen. *Methodologies for Multi-Radio Coexistence*. PhD thesis, Eindhoven University of Technology, Sep. 2013.

[18] D. Robertson and T. Montalvo. Issues and trends in RF and mixed signal integration and partitioning. *IEEE Communications Magazine*, 46(9):52 –56, Sep. 2008.

[19] Jing Zhu, A. Waltho, Xue Yang, and Xingang Guo. Multi-radio coexistence: challenges and opportunities. *Proceedings of 16th International Conference on Computer Communications and Networks, 2007. ICCCN 2007.*, pages 358 –364, Aug. 2007.

[20] L. Maurer. Adaptive digital front-end enhanced CMOS-based RF transceivers a brief overview. *Workshop on Integrated Nonlinear Microwave and Millimetre-Wave Circuits. INMMIC 2008*, pages 111 –114, Nov. 2008.

[21] Behzad Razavi. *RF Microelectronics*. Prentice-Hall, Inc., Upper Saddle River, NJ, USA, 1998.

[22] A. Dejonghe, B. Bougard, S. Pollin, J. Craninckx, A. Bourdoux, L. Ven der Perre, and F. Catthoor. Green reconfigurable radio systems. *IEEE Signal Processing Magazine*, 24(3):90 –101, May. 2007.

[23] M. Valkama, A. Shahed hagh ghadam, L. Anttila, and M. Renfors. Advanced digital signal processing techniques for compensation of nonlinear distortion in wideband multicarrier radio receivers. *IEEE Transactions on Microwave Theory and Techniques*, 54(6):2356 –2366, Jun. 2006.

[24] A. Chorti and M. Brookes. On the effects of memoryless nonlinearities on m-qam and dqpsk ofdm signals. *IEEE Transactions on Microwave Theory and Techniques*, 54(8):3301 –3315, aug. 2006.

[25] C. van den Bos, M.H.L. Ksuwenhoven, and W.A. Serdijn. Effect of smooth nonlinear distortion on ofdm symbol error rate. *IEEE Transactions on Communications*, 49(9):1510 –1514, Sep. 2001.

[26] G. Chien, Weishi Feng, Y.A. Hsu, and L. Tse. A 2.4GHz CMOS transceiver and baseband processor chipset for 802.11b wireless LAN application. *IEEE International Solid-State Circuits Conference, 2003. Digest of Technical Papers. ISSCC 2003*, pages 358 – 499 vol.1, 2003.

[27] G. Jacovitti and G. Scarano. Discrete time techniques for time delay estimation. *IEEE Transactions on Signal Processing*, 41(2):525 –533, Feb. 1993.

[28] A. Papoulis. *Probability, Random Variables, and Stochastic Processes.* McGraw-Hill Science, 3rd edition, 1991.

[29] R.H. Walden. Analog-to-digital converter survey and analysis. *IEEE Journal on Selected Areas in Communications*, 17(4):539 –550, April 1999.

[30] A. Raghavan, E. Gebara, M. Tentzeris, and J. Laskar. An active interference canceller for multistandard collocated radio. In *2005 IEEE MTT-S International Microwave Symposium Digest*, page 4 pp., june 2005.

[31] P. Baier and K.-J. Friederichs. A nonlinear device to suppress strong interfering signals with arbitrary angle modulation in spread-spectrum receivers. *IEEE Transactions on Communications*, 33(3):300–302, Mar. 1985.

[32] H. Habibi, Y. Wu, J.W.M. Bergmans, E.J.G. Janssen, and P.G.M. Baltus. Suppression of constant modulus interference in multimode transceivers by closed-loop tuning of a nonlinear circuit. In *IEEE 75th Vehicular Technology Conference (VTC)*, pages 1 –6, May 2012.

[33] E.J.G. Janssen, D. Milosevic, and P.G.M. Baltus. A 1.8GHz amplifier with 39dB frequency-independent smart self-interference blocker suppression. In *IEEE Radio Frequency Integrated Circuits Symposium (RFIC)*, pages 97 –100, June 2012.

[34] N. Blachman. Detectors, bandpass nonlinearities, and their optimization: Inversion of the chebyshev transform. *IEEE Transactions on Information Theory*, 17(4):398 – 404, Jul. 1971.

[35] K.-J. Friederichs. A novel canceller for strong CW and angle modulated interferers in spread-spectrum-receivers. In *IEEE Military Communications Conference, 1984. MILCOM*, volume 3, pages 478 –481, Oct. 1984.

[36] P.C. Jain, N.M. Blachman, and P.M. Chapell. Interference suppression by biased nonlinearities. *IEEE Transactions on Information Theory*, 41(2):496 –507, mar 1995.

[37] J.H. Higbie. Adaptive nonlinear suppression of interference. In *IEEE Military Communications Conference, 1988. MILCOM 88,*, pages 381 –389 vol.2, oct 1988.

[38] S.S. Mehta, D. Weber, M. Terrovitis, K. Onodera, M.P. Mack, B.J. Kaczynski, H. Samavati, S.H.-M. Jen, W.W. Si, MeeLan Lee, and K. Singh. An 802.11g wlan soc. *IEEE Journal of Solid-State Circuits*, 40(12):2483 – 2491, Dec. 2005.

[39] S. D'Amico, M. Conta, and A. Baschirotto. A 4.1-mw 10-mhz fourth-order source-follower-based continuous-time filter with 79-db dr. *IEEE Journal of Solid-State Circuits*, 41(12):2713 –2719, Dec. 2006.

[40] A. Schumitzky. Modulation products and optimum frequency conversion for an n-frequency input. *Journal of the Society for Industrial and Applied Mathematics*, 13(4):1019–1032, December 1965.

[41] P. Banelli and S. Cacopardi. Theoretical analysis and performance of ofdm signals in nonlinear awgn channels. *Communications, IEEE Transactions on*, 48(3):430 –441, Mar. 2000.

[42] A. Gelb and Vander Velde W. E. *Multiple-Input Describing Functions And Nonlinear System Design*. McGraw-Hill, 1968.

[43] R. Price. A note on the envelope and phase-modulated components of narrow-band gaussian noise. *IRE Transactions on Information Theory*, 1(2):9 –13, Sep. 1955.

[44] John Proakis and Masoud Salehi. *Digital Communications.* McGraw-Hill Science/Engineering/Math, 5th edition, 2007.

[45] J. Arias, V. Boccuzzi, L. Quintanilla, L. Enriquez, D. Bisbal, M. Banu, and J. Barbolla. Low-power pipeline ADC for wireless LANs. *IEEE Journal of Solid-State Circuits*, 39(8):1338 – 1340, August 2004.

[46] E.J.G. Janssen, D. Milosevic, P.G.M. Baltus, A.H.M. van Roermund, and H. Habibi. Digital hardware resources for steering a nonlinear interference suppressor. In *Proceedings of the 19th International Conference Mixed Design of Integrated Circuits and Systems (MIXDES)*, pages 133 –138, May 2012.

[47] Yung Ming Chiu, Tsung Ming Chen, Po Yu Chen, R. Kuan, and Yi Chang Shih. A 65nm low-power CMOS transceiver for 802.11n portable application. In *IEEE Radio Frequency Integrated Circuits Symposium, 2008. RFIC 2008.*, pages 97 –100, Apr. 2008.

[48] S. Ahmed and M. Faulkner. Mitigation of reverse intermodulation products at colocated base stations. *IEEE Transactions on Circuits and Systems I: Regular Papers*, 60(6):1608–1620, 2013.

[49] M. Omer, R. Rimini, P. Heidmann, and J.S. Kenney. A compensation scheme to allow full duplex operation in the presence of highly nonlinear microwave components for 4 g systems. In *IEEE MTT-S International Microwave Symposium Digest (MTT)*, pages 1–4, 2011.

[50] E.A. Keehr and A. Hajimiri. Successive regeneration and adaptive cancellation of higher order intermodulation products in rf receivers. *IEEE Transactions on Microwave Theory and Techniques*, 59(5):1379–1396, 2011.

[51] A. Kiayani and et. al. Modeling and dynamic cancellation of tx-rx leakage in fdd transceivers. In *IEEE Int. Midwest Symposium on Circuits and Systems (MWSCAS 2013)*, Aug. 2013.

[52] H. Habibi, E.J.G. Janssen, W. Yan, and J.W.M. Bergmans. Digital compensation of cross-modulation distortion in multimode transceivers. *IET Communications*, 6(12):1724 –1733, 14 2012.

[53] Y. Ma, Y. Yamao, K. Ishibashi, and Y. Akaiwa. Adaptive compensation of inter-band modulation distortion for tunable concurrent dual-band receivers. *IEEE Transactions on Microwave Theory and Techniques*, 61(12):4209–4219,

2013.

[54] H. Darabi. A blocker filtering technique for SAW-less wireless receivers. *IEEE Journal of Solid-State Circuits*, 42(12):2766–2773, 2007.

[55] Dinesh Bharadia, Emily McMilin, and Sachin Katti. Full duplex radios. In *ACM SIGCOMM*, 2013.

[56] H. Habibi, Y. Wu, J.W.M. Bergmans, E.J.G. Janssen, and P.G.M. Baltus. Suppression of constant modulus interference in multimode transceivers using an adaptive nonlinear circuit. In *NASA/ESA Conference on Adaptive Hardware and Systems (AHS), 2013*, June 2013.

[57] H. Habibi, Y. Wu, J.W.M. Bergmans, E.J.G. Janssen, and P.G.M. Baltus. Nonlinear interference suppressor for varying-envelope local interference in multimode transceivers. In *Proceedings of 34th Symposium on Information Theory in the Benelux*, May 2013.

[58] C. Cahn. A note on signal-to-noise ratio in band-pass limiters. *IRE Transactions on Information Theory*, 7(1):39 –43, Jan. 1961.

[59] RFM. SAW filter sf2124e data sheet, 2010.

[60] S.S. Haykin. *Adaptive filter theory*. Prentice Hall, 4th edition, 2001.

[61] Alan V. Oppenheim, Ronald W. Schafer, and John R. Buck. *Discrete-Time Signal Processing (2nd Edition)*, pages 775–802. Prentice Hall, 2 edition, January 1999.

[62] B. Farhang-Boroujeny. *Adaptive filters: theory and applications*. John Wiley & Sons, Inc., 1998.

[63] Yonghua Cong and R.L. Geiger. A 1.5-V 14-bit 100-MS/s self-calibrated DAC. *IEEE Journal of Solid-State Circuits*, 38(12):2051 – 2060, Dec. 2003.

[64] Zhenping Hu, R. Susitaival, Zhuo Chen, I-Kang Fu, P. Dayal, and S.K. Baghel. Interference avoidance for in-device coexistence in 3GPP LTE-advanced: challenges and solutions. *IEEE Communications Magazine*, 50(11):60 –67, November 2012.

[65] H. Habibi, Y. Wu, J.W.M. Bergmans, E.J.G. Janssen, and P.G.M. Baltus. Closed-loop adaptation of a nonlinear interference suppressor for local interference in multimode transceivers. In *Proceedings of 34th Symposium on Information Theory in the Benelux*, May 2013.

[66] Kaihui Lin, Yuanxun Ethan Wang, Cheng keng Pao, and Yi-Chi Shih. A Ka-band FMCW radar front-end with adaptive leakage cancellation. *IEEE Transactions on Microwave Theory and Techniques*, 54(12):4041 –4048, Dec. 2006.

[67] ISO/IEC 18000-3. Radio frequency identification for item management, 2004.

[68] N. Blachman. Band-pass nonlinearities. *IEEE Transactions on Information Theory*, 10(2):162 – 164, Apr. 1964.

[69] Joel Vuolevi and Timo Rahkonen. *Distortion in RF power amplifiers*. Artech house, 2003.

[70] M. Valkama, A. Springer, and G. Hueber. Digital signal processing for reducing the effects of RF imperfections in radio devices- an overview. In *Proceedings of 2010 IEEE International Symposium on Circuits and Systems (ISCAS)*, pages 813 –816, 30 2010-june 2 2010.

[71] G. Fettweis, M. Lohning, D. Petrovic, Marcus Windisch, P. Zillmann, and W. Rave. Dirty rf: a new paradigm. In *IEEE 16th International Symposium on Personal, Indoor and Mobile Radio Communications, 2005. PIMRC 2005.*, volume 4, pages 2347–2355 Vol. 4, 2005.

[72] Zhaolong Li and Ke Wu. On the leakage of FMCW radar front-end receiver. In *Global Symposium on Millimeter Waves, 2008. GSMM 2008.*, pages 127–130, 2008.

[73] M. Skolnik. *Radar Handbook, Third Edition*. Electronics electrical engineering. McGraw-Hill Education, 2008.

[74] P.D.L. Beasley, A. Stove, B. J. Reits, and B. As. Solving the problems of a single antenna frequency modulated CW radar. In *Record of the IEEE 1990 International Radar Conference, 1990.*, pages 391–395, 1990.

[75] Shi Xiu-kun and Huang Jian. Development of rf front-end with high T/R isolation for ka band mono-antenna fmcw radar. In *2011 IEEE CIE International Conference on Radar*, volume 1, pages 276–279, 2011.

Acknowledgement

Firstly, I would like to thank my first promotor, Prof. Jan Bergmans, whom without his meticulous criticism and patience I would not be able to conclude my work. During the unfortunate events that occurred to our family in the first year of my PhD, he showed an extreme sympathy and assistance, which I am grateful for that. After these events he encouraged me and guided me to work as efficient as possible to catch up. Although he has a busy schedule, he has been always present to assist me. I remember that during an approaching deadline I sent him a draft of my paper at about 5:00am. After taking a short nap, I was surprised to see my paper back with many comments! I am thoroughly indebted to him for teaching me a highly structured and goal oriented approach to scientific research, writing, and presentation. I am indebted to my daily supervisor, Dr. Wu Yan, who helped me to carefully dissect the motivation of my work step by step. Our numerous discussions allowed me to clarify my writings and presentations. I appreciate his support during these years and his efforts in reading this thesis. I also like to thank Prof. Peter Baltus, my second promotor, for his inspiring comments and ideas during our meetings. Peter has always been extremely helpful and encouraging.

I had the opportunity to have Erwin Janssen as my colleague during these years. I enjoyed working with him and learned from his way of conducting research. I would like to thank Rick Hilkens for his contribution in the experimental part of this work and Mojtaba Zamanifekri for his assistance in simulations of appendix I of the first chapter. I wish to thank members of the SPS group for contributing to a pleasant working environment, especially our secretaries Anja and Diana who have always been ready to help with a smile. I enjoyed sharing a sunny office with Iman, Brian, Joep, Maarten, and Marija. Although I will miss my time in that office, we all wished for a room which was less hot in the summer. Especial thanks go to Iman for all the interesting discussions and walks around Eindhoven.

I would like to thank other members of my doctoral committee, Prof. Bram Nauta, Prof. Gerd Ascheid, Prof. Erik Fledderus, and Dr. Dusan Milosevic for taking a seat in the committee, reading this thesis, and giving comments. I would also like to thank STW for financial support and preparing an environment to conduct our research and share its result. I wish to thank all the members of the user committee, especially, Jan Prummel for reading a part of this thesis and his comments, Henk ten Pierick and Dr. Hendrik van der Ploeg for actively participating in our monthly meetings.

I would like to express my gratitude to Dr. Behnia, Dr. Bastani, Dr. Nasiri, and Dr. Pakravan for teaching me the fundamentals of communications systems and Mehdi Rezaei for valuable lessons in practical aspects of electronics and radio frequency systems.

I was lucky to have wonderful friends around me during my PhD, in the times of need and happiness. I would like to thank Saeed, Saeede, Iman, Carmen, Hamid, Azar, Pooyan, Ellaheh, Salman, Leila, Hosein, Samane, Aisan, Vahid, Ali, Elham, Amir, Mojtaba, Ehsan and many other dear friends for their company and sincere help. Especial thanks go to my old friend Pooyan for his assistance with so many things on so many occasions.

I am grateful to my parents for all their sacrifices and efforts. They always encouraged me to continue my education to a doctorate degree and without their support this would not be possible.

Last but not least I would like to thank my lovely wife Negar, who has been by my side during these years in both happiness and sadness. She encouraged me, celebrated my achievements, and has been a true friend. I burrowed many hours from our time together to spend on this thesis. I cannot wait to redeem these hours.

A part of the second chapter of this thesis was developed during the time that Sophie was still with us. I cannot do anything except to wish that she was still here!

Curriculum vitae

Hooman Habibi was born in Iran, in 1981. He obtained his B.Sc. and M.Sc. degrees in electronics and communication systems from Sharif University of Technology, Iran, in 2004 and 2007. From 2007 to 2009 he was involved in design and implementation of various signal processing and telecommunications systems. From 2009 to 2013, he was a PhD candidate at Signal Processing group of Electrical Engineering Department of Eindhoven University of Technology, Eindhoven, the Netherlands. The goal of his PhD research was development of mixed analogue and digital techniques to enable handling of strong interferers by radio frequency receivers with low complexity and power consumption. His research interest mainly lies in application of signal processing for communication systems, statistical signal processing and adaptive systems.